# THERMOELECTRIC POWER IN DILUTE AND CONCENTRATED MAGNETIC ALLOYS

by

JEROLD TOUGER

A dissertation submitted to the Graduate Faculty in Physics in partial fulfillment of the requirement for the degree of Doctor of Philosophy, The City University of New York.

1974

This manuscript has been read and accepted for the Graduate Faculty in Physics in satisfaction of the dissertation requirement for the degree of Doctor of Philosophy.

October 4, 1974
date

Myriam P. Sarachik
Chairman of Examining Committee

10/4/74
date

Warren I. Mattheisen
Executive Officer

Prof. Myriam P. Sarachik (City)
Prof. C. Rutherford Fischer (Queens)
Prof. Frederick Smith (City)

Prof. Narkis Tzoar (City)
Dr. Klaus Andres (Bell Labs)

Supervisory Committee

The City University of New York

## ACKNOWLEDGEMENTS

The author would like to acknowledge the efforts of his mentor Professor Myriam P. Sarachik. Her guidance, assistance, discussion, and enthusiastic support were most valuable and are greatly appreciated.

The advice of Dr. Robert W. Houghton was very helpful in the design of the experimental apparatus. The contributions of the men of the machine shop of the City College Physics Department to the construction and maintenance of the experimental apparatus were invaluable.

Useful discussions and assistance in various aspects of the experimental work were forthcoming from Professor Frederick W. Smith, Dr. James B. Haddad, Dr. Randall . Caton, and Mr. Jing-cheng Liu, and are gratefully acknowledged.

The section of this thesis dealing with Boltzmann transport theory and thermopower draws heavily on notes taken by the author in a course taught by Professor Narkis Tzoar.

Finally, the author would like to express special thanks to his wife Hallie for the typing of this thesis, and for her patience and endurance during the years of work on which it is based.

## TABLE OF CONTENTS

## TABLE CAPTIONS

Table 1 Characteristic temperature $T_C$ and spin fluctuation temperature $T_S$ of alloys characterized by local spin fluctuations (taken from Ref. 2)

Table 2 Comparison of the variations of $\Delta\rho(\Delta T)$, $\Delta\rho(\Delta H)$, and the concentration C of polarization clouds with composition in Cu-Ni alloys. $\Delta\rho(\Delta T) = \rho(1.75°K) - \rho(20°K)$, $\Delta\rho(\Delta H) = \rho(H=0) - \rho(50kG)$, and values of C are deduced from the susceptibility measurements of Ref. 82 (taken from Ref. 92)

Table 3 Approximate rate dT/dt at which the ambient temperature changes at various ambient temperatures T

## FIGURE CAPTIONS

Fig. 1. Basic thermoelectric circuits (taken from D.K.C. MacDonald, Ref. 4, p. 2): (a) Closed circuit. If 1 and 2 are different conduction materials, a thermoelectric current will generally flow. (b) Open circuit. If 1 and 2 are different conducting materials, the thermoelectric potential difference generated, $\Delta V_{12}$, will be proportional to $\Delta T$ if $\Delta T/T \ll 1$. With the polarity of $\Delta V_{12}$ as shown, and with $\Delta T > 0$, $S_1 > S_2$.

Fig. 2. Sketch of idealized absolute thermoelectric power of a single quasi-free electron metal. (taken from D.K.C.MacDonald, Ref. 4, p. 23)
A: Electron diffusion component of thermoelectric power approximately proportional to T.
B: Phonon-drag component with magnitude increasing as $T^3$ for $T \ll \Theta_D$ and decaying as for $T \gtrsim \Theta_D$.

Fig. 3. Typical behavior of the incremental thermoelectric power in Kondo systems resultimg from the addition of various small concentrations $c_1, c_2$, and $c_3$ of a magnetic impurity to a nonmagnetic host metal. (taken from M.D.Daybell and W.A.Steyert, Ref. 14)

Fig. 4. Curie-Weiss curve fit approximately to G.S. Knapp's susceptibility data for $Ir_{.995}Fe_{.005}$ (from data in Ref. 70).

Fig. 5. Excess resistivity per percent Fe impurity in Ir, as a function of temperature. (c refers to iron concentration) (taken from M.P.Sarachik, Ref. 54)

Fig. 6. Thermoelectric power as a function of temperature in Pd-Ni alloys and in pure Pd and Ni. (taken from C.L.Foiles and A.I.Schindler, Ref. 71) Curve A is the pure Pd data of Fletcher and Greig (Ref. 125) and Taylor and Coles (Ref. 126); Curve B is the unannealed pure Ni data of Blatt et al. (Ref. 117); Curves C, D, E, and F are the data for Pd-Ni alloys with the at.% of Ni as follows: C=0.5; D=1.0; E=1.66; and F=6.16.

Fig. 7a. Thermoelectric power of pure Ir and Ir with ½ and 1 at.% Fe, plotted as a function of temperature between 4.2 and 300°K.

Fig. 7b. Details of the plot shown in Fig. 7a, showing actual data points between 4.2 and 100°K.

Fig. 8. $\Delta S$ vs. temperature between 4.2 and 300°K for $Ir_{.995}Fe_{.005}$ and $Ir_{.99}Fe_{.01}$, where S is the difference between the thermopower of Ir-Fe and that of pure Ir.

Fig. 9. Thermoelectric power of pure Ir as a function of temperature between 4.2 and 1800°K (high temperature data taken from Ref. 78).

Fig. 10. The electrical resistivity of Cu-Ni alloys as a function of temperature (taken from Houghton et al., Ref. 91).

Fig. 11. Low temperature resistivity of Cu-Ni alloys as a function of temperature. The scale is the same for all curves, as shown at the top of the figure, but the baslines have been shifted to allow all curves to appear in detail on the same graph. (taken from Houghton et al., Ref. 92)

Fig. 12. Resistivity of Rh-Ni alloys as a function of temperature from 2 to 700°K. The five curves have been separated vertically for clarity. The resistivity of all alloys is ~39 Ω-cm at 77°K. (taken from Houghton et al., Ref. 93)

Fig. 13. Thermoelectric power of Cu-Ni alloys having from 30 to 50 at.% Ni, shown as a function of temperature between 4.2 and 300°K. The seven curves have been separated vertically for clarity.

Fig. 14. Details of thermopower vs. temperature curve for $Cu_{70}Ni_{30}$ between 4.2 and 100°K, showing actual data points.

Fig. 15. Details of thermopower vs. temperature curve for $Cu_{66}Ni_{34}$ between 4.2 and 100°K, showing actual data points.

Fig. 16. Details of thermopower vs. temperature curve for $Cu_{62}Ni_{38}$ between 4.2 and 100°K showing actual data points.

Fig. 17. Details of thermopower vs. temperature curve for $Cu_{58}Ni_{42}$ between 4.2 and 100°K, showing actual data points.

Fig. 18. Details of thermopower vs. temperature curve for $Cu_{57}Ni_{43}$ between 4.2 and 100°K, showing actual data points.

Fig. 19. Details for thermopower vs. temperature curve for $Cu_{56}Ni_{44}$ between 4.2 and 100°K, showing actual data points.

Fig. 20. Details of thermopower vs. temperature curve for $Cu_{54}Ni_{46}$ between 4.2 and 100°K, showing actual data points.

Fig. 21. Details of thermopower vs. temperature curve for $Cu_{50}Ni_{50}$ between 4.2 and 100°K, showing actual data points.

Fig. 22. Absolute value of thermoelectric power vs. Ni concentration at constant temperature in Cu-Ni alloys. Basic idea of plot and circled data points are from Ref. 106. Uncircled data points are our own. Data points enclosed in squares are from Ref. 103. These enclosed in triangles are from Ref. 86.

Fig. 23. Comparison of thermoelectric power vs. temperature in freshly annealed $Cu_{58}Ni_{42}$ and in $Cu_{58}Ni_{42}$ with a shelf life of roughly four years. Data is shown between 4.2 and 140°K. Between 140°K and room temperature the two curves coincide, and are as shown in Fig. 13.

Fig. 24. Thermoelectric power of Rh-Ni alloys having from 56 to 64 at.% Ni, shown as a function of temperature between 4.2 and 300°K. The four curves have been separated vertically for clarity.

Fig. 25. Details of thermopower vs. temperature curve for $Rh_{44}Ni_{56}$ between 4.2 and 100°K, showing actual data points.

Fig. 26. Details of thermopower vs. temperature curve for $Rh_{40}Ni_{60}$ between 4.2 and 100°K, showing actual data points.

Fig. 27. Details of thermopower vs. temperature curve for $Rh_{38}Ni_{62}$ between 4.2 and 100°K, showing actual data points.

# I. INTRODUCTION

This work presents data for the absolute thermoelectric power in two distinct types of metal alloy systems, containing dilute and concentrated amounts of a magnetic impurity, respectively, and examines this data in the light of existing theories and ideas.

Resistivity and susceptibility data in certain dilute magnetic alloys have been explained in terms of a theory of local spin fluctuations[1,2], in which it is assumed that because strong repulsive Coulomb interactions between d-electrons of opposite spin, the long wavelength, low frequency fluctuations in the spin density of the d-electrons will have a greatly enhanced amplitude in the vicinity of the magnetic impurity, and s-d spin flip scattering of the conduction electrons will occur. In 1968, Rivier and Zuckermann[3] argued that the results predicted by local spin fluctuation theory for all physical observables are the same as those predicted by the Kondo-Nagaoka spin-compensated state, in which one assumes the existence of an impurity spin, and this spin is considered to be screened at low temperatures by a cloud of antiferromagnetically coupled conduction electrons -- that is, the impurity spin is compensated.

This aroused interest among experimentalists in seeing whether some observable property could be measured for which different results were predicted by the Kondo-Nagaoka and local spin fluctuation theories. A private

communication from A.B.Kaiser suggested that a possibility for such a property might be the thermoelectric power of Ir-Fe, one of the systems which had been successfully treated in terms of local spin fluctuations, and for which, according to qualitative arguments put forward by Kaiser, widely divergent results were predicted by Kondo-Nagaoka and local spin fluctuation theories. Our Ir-Fe measurements were undertaken with this motivation, and the thermoelectric power was measured for pure Ir and for Ir with ½ and 1 at.% Fe.

The second portion of this work deals with thermoelectric power measurements in concentrated Cu-Ni and Rh-Ni alloys, where the problem of interest is quite different. In these alloys, the low-temperature spontaneous magnetization in the weakly ferromagnetic concentration range is located in magnetic polarization clouds of large total moment, and these clouds have been shown to persist well into the paramagnetic range.

The resistivity of Cu-Ni in a range of concentrations straddling the critical concentration for ferromagnetism showed anomalous behavior which has been interpreted in terms of these giant moment clouds. However, the resistivity of Rh-Ni in a similar concentration range showed no such anomalous behavior. We undertook to measure the thermoelectric power of Cu-Ni and Rh-Ni over the concentration ranges of interest in order to determine what effect the giant moments might have on another (and rather

sensitive) transport property, and to see whether the thermopowers for these systems differ as their resistivities do. The thermoelectric power was measured between 4.2 and 300 K in a series of Cu-Ni alloys containing from 30 to 50 at.% Ni and in a series of Rh-Ni alloys containing from 56 to 64 at.% Ni.

Since this thesis deals with two distinct problems, much of the body of the thesis will be divided into two sections (IV and V). For this reason an introduction to the experimental apparatus and procedure and general information on thermoelectric power are presented prior to the sections which discuss results for the dilute and concentrated magnetic alloys.

## II. THERMOELECTRIC POWER: GENERAL THEORY

### A. The Basic Thermoelectric Phenomena

Thermoelectricity, known to physicists since the early part of the nineteenth century, has received increasing attention in recent years as a tool for studying the scattering of electrons and various excitations, e.g. phonons, magnons, and perhaps paramagnons (see Section IV) in solids, and for obtaining information about the Fermi surface in metals and alloys. A survey of thermoelectricity was published in 1962 by D.K.C.MacDonald[4], and a recent review article by R.P.Huebener[5] reflects the considerable progress made in the field since that date.

Three thermoelectric phenomena are commonly considered:

(1) The Seebeck Effect: In an open circuit consisting of two different conductors joined as shown in Fig. 1(b)[4], if the junctions are maintained at temperatures differing by T, a thermovoltage $V_{12}$ can be measured across the terminals. This effect is known as the Seebeck effect, after the man who discovered it in 1822. The relative thermoelectric power is defined by $S \equiv S_1 - S_2 = dV_{12}/dT$, where $S_1$ and $S_2$ are the absolute thermoelectric powers of conductors 1 and 2. S is taken to be positive for the polarity shown in Fig. 1. If conductor 1 is a superconductor $S_1=0$, and for the polarity shown $S_2$ is negative. In this situation, if the circuit were closed, electrons would flow from the hot end of conductor 2 to the cold end, as one would expect. Hence, in ordinary

metals one expects a negative thermoelectric power.

The thermoelectric power is the most commonly measured of the thermoelectric phenomena. The others are of interest here insofar as they relate to the thermopower.

(2) Peltier Heat: If two conductors are now joined in series at constant temperature and a current flows from conductor 1 to conductor 2, heat may be evolved or absorbed at the junction of the two metals according as the heat current density associated with the electric current is greater or smaller in conductor 1 than in conductor 2. The Peltier coefficient of a metal is defined by $\pi = U_x/J_x$, the ratio of heat current density to electrical current density. The property one actually measures is $\pi_{12} = \pi_1 - \pi_2$, the so-called Peltier heat. For the given current direction represents the heat evolved or absorbed per unit time per unit electrical current according as $\pi_{12}$ is positive or negative. From thermodynamic arguments[6] or from Boltzmann transport theory, one finds that $\pi = TS$. A negative S indicates a negative $\pi$. Physically, if the heat current is in the direction of electron flow, it is opposite to the conventional electric current and hence $\pi = J_x/U_x$ is negative as is S for ordinary metals.

It should be noted that while the properties one ordinarily measures, $S_{12}$ and $\pi_{12}$, are relative properties of two conductors, $\pi$ and S are bulk properties of a single conductor.

(3) The Thomson Effect: If a current flows through a conductor along which a temperature gradient is maintained, the heat generated per unit volume is

$$\dot{Q} = \frac{J_x^2}{\sigma} + \frac{d}{dx}\left(\kappa \frac{dT}{dx}\right) - \mu J_x \frac{dT}{dx} .$$

$\sigma$ and $\kappa$ are the electrical and thermal conductivities. The first term on the right represents Joule heating. The second term involves the divergence of the heat current density. The last contribution requires both an electrical current and a temperature gradient. This contribution is the Thomson effect, and $\mu$ is called the Thomson coefficient. From thermodynamic arguments[6] or Boltzmann transport theory, one finds that $\mu = TdS/dT$.

has the advantage of being a directly measurable bulk property of a single conductor. By integral methods, one can then obtain the thermoelectric power of a single metal from $S(T)-S(0)=\int_0^T \frac{\mu}{T} dT$, or, since $S \to 0$ as $T \to 0$ by the third law of thermodynamics[6], $S(T)= \int_0^T \frac{\mu}{T} dT$. Hence, an absolute scale of thermoelectric power can be established for a metal at all temperatures (at sufficiently low temperatures one measures the thermopower of the metal in question vs. a superconductor) as has been done for Pb.[7] Once an absolute scale of thermopower exists for one material, it is possible to obtain the absolute thermopower of any other material by relative thermopower measurements, i.e. by measuring $V_{12}$ and $\Delta T$ in a set-up such as that shown in Fig. 1b.

The Thomson heat is also useful in understanding the temperature dependence of the thermoelectric power, since for simple power laws, $\mu = TdS/dT$ will have the same T-dependence as S. Neglecting other heating terms, the Thomson effect is described by $\dot{Q} = -\mu J_x \, dT/dx$ . Hence $\frac{dQ}{dT} = -\mu n e v \frac{dT}{dx}$, so that $\frac{dQ}{dT} = -\mu n e v \frac{1}{\frac{dx}{dt}} = -\mu n e$, and one gets $\mu = -\frac{1}{ne}\frac{dQ}{dT}$ . One can thus think of $\mu$ as something like a specific heat per unit charge of the conduction electrons. Maxwellian statistics would thus suggest a value for $\mu$ of $\frac{3}{2}\frac{k_B}{e}$ . However, because electrons obey Fermi statistics, this value must be reduced by a factor $\frac{k_B T}{E_F}$ , the fraction of electrons sufficiently close to the Fermi surface to be able to exchange thermal energy ($E_F$ is the Fermi energy). This gives us a linear variation of $\mu$ with T, and hence of S with T. A more rigorous calculation of the conduction electron specific heat for a free electron metals gives $C_v = \pi^2 k_B^2 nT/2E_F$ ,[5] so that $\mu = \pi^2 k_B^2 T/2eE_F$ , and $S = \int_0^T \frac{\mu}{T} dT = \pi^2 k_B^2 T/2eE_F$ , differing from our previous result only by a small numerical factor. S is still linear in T, and is negative because e is negative.

The result we have obtained thus far is for the electron diffusion thermopower. Only the heat associated with the electrons themselves is considered. Interactions of electrons with a non-equilibrium phonon system are neglected. Even for the electron diffusion thermo-

power, however, actual thermopowers may differ substantially from the values predicted by the free electron model, in magnitude (as in many transition metals) and/or sign (as in the noble metals).

B. Boltzmann Transport Theory and Thermoelectric Power

A more general expression for the diffusion thermoelectric power is obtained from the Boltzmann equation. One assumes that in equilibrium the electron distribution is given by the Fermi-Dirac distribution function $f_o = \frac{1}{e^{\beta(\epsilon-\zeta)}+1}$ ($\beta=1/k_BT$). If a field or temperature gradient is applied, the equilibrium distribution is disturbed, and in a steady state situation one assumes a distribution function f which differs from $f_o$ by a small amount, i.e. $f=f_o+f_1(k,r,t)$. For the steady state, Boltzmann's equation says that $\frac{\partial f}{\partial t} = \left(\frac{\partial f}{\partial t}\right)_{drift} + \left(\frac{\partial f}{\partial t}\right)_{coll} = 0$, implying a balance between the fields and temperature gradients which disturb equilibrium conditions, and collisions which tend to restore them.

In linearized Boltzmann theory, one regards $\left(\frac{\partial f}{\partial t}\right)_{drift}$ as the drift term occurring in the absence of collisions to which one then adds the collision term. The Liouville theorem says that $\left(\frac{df}{dt}\right)_{drift}=0$. Thus, $-\left(\frac{\partial f}{\partial t}\right)_{drift} = \nabla_x f \frac{\partial \vec{x}}{\partial t} + \nabla_v f \frac{\partial \vec{v}}{\partial t}$ . In one dimension, neglecting magnetic fields (the theory for thermoelectric power in the presence of a magnetic field is quite complex and not relevant to our work), we can write

$-\left(\frac{\partial f}{\partial t}\right)_{drift} = \frac{\partial f}{\partial T}\frac{\partial T}{\partial x}v_x + \frac{\partial f}{\partial v_x}\frac{eE_x}{m}$ .

For the collision term one makes a relaxation time approximation; i.e. one assumes that the rate of restoration to equilibrium is proportional to the deviation from equilibrium. Hence, $\left(\frac{\partial f}{\partial T}\right)_{coll} = -\frac{(f-f_0)}{\tau} = \frac{-f_1}{\tau}$ , so that $f-f_0 \sim e^{-t/\tau}$. The Boltzmann equation thus becomes $\frac{\partial f}{\partial v_x}\frac{eE_x}{m} + \frac{\partial f}{\partial T}\frac{\partial T}{\partial x}v_x = -f_1/\tau$ , or, keeping only terms of lowest order, $\frac{\partial f}{\partial v_x}\frac{eE_x}{m} + \frac{\partial f_0}{\partial T}\frac{\partial T}{\partial x}v_x = -f_1/\tau$ .
One can assume a well-defined temperature at each r in order to write down a quasi-equilitrium distribution function $f_0(r)$ or, equivalently, $f_0(T)$, and hence one calculates $\frac{\partial f_0}{\partial T}$ . One also calculates $\frac{\partial f}{\partial v_x} = \frac{\partial \epsilon}{\partial v_x}\left(\frac{\partial f_0}{\partial \epsilon}\right)$ .
With these calculations the Boltzmann equation becomes

$$\frac{\partial f_0}{\partial \epsilon}\left(ev_xE_x + T\frac{\partial}{\partial T}\left(\frac{\epsilon_k - \zeta(T)}{T}\right)v_x\frac{\partial T}{\partial x}\right) = -\frac{f_1}{\tau} .$$

We next set $f_1 = \left(-\frac{\partial f_0}{\partial \epsilon}\right)\varphi_k$ . ( $-\frac{\partial f_0}{\partial \epsilon}$ behaves essentially like $\delta(\epsilon-\epsilon_F)$, which is reasonable, since we expect transport properties to involve only electrons near the Fermi surface). Thus, $ev_xE_x + T\frac{\partial}{\partial T}\left(\frac{\epsilon_k-\zeta(T)}{T}\right)v_x\frac{\partial T}{\partial x} = \frac{\varphi_k}{\tau}$ .

Since only $f_1$, the non-equilibrium part of the distribution function, contributes to transport properties, the current $j_x = nev_x \rightarrow \frac{-2e}{(2\pi)^3}\int \varphi_k v_k^x \frac{\partial f_0}{\partial \epsilon_k} d^3k$ .
We then use the Boltzmann equation to write $\varphi_k$ explicitly, and if for one-dimensional isotropic situations we define a set of integrals $K^{(n)} = \frac{1}{12\pi^3}\int \tau(k)v_k^2 \frac{\partial f_0}{\partial \epsilon_k}(\epsilon_k-\zeta)^{n-1} d^3k$ , one then gets $j = eK^{(1)}\left[eE - T\frac{\partial}{\partial T}\left(\frac{\zeta}{T}\right)\frac{\partial T}{\partial x}\right] - eK^{(2)}\frac{1}{T}\frac{\partial T}{\partial x}$ (Eq. 1).

The electrical conductivity $\sigma$ is defined in the absence of a temperature gradient by $\vec{j} = \sigma\vec{E}$ .

Eq. 1 with $\frac{\partial T}{\partial x}=0$ thus gives $\sigma = e^2 K^{(1)}$ .

We now consider a situation with a temperature gradient but no external field, such as is shown in Fig. 1a.[4] In this situation a current results, which we can associate with an internal field $E' = \frac{j}{\sigma} = \frac{j}{e^2 K^{(1)}} = -\frac{1}{e}\left[\frac{\partial \zeta}{\partial T} + \frac{1}{T}\left(\frac{K^{(2)}}{K^{(1)}} - \zeta\right)\right]\frac{\partial T}{\partial x}$ The thermal EMF is then $\mathcal{E} = \oint \vec{E}' \cdot d\vec{l}$ . Since the chemical potential does not change in going from one metal to the other, $\oint \frac{d\zeta}{dx}\,dx = 0$ and $\mathcal{E} = -\frac{1}{e}\oint \frac{1}{T}\left(\frac{K^{(1)}}{K^{(1)}} - \zeta\right)\frac{\partial T}{\partial x}\,dx$

$$= -\frac{1}{e}\int_{T}^{T+\Delta T}\frac{1}{T}\left(\frac{K^{(2)}}{K^{(1)}}\right)_1 dT - \frac{1}{e}\int_{T+\Delta T}^{T}\frac{1}{T}\left(\frac{K^{(2)}}{K^{(1)}}\right)_2 dT$$

Hence, the relative thermopower is given by

$$S_{12} = \frac{d\mathcal{E}}{dT} = \frac{1}{eT}\left(\frac{K^{(2)}}{K^{(1)}}\right)_1 - \frac{1}{eT}\left(\frac{K^{(2)}}{K^{(1)}}\right)_2 \equiv S_1 - S_2$$

and the absolute thermopower is $S = \frac{1}{eT}\frac{K^{(2)}}{K^{(1)}}$ .

The same result for S can also be obtained from Eq. 1 if one defines S by $S = \left(\frac{E}{dT/dx}\right)_{j_x=0} - \frac{1}{e}\frac{d\zeta}{dT}$ .[4] Another alternative defining expression for S is

$$S = \frac{1}{eT}\int(\epsilon-\zeta)\sigma(\epsilon)\frac{\partial f_0}{\partial \epsilon}\,d\epsilon \Big/ \int \sigma(\epsilon)\frac{\partial f_0}{\partial \epsilon}\,d\epsilon ,$$

where $\sigma(\epsilon)$ is defined by $\sigma = \int \sigma(\epsilon)\frac{\partial f_0}{\partial \epsilon}\,d\epsilon$ . This expression corresponds to the relationship $\pi = T \cdot S$ between S and the Peltier heat $\pi$ , since $\epsilon - \zeta$ is the internal energy minus the free energy of an electron, hence its "heat".[8]

We shall consider briefly some implications of these expressions, In particular, using the fact that $\sigma = e^2 K^{(1)}$ we note that $S = \frac{1}{eT}\frac{K^{(2)}}{K^{(1)}} = \frac{\pi^2 k_B^2 T}{3e}\left[\frac{\partial \ln \sigma(\epsilon)}{\partial \epsilon}\right]_{\epsilon=\zeta}$

Writing out $K^{(1)}$ explicitly, we get

$$\sigma = \frac{e^2}{12\pi^3}\int \tau(k) v_k^2 \left(\frac{-\partial f_0}{\partial \epsilon_k}\right) d^3k = \frac{e^2}{12\pi^3}\iint \tau(k) v_k^2 \left(\frac{-\partial f_0}{\partial \epsilon_k}\right)\frac{dS}{\hbar v_k}\,d\epsilon = \frac{e^2}{12\pi^3}\frac{\tau}{\hbar}\int v_k\,dS_F = \frac{e^2\lambda}{12\pi^3}\frac{S_F}{\hbar}.$$

Here $-\frac{\partial f_0}{\partial \epsilon_k}$ acts like $\delta(\epsilon-\epsilon_F)$ in reducing the integral over

volumes $dSd\epsilon$ in energy-space to an integral over the Fermi surface[8], and $\lambda = v_k \tau$ is the electron mean free path. With this expression for $\sigma$, one obtains $S = \frac{\pi^2 k_B^2 T}{3e} \left[ \frac{\partial \ln \lambda}{\partial \epsilon} + \frac{\partial \ln S_F}{\partial \epsilon} \right]$. One expects $\lambda$ to increase with energy, since higher energy particles are less easily scattered; thus $\frac{\partial \ln \lambda}{\partial \epsilon}$ should be positive, and since $e$ is negative, the first term in the expressions for S above should be negative as one ordinarily expects for metals.

However, the area $S_F$ of the Fermi surface increases until the Fermi surface touches the Brillouin zone boundary, then decreases for further increases in $\epsilon$. When the Brillouin zone is nearly full, then, one gets a positive contribution to S and, in fact, S itself can be positive. This is reasonable in view of the fact that as one approaches the zone boundary, the dynamical mass of the electrons becomes negative, and one is dealing with holes. In any event, it is clear that the thermoelectric power can be sensitive to change in the Fermi surface.

In transition metals, the $\frac{\partial \ln \lambda}{\partial \epsilon}$ term becomes important. Here the high resistivities observed are considered to be due to the scattering of s-electrons into the high density states in the d-band[9], so that $\lambda \sim \frac{1}{N_d(\epsilon)}$ and one gets a term $-\frac{\pi^2 k_B^2 T}{3e} \frac{\partial \ln N_d(\epsilon)}{\partial \epsilon}$ in the thermopower. This term will be considered further in Section V.

In many situations the thermoelectric power is

calculated from $S = \frac{1}{eT}\frac{K^{(2)}}{K^{(1)}}$, where $K^{(2)}$ and $K^{(1)}$ are written explicitly in terms of the relaxation time for the system of interest. (This is done, for example, to obtain the Kondo thermopower -- See Section V.) It should be noted from the form of the $K^{(n)}$ that since $-\frac{\partial f_o}{\partial \epsilon}$ is only non-zero in the vicinity of the Fermi surface, the thermopower is sensitive to the behavior of the relaxation time $\tau(\epsilon)$ in this vicinity. In particular $K^{(1)}$ will be large and $K^{(2)}$ small if $\tau(\epsilon)$ is an even function with respect to the Fermi energy, and alternatively $K^{(2)}$ will be large and $K^{(1)}$ small if $\tau(\epsilon)$ is odd. (This point is elaborated on by Bailyn[10] and Huebener[5]). If $\tau(\epsilon)$ is odd, one would expect a significant contribution to the resistivity since $\rho \sim \frac{1}{\sigma} \sim \frac{1}{K^{(1)}}$, but a more pronounced contribution to the thermopower is expected since $S \sim \frac{K^{(2)}}{K^{(1)}}$, and while $K^{(1)}$ is diminished, $K^{(2)}$ is enhanced.

C. Phonon Drag and Other Drag Effects

We next take into account the fact that a temperature gradient will result in a non-equilibrium phonon distribution, i.e. a flow of lattice energy from the hot end of a sample to the cold end. "Momentum" (actually $\hbar\vec{k}$, rather than a true momentum) must be lost by the phonons going from the hot end to the cold end, or the thermal conductivity would be infinite. At sufficiently low temperatures in nearly perfect metals, this "momentum" is transferred to the conduction electrons by means of

electron-phonon collisions, and the electrons in effect get dragged along by the phonons. This process is known as "phonon drag". Its contribution to the thermoelectric power can be understood qualitatively in terms of the lattice specific heat. The change in lattice energy occurs spatially as one goes from the hot end to the cold. If all this energy is transferred to the conduction electrons, the energy gained per $^{\circ}K$ per unit conduction charge (which is how we interpreted $\mu$) will be $\frac{C_g}{ne}$, where $C_g$ is the lattice specific heat and $n$ the density of conduction electrons. S, as noted previously, will have the same T-dependence as $\mu$. If other processes compete with electron-phonon collisions as mechanisms for the loss of lattice energy, we must multiply $\frac{C_g}{ne}$ by a factor $\alpha$ ($0 \leq \alpha \leq 1$), the relative probability of a phonon colliding with a conduction electron as compared with all other things the phonon might collide with. Thus one gets $S_g \approx \frac{C_g}{ne}\alpha$.

At sufficiently low temperatures the total phonon "momentum" is unaffected by phonon-phonon collisions. "Normal" collisions only redistribute the energy flow among the phonons, so that in a perfect metal, collisions with conduction electrons are the only mechanism by which lattice energy is dissipated. At temperatures small compared with the Debye temperature $\vartheta_D$, we therefore have $\alpha \approx 1$. At these temperatures $C_g \sim T^3$ and therefore the phonon-drag thermopower $S_g \sim T^3$.

At temperatures larger than $\Theta_D$, umklapp collisions, in which lattice momentum is not conserved, are common, and phonon-phonon collisions become a viable energy-dissipating mechanism. The phonon-phonon mean free path $\lambda_{pp} \sim \frac{1}{T}$ at these temperatures[4], so that the phonon-phonon collision probability increase linearly with T, and $\alpha \sim \frac{1}{T}$. is roughly temperature-independent at high temperatures, so that $S_g \sim \frac{1}{T}$ for $T \gtrsim \Theta_D$. For ideal pure metals, then, one expects the total thermoelectric power to behave as shown in Fig. 2, i.e. S is the sum of a phonon drag contribution, which peaks at about 1/5 $\Theta_D$, and an electron diffusion term linear in T.

If the predominant electron-phonon collisions are umklapp rather than normal processes (as may happen, for example, when the Fermi surface is very close to the Brillouin zone boundary[5,11]) the change in electron momentum will be opposite in direction to the heat flow and the phonon-drag peak will be positive rather than negative.

In metals with impurities (including dilute alloys and metals with lattice defects), the impurities act as an alternate scattering mechanism to the conduction electrons for reducing the total phonon "momentum". $\alpha$ therefore decreases with increasing impurity concentration, and for more than a few atomic percent of the impurity, the phonon drag peak will ordinarily be completely suppressed.

Drag peaks due to excitations other than phonons may be understood analogously to phonon drag. For instance, magnon drag[12] will have the same T-dependence as the specific heat of the magnon or spin-wave system, i.e. it will vary as $T^{3/2}$[5]. In Section IV we will consider a similar picture with regard to the possible existence of a paramagnon drag effect.

D. Multiple Contributions to the Diffusion Thermoelectric Power

Although the electron diffusion and drag terms are directly additive, if there are two or more contributions to the diffusion thermoelectric power, the total diffusion power is not ordinarily the simple sum of these.

If, for example, one considers thermoelectric power due to two (or more) conduction bands, one treats these bands as conductors in parallel. If parallel conductors 1 and 2 have electrical conductivities $\sigma_1$ and $\sigma_2$ and heat current densities $U_1$ and $U_2$ respectively, their respective Peltier coefficients are $\pi_1 = \frac{U_1}{\sigma_1 E}$ and $\pi_2 = \frac{U_1}{\sigma_2 E}$. Since for parallel circuits in general, the heat currents and conductances add directly, and since for parallel bands within the same metal the physical dimensions are the same for the individual bands as for the total circuit, it follows that for parallel bands the heat current densities and electrical conductivities add directly, i.e. $U = U_1 + U_2$ and $\sigma = \sigma_1 + \sigma_2$. Thus the Peltier coefficient for the total circuit is given

by $\pi = \frac{U}{\sigma E} = \frac{U_1 + U_2}{\sigma E} = \frac{\pi_1 \sigma_1 + \pi_2 \sigma_2}{\sigma}$.

Since $\pi = TS$, $S = \frac{\sigma_1 S_1 + \sigma_2 S_2}{\sigma}$ for two conduction bands, and for n conduction bands $S = \sum_{j=1}^{n} \sigma_j S_j / \sigma$, where $\sigma = \sum_{j=1}^{n} \sigma_j$.[5]

If one considers a single conduction band but two independent scattering mechanisms (such as phonons and impurities, or the two components of a binary alloy), one may consider the total temperature difference $\Delta T$ across the conduction band to be the sum of two contributions $\Delta T_1$ and $\Delta T_2$ sustained by the thermal resistivities $W_1$ and $W_2$ respectively, of the two scattering mechanisms, just as if the mechanisms were two conductors in series. The size of each contribution is proportional to the thermal resistivity associated with it. Hence, $\Delta T = \Delta T_1 + \Delta T_2$, where $\Delta T_1 = \frac{W_1 \Delta T}{W_1 + W_2}$ and $\Delta T_2 = \frac{W_2 \Delta T}{W_1 + W_2}$. For a series circuit $\Delta V$ (where $\Delta V = S \Delta T$), the thermovoltage produced by $\Delta T$, must equal the sum of the thermovoltages $\Delta V_1$ and $\Delta V_2$ across the two circuit components. Specifically, $\Delta V_1 = S_1 \Delta T_1$, and $\Delta V_2 = S_2 \Delta T_2$. Thus $S \Delta T = S_1 \Delta T_1 + S_2 \Delta T_2$ $= \frac{W_1 S_1 \Delta T}{W_1 + W_2} + \frac{W_2 S_2 \Delta T}{W_1 + W_2}$, or $S = \frac{W_1 S_1}{W_1 + W_2} + \frac{W_2 S_2}{W_1 + W_2}$.[5] For more than two scattering mechanisms, $S = \sum_i W_i S_i / \sum_i W_i$. In situations where the Lorentz number is constant, this becomes $S = \frac{\sum_i \rho_i S_i}{\sum_i \rho_i}$, where the $\rho_i$ are the electrical resistivities associated with the several mechanisms.

Further considerations of thermoelectric power are deferred to subsequent sections of this work, where

their introduction seems more appropriate.

## III. OUTLINE OF EXPERIMENTAL PROCEDURE

Thermoelectric powers for all alloys studied were measured as a function of temperature between 4.2 K and 300 K. To measure thermoelectric power, a heater is placed at the free-standing end of a rod-shaped sample which is anchored at the other end to a heat sink. The heater is used to impose a small temperature difference $\Delta T$ (0.1-0.2 K) across the sample. $\Delta T$ is measured by a differential thermocouple, the junctions of which are anchored at the two ends of the sample. The voltage across the sample, $\Delta V$, is measured directly by a nanovoltmeter, thus enabling us to calculate the thermoelectric power S, given by $S = \Delta V / \Delta T$.

The ambient temperature is achieved by using the following arrangement. The heat sink is a copper block in direct thermal contact with a large reservoir of activated charcoal. The charcoal is immersed in liquid helium, and the liquid helium is then boiled off. The temperature of the charcoal, which has adsorbed a good deal of helium, then rises very slowly because of the large heat of adsorption, and quasi-steady state conditions suitable for measuring S are achieved. The ambient temperature is measured by a thermocouple with one junction anchored to the heat sink and the other immersed in an ice-water bath. Cu-constantan thermocouples are used throughout.

The error in our thermoelectric power measurements is estimated to be no more than 2-3% for most of the temperature range considered. The principal sources of error were thermovoltages arising in the leads, and possible discrepancies between (a)$\Delta T$ between the two points at which the differential thermocouple junctions make contact (the measured $\Delta T$) and (b) $\Delta T$ between the two points at which the voltage leads make contact (the $\Delta T$ actually producing the measured thermovoltage. $\Delta V$).

For the details of the experimental procedure, see Appendix A.

## IV. DILUTE MAGNETIC ALLOYS

### A. The Dilute Impurity Problem: Background

The problem of understanding the electronic structure associated with magnetic impurity atoms in dilute magnetic metal alloys, and the local magnetic moments which often arise from such structure, has been considered quite extensively in recent years. The phenomena associated with these moments fall loosely into two categories -- local effects, which are studied primarily by various types of magnetic measurements, and modifications in properties of the electron gas away from the impurity site, as manifested in the transport properties. The problem has been treated in depth both theoretically and experimentally in several reviews[10, 13-19], so that most of the theory will simply be outlined here, with amplification of those aspects which bear directly on the present work.

A dilute alloy is considered to be one in which the effect of impurity-impurity interactions is negligible, so that calculations can be done for a single impurity and results for n impurities are obtained by superposition.

A useful concept in the understanding of local moment formation is that of the "virtual bound state", as developed by Friedel[20-22]. When one of an impurity's outer atomic orbitals (d-states in transition metals) falls within the conduction band of the host, the d-state will resonate with conduction electron states of like

energy, and the correct electron states will be linear combinations of the d- and conductive states. The result is a state which is strongly d-like, occupying a small spread of energies about the original resonant energy, and localized in space about the impurity rather than truly bound like the core states -- hence a "virtual bound state".

In the formal treatment, for simplicity, the perturbing potential of the impurity is regarded as spherical, and the wave functions of the alloy can be analyzed in spherical harmonics, with the states of quantum number $\ell$ undergoing a phase shift $\eta_\ell$. This results in a Lorentzian broadening of the density of states about the resonant energy, which can be regarded as a virtual bound state of energy $E_0$ and width $\Delta$.

Friedel's calculation subjects the phase shifts $\eta_\ell$ to a condition of local electrical neutrality, i.e. a net screening charge must arise from the conduction electrons equal in magnitude to the excess charge of the impurity relative to the host. This condition is expressed formally as the Friedel sum rule, $Z = \frac{1}{\pi} \sum_\sigma \sum_\ell (2\ell+1)\, \eta_{\ell\sigma}(E_F)$, where Z is the excess charge, and the phase shifts $\eta_{\ell\sigma}$ are evaluated at the Fermi energy.

Friedel noted that the distributions of spin-up and spin-down electrons would be separated in energy because of Hund's rule and the Coulomb repulsion acting between

electrons of opposite spin. If the virtual bound state is sufficiently narrow, the number of spin-up levels will exceed the number of spin-down levels for energies below $E_F$. The $d^{10}$ level is thus split into two $d^5$ levels. Using the Friedel sum rule to estimate occupation numbers for spin-up and spin-down levels, Blandin and Friedel[21] constructed a table predicting whether a local moment would occur in various alloys.

Anderson[23] treated these ideas qualitatively by means of a self-consistent Hartree-Fock calculation. He began with a Hamiltonian of the form

$$H = H_{of} + H_{od} + H_{corr} + H_{sd} = \sum_{k,\sigma} \epsilon_k n_{k\sigma} + \sum_{\sigma} E n_{d\sigma} + U n_{d\uparrow} n_{d\downarrow} + \sum_{k,\sigma} V_{dk} (c^*_{k\sigma} c_{d\sigma} + c^*_{d\sigma} c_{k\sigma})$$

The first two terms are the unperturbed energies of the free electrons and the impurity d-state, the third term represents the repulsive Coulomb exchange interaction between d-electrons of opposite spin, and $H_{sd}$ is an exchange term between the conduction s-states and the impurity d-states, which accounts for the broadening of the virtual bound state. $n_\alpha = c^*_\alpha c_\alpha$ is the number operator for a state $\alpha$, where $c^*_\alpha$ and $c_\alpha$ are the creation and annihilation operators for that state.

The problem is then solved self-consistently by letting $U n_{d\uparrow} n_{d\downarrow} \rightarrow U\langle n_{d\uparrow}\rangle n_{d\downarrow} + U\langle n_{d\downarrow}\rangle n_{d\uparrow} - U\langle n_{d\uparrow}\rangle\langle n_{d\downarrow}\rangle$ so that the Hamiltonian is now given in terms of average interaction strengths $\langle n_{d\sigma}\rangle$ and one-body operators. One then gets $H_{od} + H_{corr} = E_\uparrow n_{d\uparrow} + E_\downarrow n_{d\downarrow}$ - constant term, where $E_{\uparrow\downarrow} = E + U\langle n_{d\uparrow\downarrow}\rangle$.

From here Anderson gets Lorentzian densities of states $A_{\uparrow\downarrow}(E) = \frac{\Delta/\pi}{(E-E_{\uparrow\downarrow})^2+\Delta^2}$, where the level width $\Delta = \pi(V_{dk})^2\rho(E)$ is obtained by the golden rule. The result is that the centers of the virtual levels for spin up and spin down have been shifted, and not necessarily by the same amount, so that the average occupancies $\langle n_{d\uparrow\downarrow}\rangle = \int A_{\uparrow\downarrow}(E)\,dE$ may also differ. Through further calculation, Anderson arrives at the criterion $\frac{U}{\pi\Delta} > 1$ for magnetism.

A commonly presented[13,21,24,25] heuristic argument for this criterion is as follows. If virtual bound states for up and down spins, initially with equal occupation number n, are split, there will be a splitting energy $\Delta E$ and a moment will be formed by the transferral of $\delta n$ electrons from spin down to spin up. This represents an increase $\Delta K.E. = \delta n\,\Delta E$ in the kinetic energy of the system. The corresponding change in potential energy will be $\Delta P.E. = U\langle n+\delta n\rangle\langle n-\delta n\rangle - U\langle n\rangle^2 = -U(\delta n)^2$ The moment will be stable if the energy of the system is decreased by moment formation, i.e. if $\Delta K.E. + \Delta P.E. < 0$. Now $\Delta K.E. + \Delta P.E. = \delta n[\Delta E - U\delta n]$, or, since in the Anderson model $\delta n = A(E_F)\Delta E$, the change in energy is $\Delta E(1 - UA(E_F))$, so that the criterion for moment formation is $UA(E_F) > 1$. Since we see from the criterion of $A_{\uparrow\downarrow}(E)$ that the maximum value of $A(E_F)$ is $1/\pi\Delta$, one then gets $\frac{U}{\pi\Delta} > 1$ as the condition for magnetism.

A similar criterion is obtained by Friedel[21] by

relating $\delta_n$ to a splitting of the $\ell = 2$ (d-band) term in Z. The contribution for $\ell \neq 2$ are small. We note from the condition for magnetism that the likelihood of moment formation varies inversely with the width of the virtual bound state. The s and p bands are too broad to allow moment formation, but the d band is narrow and thus conducive to such formation.

Kondo[26] took a different approach to the dilute impurity problem. Rather than explain the formation of local moments, he <u>assumed</u> the existence of a local moment at the impurity site, assigned to it a spin $\vec{S}$, and considered the effect on physical properties of an interaction of the form $-J\Omega \sum_i \vec{S}\cdot\vec{s}_i\, \delta(\vec{r}-\vec{r}_i)$, where J is the exchange integral, $\Omega$ is an atomic volume, and the $\vec{s}_i$ are the conduction electron spins. By applying a second Born approximation to this Hamiltonian, Kondo was able to explain the existence of the low-temperature resistivity minimum which is one of the most notable features of local magnetic moment systems.

Schrieffer and Wolff[27] used a canonical transformation to relate the Anderson and Kondo models, and found them to be equivalent, i.e. they gave the same interaction matrices in the limit of small s-d mixing, which is the optimum condition for local moment formation. Noting that the exchange integral is of interest only near the Fermi surface, they obtained the result $J_{k_F k_F} = J_o = 2|V_{k_F d}|^2 \frac{U}{\epsilon_d(\epsilon_d+U)}$.

If a local moment exists, $\epsilon_d < 0$ and $\epsilon_d + U > 0$ , and so $J_o$ is negative. More recently, Schotte[28] included zero- and two-particle states, and obtained a J for the Kondo model equal to half the value predicted by the Schrieffer-Wolff transformation. Difference in other parameters as well led Schotte to conclude "that the Kondo and the Anderson model are not that intimately connected."

The Kondo calculation treats the scattering amplitude $T = \langle f | -JS_z s_{iz} | i \rangle$ between initial states $|i\rangle = |k\uparrow, d\downarrow\rangle$ and the final states $|f\rangle = |k'\uparrow, d\downarrow\rangle$. The first order Born approximation gives a value $T^{(1)} = \frac{J}{4}$, and does not account for any of the interesting temperature dependence of the resistivity. The second order Born approximation gives a contribution $T^{(2)}$ containing terms from three second order processes:

(1) $k\uparrow$ goes to $k'\uparrow$ via $k''\uparrow$

(2) the exchange of (1)

(3) $k\uparrow$ goes to $k'\uparrow$ via $k''\downarrow$ . In the intermediate state, the impurity is also spin-flipped to conserve angular momentum.

In the exchange of (3), the impurity must first interact with an electron in state $k''\downarrow$ and have its spin flipped up. This does not conserve angular momentum, and therefore cannot occur. Calculating the three second order terms and summing these and the first order term gives

a scattering amplitude $T_{total} = \frac{J}{4}\left(1 + J \ln \frac{k_B T}{D}\right)$ where D is the conduction band width. The resistivity varies as $\frac{1}{\tau}$, which by the golden rule varies as $T^2_{total}$. Kondo's result for the total resistivity, including the standard phonon term (first term below) and a term due to potential scattering from the impurity (second term below) is (keeping ln terms to first order)

$$\rho = aT^5 + c\rho_A + c\rho_M\left[1 + 4JN \ln\left(\frac{k_B T}{D}\right)\right]$$

where N is the density of states per atom of the crystal at the Fermi surface and c is the impurity concentration. When J is negative (which is the prediction of the Anderson model for a magnetic state), a minimum occurs in the resistivity. Moreover, when $J < 0$, setting

gives for the temperature at which the minimum occurs $T_{min} = \left(\frac{4|J|N\rho_M}{5a}\right)^{1/5} c^{1/5}$. This $c^{1/5}$ law had previously been known from experiments.

The main difficulty with the Kondo treatment is that for sufficiently small T, the second Born term is larger than the first. Hence, the Born series may diverge, and as is perhaps more evident, the resistivity diverges logarithmically as $T \to 0$. The divergence is considered to occur below a characteristic "Kondo temperature" $T_K$, usually defined by $kT_K = D e^{-\frac{1}{|J|N}}$ in accordance with Abrikosov.[29]

The breakdown in perturbation theory below a characteristic temperature suggested to Nagaoka[30] an analogy

to the case of superconductivity, where perturbation theory breaks down below the critical temperature, and correlations between electrons must be considered, giving rise to a bound state (Cooper Pairs).[31] Nagaoka treated the correlation between localized spin and conduction-electron spin using retarded double-time Green's functions, and showed the existence below $T_K$ of a quasi-bound state near the Fermi surface in which the nearby conduction electron spins are antiferromagnetically coupled to the impurity spin and effectively screen it. This quasi-bound state seems to form gradually over a range of temperatures in the vicinity of $T_K$. Above this range, Nagaoka confirmed the ln T resistivity behavior calculated by Kondo. Below this range he calculated a resistivity behavior of the form $\rho = \rho_0 \left[1 + \frac{\pi^2}{3}\left(\frac{T}{T_K}\right)^2\right]^{-1}$ which for $T \ll T_K$ becomes $\rho \approx \rho_0 \left[1 - \frac{\pi^2}{3}\left(\frac{T}{T_K}\right)^2\right]$ and reduces to a constant $T \to 0$.

Other models, based on many-body perturbation theory[29] or dispersion theory[32,33] have been shown to be closely related to that of Nagaoka[34,35]. Many authors, though not all, still consider the spin-compensated picture to be a valid one.[36]

In certain situations, the single electron picture proved unsatisfactory. Theoretically the Hartree-Fock approximation predicted the existence of a local magnetic moment for $\frac{U}{\pi\Delta} > 1$. But it is precisely in this region that the Hartree-Fock theory breaks down, since, as Schrieffer[37]

points out, if $U > \pi\Delta$ "the interaction time $\tau_U = \frac{\hbar}{U}$ is less than the time $\tau_\Delta = \frac{\hbar}{\Delta}$ required for electrons to hop on or off the impurity into the conduction band." Physically, the failure comes about when an electron on the impurity interacts sufficiently strongly with nearby electrons that one can no longer regard the electron on the impurity as seeing an average potential through interaction with all the electrons, as Hartree-Fock theory assumes. It then becomes necessary to treat the situation as a true many body problem.

Experimentally, as well, it was found that despite the considerable success of the scheme used by Blandin and Friedel[21] in predicting whether or not a localized moment would occur in a given alloy, evidence of local moments was found in the resistivity behavior of certain alloys where none was predicted by a straightforward application of the Friedel virtual-bound-state viewpoint. Caplin and Rizzuto[38,39] observed a weak low temperature resistance minimum (a characteristic feature of a magnetic impurity) in Zn-Fe, Al-Mn, and Al-Cr, which in Al-Mn, at least, was sufficiently pronounced to indicate a negative $T^2$ temperature dependence of the impurity resistance at very low temperatures. They suggested that local spin fluctuations were responsible for the behavior.

Similar resistivity behavior, but with a positive $T^2$ term, was observed by other experimentalists in Pd-Ni,

Ir-Fe, and Rh-Fe. The behavior of these systems has since been explained in terms of local spin fluctuations.

B. Local Spin Fluctuations

The theory of local spin fluctuations is a many-body theory which treats specifically the strong local interactions responsible for the breakdown of Hartree-Fock theory when $\frac{U}{\pi\Delta} > 1$.

Just as one finds that appreciable short range order is retained in a ferromagnet above its Curie temperature $T_C$, as was evidenced by early neutron scattering experiments,[40] one might reasonably expect similar short-range spin order in what Schrieffer[41] calls "incipient ferromagnets", i.e. systems which have greatly enhanced susceptibilities. In these systems the magnetic susceptibility may be given by $\chi = \chi_p [1 - UN(0)]^{-1}$ where $\chi_p$ is the Pauli free-electron susceptibility, and $[1-UN(0)]$ is the so-called Stoner exchange enhancement factor, in which N(0) is the density of states at the Fermi surface and U is the same repulsive Coulomb electron-electron interaction that enters into the Anderson Hamiltonian. Since the spin-spin correlation time increases as one approaches ferromagnetism in either of the two situations described above, the dynamic susceptibility $\chi(\vec{r},\omega)$ in incipient ferromagnets depends predominantly on small $\omega$ (i.e. $\omega \sim \frac{1}{\tau}$ and is small compared to $E_F$). One therefore expects long-wavelength, low frequency intrinsic fluctuations in the spin density to

play an important role in determining the properties of such systems.[41] These intrinsic fluctuations arise because even as $T \rightarrow 0$ the ground state of the local cell interacts at least residually with the conduction electrons through direct Coulomb and exchange interactions and also via residual crystal fields and residual spin-orbit coupling.[42] Lederer and Mills[1] argued that if one adds a small amount of magnetic impurity to such a system (e.g. if Ni is added to a Pd matrix) the spatial homogeneity of the Coulomb exchange field greatly enhances the intrinsic spin fluctuations locally and in effect produces local spin-density fluctuations in the vicinity of the impurity cell with amplitude large compared to that of the host metal. In this picture one may also regard the local spin fluctuations as critically damped spin waves.[43]

Theoretically, Lederer and Mills treat their model of locally enhanced spin-fluctuations as an extension of the Stoner exchange enhancement idea. In the Stoner theory for exchange-enhanced pure metals, one considers the response of the electrons to a spatially uniform static magnetic field. A Hartree-Fock calculation taking into account the Coulomb exchange interaction then gives rise to the Stoner exchange-enhancement factor mentioned earlier. The paramagnon theory considers the response of the pure matrix to an applied magnetic field

that varies in space and time. Then, invoking the fluctuation-dissipation theorem, the dynamic sysceptibility (defined below) which is thus developed is used to obtain the amplitude of the spin-density fluctuations in the alloy, which do not require an externally applied field.

More specifically, Lederer and Mills begin with a Hamiltonian for the electrons of the form

$$H = T + (U_0+\Delta U)\sum_i n_{i\uparrow}n_{i\downarrow} + V\sum_\sigma n_{i\sigma} + H_z \ .$$

T is the kinetic energy of the electrons; $U_0$ and $\Delta U$ respectively are the Coulomb interaction potential in the host and the change from the host potential in the impurity cell; V is the deviation from the periodic potential of the lattice, which is largely restricted to the impurity cell; and $n_{i\sigma}(\sigma=\uparrow,\downarrow)$ is the number operator for electrons in the Wannier function centered at the $i$th cell. Finally, $H_z$ is the Zeeman energy due to a field $\vec{h}$ of frequency $\Omega$, and is given by $H_z = -\frac{1}{2}\sum_i (n_{i\uparrow} - n_{i\downarrow}) h_i e^{i\Omega t}$, where $h_i$ is the amplitude of the field in the $i$th cell.

The expectation value of the spin component parallel to the field in cell i is then given by $\langle s_i^z \rangle = \frac{1}{2}\sum_j \chi(i,j,\Omega) h_j$. $\chi(i,j,\Omega)$ is called the dynamic susceptibility and represents the response of conduction electrons in cell i to a field $\vec{h}$ of frequency $\Omega$ applied to cell j.

One now lets $(U_0+\Delta U)\sum_i n_{i\uparrow}n_{i\downarrow} = (U_0+\Delta U)(\sum_i \langle n_{i\uparrow}\rangle n_{i\downarrow} + \sum_i \langle n_{i\downarrow}\rangle n_{i\uparrow})$ where $\langle n_{i\uparrow\downarrow}\rangle = \bar{n}_i \pm \langle s_i^z \rangle e^{i\Omega t}$ in the presence of the external field, and $\bar{n}_i$ is time-independent.

The Hamiltonian can then be re-arranged so that the effective part of the Hamiltonian can be rewritten as $H_{eff} = T + V_{HF}\sum_{I\sigma} n_{I\sigma} + \frac{1}{2} e^{i\Omega t}\sum_i (n_{i\uparrow} - n_{i\downarrow}) h_i^{(eff)}$, where $V_{HF} = V + \Delta U \bar{n}_I$ is the Hartree-Fock approximation to the change in crystal potential produced by the impurity, and

$$h_i^{(eff)} = h_i + 2U_o \langle s_i^z \rangle + 2\Delta U \langle s_i^z \rangle \delta_{i,I}$$

is the effective magnetic field seen by an electron in cell i.

$V_{HF}$ should be quite small in Pd-Ni, since Pd and Ni are isoelectronic. In the approximation that $V_{HF}=0$ (the case for $V_{HF}\neq 0$ has also been treated by Lederer and Mills[1]), the effective Hamiltonian describes the response of a non-interacting electron gas in the pure matrix to the effective field. In this case $\chi(i,j;\Omega) \to \chi_o(i-j;\Omega)$ and $\langle s_i^z \rangle = \frac{1}{2}\sum_j \chi_o h_j^{(eff)} = \frac{1}{2}\sum_j \chi_o(i-j;\Omega) h_j + U_o \sum_j \chi_o(i-j;\Omega)\langle s_j^z \rangle + \Delta U \chi_o(i-I)\langle s_I^z \rangle$

But $\langle s_i^z \rangle = \frac{1}{2}\sum_j \chi(i,j,\Omega) h_j$ . Equating the two expressions for $\langle s_i^z \rangle$ and solving for $\chi(i,j,\Omega)$ , [1] Lederer and Mills arrive at the result that

$$\chi(i,j;\Omega) = \tilde{\chi}(i-j;\Omega) + \Delta U \frac{\tilde{\chi}(i-I;\Omega)\tilde{\chi}(I-j;\Omega)}{1 - \Delta U \bar{\chi}(\Omega)}$$

which may be understood in terms of the following definitions:

$$\chi_o(\vec{q},\Omega) \equiv N^{-1}\sum_i e^{i\vec{q}\cdot\vec{x}} \chi_o(i,\Omega)$$

$$\tilde{\chi}(\vec{q},\Omega) \equiv \frac{\chi_o(\vec{q},\Omega)}{1 - U_o \chi_o(q,\omega)}$$

$$\tilde{\chi}(i-j;\Omega) \equiv N^{-1}\sum_{\vec{q}} e^{-i\vec{q}\cdot(\vec{x}_i - \vec{x}_j)} \tilde{\chi}(\vec{q},\omega)$$

and $\bar{\chi}(\Omega) \equiv N^{-1}\sum_{\vec{q}} \tilde{\chi}(\vec{q},\Omega) = \tilde{\chi}(i-j;\Omega)|_{i=j}$

The expression for $\tilde{\chi}(\vec{q},\omega)$ has also been obtained from the random phase approximation (RPA) of many-body theory[45] and is central to the arguments of Berk and

Schrieffer[46] and Doniach and Engelsberg[43] for enhanced spin fluctuations in Pd. In the static long wavelength limit, $\tilde{\chi}(0,0) = \chi_p [1 - UN(0)]^{-1}$ -- again the Stoner expression. As Mills et al[44] point out, introducing the effective field to obtain $\chi(i,j;\Omega)$ is equivalent to RPA.

The physical significance of the result is as follows. In the static limit, where $\bar{\chi}(\Omega) = \bar{\chi}(0) \equiv \chi_s$, etc., the result for $\chi(i,j;\Omega)$ gives $\langle S_i^z \rangle = \frac{1}{2} h_0 \tilde{\chi}_s (1 + \alpha \Delta U \tilde{\chi}_s (i-I))$, where $\alpha = (1 - \Delta U \bar{\chi}_s)^{-1}$ and is called the local exchange enhancement factor. Far from the impurity $\tilde{\chi}_s (i-I) \to 0$ and $\langle S_i^z \rangle = \frac{1}{2} h_0 \tilde{\chi}_s$, the value for the pure metal. At the impurity $\langle S_I^z \rangle = \frac{1}{2} h_0 \tilde{\chi}_s \alpha$ and is enhanced.

If one defines a correlation function $S_{ij}(\Omega) = \int_{-\infty}^{+\infty} \frac{dt}{2\pi} e^{i\Omega t} \langle S_i^z(0) S_j^z(t) \rangle$, then $S_{ii}(\Omega)$ is the spectral density and is a measure of the amplitude of a spin fluctuation of frequency at the $i$th cell. The fluctuation-dissipation theorem then says that $S_{ij}(\Omega) = \frac{1}{2\pi i} n(\Omega) \, \mathrm{Im}\, \chi(i-j;\Omega)$ where $n(\Omega) = \frac{1}{e^{\hbar\Omega/k_B T} - 1}$ is the Bose-Einstein factor (magnons and paramagnons are bosons). If one takes $\mathrm{Im}\, \tilde{\chi}(\Omega) = i\chi'(\Omega)$ for small $\Omega$, one can calculate that far from the impurity $S_{ii}(\Omega) = \frac{\bar{\chi}'}{2\pi} n(\Omega) \, \Omega$ for small $\Omega$, and at the impurity $S_{II}(\Omega) = \frac{n(\Omega)}{2\pi} \frac{\chi'(\Omega)}{\alpha^{-2} + (\Delta U \bar{\chi}')^2 \Omega^2}$, which for small $\Omega$ becomes $S_{II} = \frac{n(\Omega)}{2\pi} \alpha^2 \chi' \Omega$. Hence the spin-fluctuation amplitude is enhanced by a factor $\alpha^2$ at the impurity site.

$S_{II}$ peaks at the frequency $\Omega_S = (\Delta U \tilde{\chi}' \alpha)^{-1}$ , from which one can obtain a characteristic spin fluctuation lifetime $\tau_S = \frac{2\pi}{\Omega_S}$ , or a spin fluctuation temperature $T_S$ defined by $k_B T_S = \hbar \Omega_S$.

The lifetime of the spin fluctuations is of central interest in the question of local moment formation. As one reaches temperatures of order $T_S$ the motion of the axes of local moments (and hence the fluctuations in their field-parallel or z-components) comes to be dominated by thermal fluctuations rather than by intrinsic spin fluctuations[42,3], i.e. one gets thermal fluctuations of frequency $\frac{k_B T}{\hbar} > \Omega_S$ . Above $T_S$, then, the spin-fluctuations are long-lived compared to the thermal fluctuations, and for the duration of a thermal fluctuation one sees a well-defined spin, or Curie paramagnetism. Otherwise stated, if one regards the susceptibility as showing Curie-Weiss-like behavior, $\chi = \frac{N\mu_{eff}^2}{3k(T+\Theta)}$, one gets Curie behavior ( $\chi \sim \frac{1}{T}$ ) when T is large compared to .

A failing of the RPA description of local spin fluctuations is that "starting from the HF criterion for formation of a local moment ($\alpha \to \infty$), all the corrections to the RPA happen to be equally important and to diverge to infinite order."[44] Attempts to renormalize the theory have included the "Renormalized Random Phase Approximation" or RRPA of Suhl and co-workers,[47-49] and the functional integral method of Wang et al.[50] Neither of these approaches has been fully successful. However, the

expression obtained for $\chi(i,j;\Omega)$ from the RPA is a general one, even if the RPA is not itself valid, provided $\tilde{\chi}(i-j;\Omega)$ and $\tilde{\chi}(\Omega)$ are replaced by suitable particle-hole propagators, and the physical results derived from the RPA treatment may have more general validity if $\Omega_S$ is treated as a phenomenological parameter which can differ from the RPA-predicted value.

We next consider the effect of local spin fluctuations on the physical properties of dilute alloys.

(1) Susceptibility: from the expression for $\langle S_i^z \rangle$ obtained by Lederer and Mills, one gets the static susceptibility $\chi_S^{(A)}$ of the alloy, given by

$$\langle S_{tot}^z \rangle = \sum_i \langle S_i^z \rangle = \frac{N}{2} h_0 \chi_S^{(A)} = \frac{N h_0}{2} \left[ \tilde{\chi}_S + \alpha \frac{\Delta U}{N} \tilde{\chi}_S^2 \right];$$

<u>i.e.</u> $\chi_S^{(A)} = \tilde{\chi}_S + \alpha \frac{\Delta U}{N} \tilde{\chi}_S^2$ is the sum of host and impurity contributions. For low impurity concentrations, the impurity susceptibility varies linearly with impurity concentration c, and it follows that $\frac{1}{\chi}\frac{d\chi}{dc} = \Delta U \tilde{\chi}_S \alpha$. Thus for large local enhancement $\alpha$, one gets a large change in $\chi$, which is even greater if the static susceptibility $\tilde{\chi}_S$ of the host is itself large, as it is in Pd. The data of Shaltiel <u>et al</u>[51] suggests that in Pd-Ni $\frac{1}{\chi}\frac{d\chi}{dc} \approx 100$ and $\alpha \approx 20$.

(2) Specific Heat: One also obtains a strong concentration dependence of $\gamma$, the coefficient of the term linear in temperature in the specific heat. A general expression developed by Brinkman <u>et al</u>.[40] re-

lates $\frac{1}{\gamma}\frac{d\gamma}{dc}$ to the concentration-dependent change in susceptibility $\frac{1}{\chi}\frac{d\chi}{dc}$. Qualitative corroboration is provided by experimental data[52] but numerical values are a factor of 3 smaller than predicted. (See also Sec. IV-D.)

(3) Transport Properties: We shall discuss these in greater detail since they are of more direct relevance to the present work.

At very low temperatures a positive impurity contribution to the resistivity of Pd-Ni varying at $T^2$ and strongly dependent on impurity concentration was observed by Schindler and Rice.[53] A good account of this behavior was provided by the calculations of Lederer and Mills. These authors assume that the conduction s-electrons sample the spin-fluctuations in the d-band through an s-d interaction in the form $J\vec{S}\cdot\vec{s}$. From this interaction, an expression is obtained for the relaxation time $\tau$ for spin-flip scattering in terms of a spectral density function $A(\vec{q},\Omega)$, which is essentially a Fourier transform of $S_{ii}$. $A(\vec{q},\Omega)$ is in turn given by

$$A(\vec{q},\Omega) = i\left[\chi_r(\vec{q},\vec{q};\Omega+i\epsilon) - \chi_r(\vec{q},\vec{q},\Omega-i\epsilon)\right]$$

where $\epsilon$ is an infinitesimal positive number and $\chi_r(\vec{q}',\vec{q},\Omega)$ is a Fourier transform of the response function $\chi(i,j;\Omega)$ discussed at length previously. Hence Lederer and Mills proceed from their result for $\chi(i,j;\Omega)$ through a formidable sequence of calculations to obtain $\frac{1}{\tau} = A(\vec{c})T^2$, where $A(\vec{c})$ is given explicitly and is roughly linear in

c at low concentrations. A calculation of gives the very large value of 750, in good agreement with the data of Schindler and Rice.

The resistivity calculations of Lederer and Mills were extended to higher temperatures by Kaiser and Doniach,[2] giving a good account of the resistivities observed in Ir-Fe[54] and Rh-Fe[55] as well as in Pd-Ni. In broad outline, a procedure somewhat like that used by Lederer and Mills is used to obtain a general expression or universal curve for the resistivity: The resistivity is written down in terms of a transition probability $Q(\vec{k}\to\vec{k}')$ for paramagnon absorption, which in turn is given in terms of the spectral density function A. One then gets an expression for $\rho$ of the form

$$\rho = \frac{\rho_0}{k_B T}\int_0^\infty d\omega\, I(\omega)\, n(\omega)\, \bar{A}(\omega)$$

in which $\omega \equiv \epsilon_{k'} - \epsilon_k$, $\rho_0 \left[\frac{JN(\epsilon_F)}{4}\right]^2 \left(\frac{\nu}{n}\right)\frac{m}{ne^2\tau_F}$ ( $\nu$ is the number of atoms per unit volume),

$$I(\omega) = \int_{-\infty}^{+\infty} d\epsilon_k\, f(\epsilon_k)\left[1-f(\epsilon_{k'})\right] = \frac{\omega}{1-e^{-\beta\omega}}$$

gives the overlap of the Fermi-Dirac distribution functions for electrons and holes separated by energy $\omega$, is the Bose distribution function (which characterizes paramagnons), and $\bar{A}(\omega) = \frac{1}{k_F^4}\int_0^{2k_F} dq\, q^3 A_I(q,\omega)\,|F(q)|^2$ is a weighted average over wave vector of the impurity portion of $A(q,\omega)$ ($|F(q)|^2$ is a form factor for the impurity d-orbital). As in the Lederer and Mills calculation, $A_I(q,\omega)$ is obtained using the fluctuation-dissipation relation $A(\vec{q},\omega) = 2\, Im\,\chi(\vec{q},\vec{q},\omega)$, using $\chi(\vec{q},q,\omega)$

as obtained from the RPA.

The central result obtained by Kaiser and Doniach is the expression $\tilde{\rho} = \frac{1}{\tilde{T}} \int_0^\infty d\tilde{\omega} \frac{\tilde{\omega}^2}{(e^{\tilde{\omega}/\tilde{T}} - 1)(1 - e^{-\tilde{\omega}/\tilde{T}})(1 + \tilde{\omega}^2)}$. Here $\tilde{\rho} = \rho \times$ a resistivity scaling factor, $\tilde{\omega} = \omega / k_B T_S$, and $\tilde{T} = \frac{T}{T_S}$, where $T_S$ is also treated as a scaling parameter. In the low and high temperature limits ($T \ll T_S$ and $T \gg T_S$),

$$\tilde{\rho}(T \to 0) = \tilde{T}^2 \int_0^\infty \frac{x^2 dx}{(e^x - 1)(1 - e^{-x})} = \frac{\pi^2}{3} \left(\frac{T}{T_S}\right)^2$$

and $\tilde{\rho}(T \to \infty) = \tilde{T} \int_0^\infty \frac{d\tilde{\omega}}{1 + \tilde{\omega}^2} = \frac{\pi}{2} \frac{T}{T_S}$.

If the scaling parameters are temperature-independent, one obtains the same temperature dependence for $\rho$. This in fact gives the $T^2$-dependence at lowest temperatures, changing gradually to linear dependence on T at about $\frac{1}{4} T_S$, which is observed in Pd-Ni, Ir-Fe, and Rh-Fe.[56] Using the scaling parameters, Kaiser and Doniach obtain a good fit of the data for these systems to their universal curve. The fact that the resistivity starts dropping below linearity in T at sufficiently high temperatures relates to the fact that the scaling factors are not truly temperature-independent but diverge significantly from their zero-temperature values at high temperatures.

Kaiser and Doniach also showed that for $T > T_S$, $\rho \sim T \Delta\chi$, where $\Delta\chi$ is the increase in static susceptibility due to impurities. Hence, at high T there is a decrease in $\Delta\chi$ which corresponds to the deviation of $\rho$ below linearity. Kaiser[57] later did a calculation for the thermal resistivity and Lorentz number of spin-fluctuation systems. No formal calculation for the thermoelectric

power has been published.

A point mentioned earlier should be repeated here, namely, that the physical results derived from the RPA may have more general validity than the RPA itself if $\Omega_S$ is treated as a phenomenological parameter which can differ from the RPA-predicted value. This is precisely what Kaiser and Doniach have done.

An alternate physical picture of how local spin fluctuations arise is given by Rivier et al.[58] One begins with a d-like virtual bound state of width $\Delta$. A conduction electron can hop onto the impurity state where it stays for a time $\Delta^{-1}$. During this time, because of the Coulomb repulsive interaction U between electrons of opposite spin the electron is surrounded primarily by conduction electrons of like spin. Hence, a "fluctuation" in the local magnetic moment density is produced. Although the electron on the impurity site remains for a time $\Delta^{-1}$, memory of its spin is kept for a longer time by the surrounding electrons because of the Coulomb repulsion, and that time may become infinite if U is much greater than $\Delta$, giving rise to a static local moment. In this model, the memory time is taken to be the lifetime of the spin fluctuation. The local spin fluctuation is taken to be "the repeated scattering between an electron and a hole of opposite spin on the impurity site."[3]

Mills et al.[44] point out that the two physical pictures are identical, and differ "only in detail." They yield the same $\Omega_S$ and low temperature susceptibility, and very similar frequencies for the self-energy of the electron on the impurity cell. However a difference arises in the way the resistivity is obtained in the two pictures.

In the case of systems like Al-Mn, as described by Rivier et al, the interaction of the conduction electrons with local spin fluctuations comes about indirectly through s-d mixing, i.e. through the $V_{dk}$ term in the Anderson Hamiltonian. In systems like Pd-Ni , on the other hand, the d-electron contribution to the electrical current is small in a host like Pd, and in the model treated by Lederer and Mills,[59] the s-electrons (which actually have an admixture of s and d character in their wavefunctions) sample the spin-fluctuations in the d-band directly through an s-d exchange interaction $J\vec{S}\cdot\vec{s}$.

Central to this difference is the presence of virtual bound states in systems like Al-Mn. Kaiser and Doniach point out that in such cases, where there is a virtual bound state at the Fermi level, the $\ell=2$ phase shift will be $\frac{\pi}{2}$ at T=0 , and the resistivity, which goes as $\sin^2 \eta_\ell$ [22], will be a maximum. Spin fluctuations at higher temperatures will then have the effect of changing the phase shifts, so that the resistivity will decrease. A negative $T^2$ - to - T

transition in the impurity resistivity similar to the positive effect treated by Kaiser and Doniach, has been calculated theoretically[60] and observed experimentally for Al-Mn.[61]

In 1968, Rivier and Zuckermann argued that in its effect on observable physical properties such as susceptibility or transport coefficients, the local spin fluctuation picture is equivalent to the Kondo-Nagaoka spin-compensated state. This aroused interest among experimentalists in finding a physical property of some system for which the two pictures might predict measurably different results.[62] This in fact was the motivation for our thermoelectric power measurements on Ir-Fe, and more will be said later in this regard.

The Rivier and Zuckermann argument is essentially the following. With increasing temperature a dilute alloy proceeds gradually from a non-magnetic regime to a magnetic regime with marked physical characteristics (resistivity minimum, Curie-law susceptibility behavior, and giant thermopower). This is so whether one associates the gradual change in properties with (1) a break-up of the spin-compensated state over a temperature range characterized by the Kondo-temperature $T_K$, or with (2) an increase in the frequency of thermal fluctuations of local moments with increasing temperature. In the latter case, at temperatures above the order of $\tau_s^{-1}$, the spin

fluctuations are long-lived compared to the thermal fluctuations and "there is no physical difference between a spin fluctuation and a genuine spin." On this basis Rivier and Zuckermann postulate a Kondo temperature obtained from spin fluctuation theory given by $kT_K^{sf} = \gamma_o^{-1}(h=1)$ rather than by Abrikosov's defining relationship $kT_K^A = De^{-\frac{1}{|J|N}}$. They then derive expressions on the basis of spin-fluctuation theory for resistivity, susceptibility, and low temperature thermopower and associate with the behavior of each property p a characteristic temperature $T_K^p$. $T_K^S$ and $T_K^\chi$ (for thermopower and susceptibility respectively) are both roughly equal to $T_K$. $T_K^\rho$ (for resistivity) is about a factor of 3 smaller. In the Kondo-Nagaoka picture as well, characteristic temperatures associated with the thermopower peak and with an extrapolation of $\frac{1}{\chi}$ at higher temperatures to a Curie-Weiss law are both equal or nearly equal to $T_K$.

Recent theoretical approaches to the Kondo problem have demonstrated continued interest in relating the concept of spin fluctuations to the Kondo model.

Many of these approaches have certain features in common. As in the original Kondo treatment, the impurity is assumed to have a spin $\vec{S}$, but now its z-component is not fixed. Rather, the spin orientation is considered to fluctuate and, in particular, can hop between spin-up and spin-down states. This hopping between spin orientations is identified as a general

kind of spin fluctuation.[28]

Feynman path-integral methods are applied, in which the various "paths" are the possible time sequences of events, each with a certain amplitude. Equivalences are obtained between the Kondo problem and certain classical one-dimensional statistical ones. The $J>0$ and $J<0$ regimes are regarded as separated by a phase transition and the Kondo problem, "really a problem of very low J values,"[63] is thus closely related to the critical-point behavior of the equivalent classical system. Numerical treatments give computer results for susceptibility behavior in good agreement with experimental observations. A fuller description of some of these approaches is given in review articles by Anderson and Yuval.[63] Hamann and Schrieffer discuss the application of similar methods to the Anderson model.[64]

Certain conclusions have been drawn from these approaches. Anderson *et al.*[65] see their approach as confirming that the ground state for the antiferromagnetic (J 0) case is the bound singlet state predicted by Nagaoka. Anderson and Yuval argue that all antiferromagnetic Kondo systems behave in the same way, and that $T_K$ is the parameter which scales a particular system to this universal behavior. This is not unlike the use of $T_S$ as a scaling parameter by Kaiser and Doniach. Anderson and Yuval also conclude that at very low temperatures

the system behaves like a localized spin fluctuation.[63] They assert that their method succeeds in dealing with the connection between the LSF and magnetic regimes, whereas more detailed LSF approaches have not dealt with this connection.

The more general approaches discussed above, however, have only just begun to yield results for physical properties. Calculations for transport properties have not yet been published. Moreover, these approaches do not concern themselves with specific kinds of physical mechanisms associated with local spin fluctuations, such as those discussed by Lederer and Mills and Kaiser and Doniach, and by Rivier and Zuckermann.

C. Thermoelectric Power in Dilute Magnetic Alloys

One of the prominent features of Kondo systems is a large peak in the thermoelectric power occurring near $T_K$. Typical behavior of the thermopower in these systems is shown in Fig. 3, taken from Daybell and Steyert.[14] The magnitude and position of the peak are concentration-independent for impurity concentrations large enough so that exchange scattering will provide the dominant contribution to the thermopower,[14] but small enough so that impurity-impurity interactions are unimportant. The sign of the peak is opposite to that of the ordinary scattering potential V of the impurity, and the magnitude also depends on V.[66] A considerable broadening in the peak is observed as the concentration is increased.

This thermopower behavior has been observed experimentally in a substantial number of systems. Results and references for many of these systems are presented in a table in Daybell's review article.[66]

Theoretical calculations of the thermoelectric power in Kondo or Kondo-Nagaoka systems have been published by a number of authors. On the basis of an S-matrix formalism, Suhl and Wong[32] obtain amplitudes for spin-flip and non-spinflip scattering of a conduction electron by a paramagnetic impurity, using an interaction energy of the form $\int [V(\vec{r})\rho(\vec{r}) + J(\vec{r})\vec{S}\cdot\vec{s}(\vec{r})]\, d^3r$. These are used to calculate a relaxation time which in turn is used to calculate $K^{(1)}$ and $K^{(2)}$ (See Sec. II for

definitions), from which the thermopower $S = \frac{1}{eT}\left(\frac{K^{(2)}}{K^{(1)}} - \epsilon_F\right)$ is obtained. (Although these authors choose to include $\epsilon_F$ in their defining equation for S, the physical results obtained for metals, as was indicated in Section II, should not differ from those predicted by the more usual defining equation, $S = \frac{1}{eT}\frac{K^{(2)}}{K^{(1)}}$, which we shall see below is used by other authors to calculate the Kondo thermopower.) Suhl and Wong do not present an analytical result for S; rather, plots of S vs. $\beta = \frac{\epsilon_F}{k_B T}$ are obtained numerically for various values of V and J. Their calculations do in fact indicate a large peak in the thermopower, the magnitude of which increases with increasing V and the sign of which opposes that of V.

Another calculation, due to Kondo[67] with a subsequent correction by Fischer[68], is based on a perturbation treatment of the sort which leads to the resistivity minimum, as discussed in Section IV.-A. Here, however, the imaginary parts of the scattering amplitudes are retained, and a rather complicated calculation leads to an expression for the inverse relaxation time of the form $\tau^{-1} = \tau_0^{-1} + \tau_1^{-1} \ln\left|\frac{\epsilon}{D}\right| + \tau_2^{-1}\left[2f(\epsilon) - 1\right]$. The first two terms are familiar from the resistivity calculation, but it is the last term which is an odd function of $\epsilon$ and hence contributes to the thermoelectric power. A rough calculation of the diffusion thermoelectric power then proceeds from $S \sim \frac{k^2 e}{T}\frac{d \ln \tau^{-1}}{d\epsilon}$,

a more general form of the $\frac{d \ln \rho}{d\epsilon}$ expression for S. Now $\frac{d \ln W}{d\epsilon} = \frac{\tau_1^{-1} \frac{d \ln |\epsilon|}{d\epsilon} + 2\tau_2^{-1} \frac{df(\epsilon)}{d\epsilon}}{\tau^{-1}}$, where $\frac{df}{d\epsilon}$ is large near the Fermi surface and dominates the numerator, and $\tau_0^{-1}$ is the dominant term in the denominator. Hence $S \sim \frac{k^2 e}{T} \frac{\tau_2^{-1}}{\tau_0^{-1}} \left(\frac{df}{d\epsilon}\right) \sim -\frac{k}{e} \frac{\tau_2^{-1}}{\tau_0^{-1}}$. When the s-d interaction is the dominant scattering mechanism $\tau_0^{-1}$ and $\tau_2^{-1}$ are proportional to the impurity concentration c and independent of temperature, and S is both concentration- and temperature- independent. This condition is observed experimentally to a reasonable approximation for a substantial range of concentrations and temperatures, as can be seen in Fig. 3.

For this range, the detailed Kondo calculation, as corrected by Fischer, leads to[16]

$$S_0 = \frac{2\pi\rho c}{\hbar}\left[V^2 + J^2 S(S+1)(1+4Jg) + 2\pi^2 \rho^2 J^3 V S(S+1)(2F-1)\right]$$

where $g = \int [f(\epsilon') - \frac{1}{2}] \frac{\rho(\epsilon')}{\epsilon' - \epsilon} d\epsilon'$. As T decreases, kT eventually drops below the Zeeman splitting energy of the impurity spins. When this happens, it is found that $S = S_0(\frac{T}{T_0})$, where $T_0 \sim \frac{\langle 2\mu H \rangle}{k_B}$, and S drops linearly to zero as $T \to 0$. An interpolation formula $S = S_0(\frac{T}{T+T_0})$ connects the two regimes.

Alloy systems which have been described in terms of local spin fluctuations also exhibit giant thermopower peaks, but the shapes of these peaks, as well as the temperatures at which they occur, differ from what one would expect from Kondo theory. A more detailed

discussion of these features appears in Section IV-D in connection with our own data.

Theoretically, no calculations based on the local spin fluctuation picture have been published to account for the thermopower peak. Rivier and Zuckermann use the self-energy of the d electron to obtain a result for S at very low temperatures which is linear in T,[3] as is the low-temperature Kondo result, but no calculation is offered for the higher temperature behavior. Their characteristic temperature for thermoelectric power $T_K^S = \frac{\pi\Delta}{k\tilde{U}\tau_s}$, is defined to make S linear in $\frac{T}{T_K}$.

Kaiser[69] has suggested that the peak observed in local spin fluctuation systems may be a "paramagnon drag" effect, analogous to the better know phonon and magnon drag peaks. This suggestion will be considered in more detail in the discussion of our own results.

D. Thermoelectric Power in Ir-Fe; Results and Conclusions

We have measured the thermoelectric power between 4.2 and 300°K for Ir with 0.5 and 1.0 at.% Fe and for pure Ir. The motivation for these measurements proceeded from arguments of Rivier and Zuckermann[3] that in its effect on observable properties, the spin-fluctuation model is entirely equivalent to the Kondo-Nagaoka spin-compensated state. On the other hand, Kaiser[69] suggested that for Ir-Fe one might expect the thermopower curve to peak at very different temperatures in the spin-fluctuation and Kondo pictures, and that a measurement of this sort might allow us to distinguish between the two models.

In the Kondo theory, the peak is expected roughly at Kondo temperature. As is seen in Fig. 4, a rough attempt to fit a Curie-Weiss curve to Knapp's[70] susceptibility data for Ir-Fe suggests a Kondo temperature on the order of 100°K, though Knapp argued that a Curie-Weiss curve could not be fit to his data over any considerable temperature range, and that therefore his data did not indicate a normal local moment.

In the spin-fluctuation picture, on the other hand, one might expect a peak for Ir-Fe at $T_C$, which in Ir-Fe is 7 K. (it should be recalled that $T_C=\frac{1}{4}T_S$ is an experimentally determined parameter marking roughly the transition from $T^2$ to T dependence in the resistivity.

This can be seen to occur at about 7°K in Sarachik's Ir-Fe[54] data, shown in Fig. 5. Table 1 lists $T_C$ and $T_S$ for the systems considered by Kaiser and Doniach.) As Fig. 6 shows, Foiles and Schindler[71] had observed a negative peak in the thermopower of Pd-Ni at 19°K, which is $T_C$ for that system. Moreover, Kaiser suggested that a peak at $\frac{1}{4}T_S$ would be reasonable for a paramagnon drag contribution, somewhat analogous to the phonon drag peak which occurs typically at about one fifth of the Debye temperature. No formal calculations of the spin-fluctuation thermopower have been published.

Anticipating a peak, then, at about 100°K for the Kondo picture, or 7°K for the spin-fluctuation picture, we performed our Ir-Fe measurements. The results are shown in Fig. 7a. (Results up to 100°K are shown in greater detail in Fig. 7b.) A large peak occurs near 28°K independently of Fe concentration for both alloys but does not occur for pure Ir. This peak is positive, whereas the Pd-Ni peak is negative. It should be noted that this peak clearly does not occur near the 100°K predicted by Kondo theory, nor does it occur at $\frac{1}{4}T_S$ as it does in Pd-Ni. Instead it occurs at 28 K, which is the spin-fluctuation temperature $T_S$ for Ir-Fe. In other words, on a universal curve the peaks for the two systems occur at temperatures differing by a factor of four. Kaiser and Doniach acknowledge that their value of $T_S$ for Pd-Ni, determined from the resistivity data of

Schindler and Rice[53], may be inaccurate, since that resistivity data did not go up to high enough temperatures to permit an accurate determination, but this inaccuracy could not account for a factor of four.

Moreover, recent thermopower measurements in Rh-Fe seem to indicate that for that system there is also a thermopower peak occurring roughly at $T_S$, which was determined by Kaiser and Doniach to be less than 1.6 K. Although measurements have not been made for a temperature range which includes $T_S$, measurements by Nagasawa[72] between 1.7 and 50°K on $Rh_{99.28}Fe_{0.72}$ show that below about 8°K the thermopower increases sharply in magnitude (it is negative) with decreasing temperature, and this increase continues down to the lowest temperatures considered. More recently Graebner et al[73] reported thermopower data for Rh-Fe with 0.1-1 at.% Fe at very low temperatures (below $T_S$) and found the magnitude of the thermopower to be monotonically increasing with increasing temperature over this range. It seems clear that a negative peak between the two temperature ranges considered is indicated, which would place it in the vicinity of $T_S$.

Returning now to our Ir-Fe data, one notes also a broader, higher-temperature shoulder or peak in the curves for the dilute alloys which is also seen in pure Ir, and is most likely related to phonon drag. It is

the larger, impurity-induced peak noted previously which is our primary concern. Fig. 8 explicitly shows $\Delta S$, the change in thermopower due to the iron impurities. The peak is larger in magnitude for the greater impurity concentration, but is not significantly broader. In these respects, the peak we observe is much like the peak found in Pd-Ni. In these respects also, as Foiles and Schindler[71] point out for the Pd-Ni peak, it is in contrast to the kind of peak one expects for Kondo systems. Fig. 3 shows typical thermoelectric power curves for Kondo systems. As the impurity concentration increases in Kondo alloys, the height of the peak remains roughly the same and the peak shows a very considerable broadening. The Ir-Fe and Pd-Ni alloys clearly do not exhibit this behavior. In both cases, the peak changes in magnitude and no broadening occurs, and it is thus likely that the behavior observed for both alloys is attributable to spin fluctuations. However, the differing temperatures at which the peaks occur poses a problem.

As noted earlier, a second difference between the two systems is that the impurity peak for Ir-Fe is positive, whereas that for Pd-Ni is negative. This is probably a less important consideration for two reasons. First, since the Rh-Fe peak is negative as in Pd-Ni, but occurs at $T_s$ as in Ir-Fe, it seems unlikely that the difference in sign is related to the difference in the temperatures at which the peaks occur. Second, a preliminary

calculation by Kaiser[69] indicated that the spin fluctuation contribution to the electron diffusion thermoelectric power is far too small to account for the peaks seen in Ir-Fe and Pd-Ni. If, instead, the spin fluctuations contribute to the thermopower by means of a drag effect, as Kaiser suggests, then the sign of the peak simply indicates whether normal or umklapp processes are dominant.

The notion of a local spin fluctuation or paramagnon drag peak is consistent with both the Kaiser and Doniach picture and the Rivier and Zuckermann pictures of local spin fluctuations. The former authors note that the linear T-dependence of the resistivity is a general consequence of electron scattering from a low-lying Bose excitation spectrum. A recent resistivity calculation based on the Rivier and Zuckermann picture[60] also shows the impurity resistivity to be linear in T over a considerable temperature range, in agreement with experimental results for Al-Mn[61]. Although negative, this term is attributed, as in the Kaiser Doniach model, "to the scattering of conduction electrons by a quasi-boson, the LSF."[60] Since it is scattering of conduction electrons from a spectrum of Bose excitations that gives rise to both the phonon and magnon drag peaks, one might reasonably expect a peak of this sort in the case of local spin fluctuations as well. Oddly, Babić et al.[61] note that as yet unpublished thermopower measurements on

Al-Mn indicate a linear behavior in the $T^2$ region of resistivity and temperature-independent behavior above about 100°K. No peak was observed. However, it should be pointed out that for Al-Mn, $T_S \sim 530^\circ$K. It is unclear whether the thermopower measurements were extended to such high temperatures. Finally, we note that $\Delta S$ for Ir-Fe (see Fig. 8) is also temperature-independent above about 150 K.

Two additional observations can be made about our Ir-Fe data. First, the temperature dependent part of $\Delta S$ as seen in Fig. 8 occurs over roughly the same range of temperatures for which a significant contribution to the specific heat of Ir-Fe has been observed by Geballe et al.[75] This is unfortunately not as useful as one would hope. For phonons and magnons, the low-temperature specific heat varies with temperature according to a simple power law ($T^3$ and $T^{3/2}$ respectively). The Thomson heat $\mu$ is taken to have the same T dependence, and in these cases the drag thermopower, given by $S=\int_0^T \frac{\mu}{T} dT$, also has the same T dependence. If the thermopower given by $S=AT+BT^x$ , i.e. if it is the sum of a linear diffusion term and a drag term obeying some power law, one can plot S/T vs. $T^{x-1}$ to determine A and B, and thus separate out the drag and diffusion terms. This analysis is not applicable to our Ir-Fe data, however, since no simple analytic expression is available for the specific heat of Ir-Fe as a function of temperature,

either from experiment or from theory. Some evidence for a $T^3$ or $T^3$ ln T dependence has been found in the specific heat of Pd-Ni at temperatures up to 4.2 K.[52,76] Contributions of both forms have also been calculated for Pd-Ni theoretically,[77,40,44] but the validity of the theoretical expressions is limited roughly to the temperature range for which measurements were made experimentally. No analytic expressions for the specific heat in local spin fluctuation systems have been calculated for the temperature range of our own measurements, and none have been calculated for Ir-Fe in any temperature range.

A second observation is that the thermoelectric power of pure Ir has only been measured previously at room temperature and above. Our data fits continuously with high temperature data (173°K and up) published by Vedernikov[78] which is a composite of the measurements of several authors. Fig. 9 combines our data with the higher temperature results and shows the thermopower of pure Ir between 4.2 and 1800°K. The thermopower of pure Rh has been measured between 83 and 1700°K[78] and behaves very similarly. Our pure Ir data may be of interest to investigators studying the properties of pure transition metals.

Of primary interest, however, are the similarities and contrasts between the thermopower data for Ir-Fe and Pd-Ni. To summarize, the two systems show similarly-

shaped impurity peaks which increase with impurity concentration but do not broaden, in contradistinction to what one would expect of Kondo systems. Moreover, the Ir-Fe curve peaks at a much lower temperature than Kondo theory would predict. But whereas Pd-Ni exhibits a peak at $T_C$, or $\frac{1}{4}T_S$, the thermopower of Ir-Fe peaks at the spin fluctuation temperature $T_S$. While there is good reason to relate the behavior of both systems to local spin fluctuations, this difference is puzzling and suggests a need for further theoretical work.

## V. CONCENTRATED MAGNETIC ALLOYS

### A. Concentrated Magnetic Alloys and Giant Moment Clouds: Background

In certain binary transition metal alloys, in which one of the two components is magnetic, the magnetic susceptibility increases rapidly as the concentration of the magnetic component is increased, and becomes infinite (the alloy becomes ferromagnetic) at a critical concentration. The properties of these systems for nearly ferromagnetic compositions are thus characterized by susceptibilities much larger than the Pauli spin susceptibility $\chi_p$ for free electrons, and have attracted considerable attention in recent years. Of particular interest have been the Pd-Ni, Pt-Ni, Cu-Ni, and Rh-Ni alloy systems, in which the susceptibility varies rapidly with Ni, becoming infinite at a critical Ni concentration which is different for each system.

Such systems are said to be "exchange enhanced"; *i.e.* the sysceptibility is enhanced because of a screened short-range intra-atomic Coulomb repulsion between electrons of opposite spin. This interaction does not occur between electrons of like spin, which have an anti-symmetric spatial wave function that keeps them further apart than the effective range of the potential.

Until the late 1960's it was thought that the behavior of these systems could be explained on the basis of a "uniform enhancement" theory.[43,53,40] In

this theory one considers a susceptibility of the form $\chi = \chi_p(\frac{1}{1-UN(0)})$, in which the Pauli spin susceptibility is amplified by the Stoner exchange enhancement factor. The theory assumes that the density of states N(0) at the Fermi surface and the exchange term U of the screened Coulomb repulsion vary with alloy composition but are roughly constant throughout a given solid. Thus UN(0) would approach one from below, and ferromagnetism would occur at the critical Ni composition which results in UN(0)=1.

For dilute alloys, such as Pd-Ni and Pt-Ni, this viewpoint has been largely superseded by a "local enhancement" theory.[1,79,77,2] Developed for the case of a host matrix containing a single impurity atom (with results obtained thereafter by superposition), this theory assumes the interelectronic interaction to be especially large in the impurity cell. Depending on the host, short-range intra-atomic Coulomb repulsions between d-electrons elsewhere in the solid may or may not be taken into account.[80] In short, this has evolved as the theory of local spin fluctuations which was of central interest in Sec. IV. Hence, dilute exchange-enhanced alloys will not be considered further in this section.

The applicability of "uniform enhancement" theory to concentrated alloys, such as Cu-Ni and Rh-Ni, assumed that the magnetization is uniform throughout the solid.

However, in 1969, neutron scattering experiments performed by Hicks et al.[81] on a series of weakly ferromagnetic Cu-Ni alloys showed that near the critical composition (44 at.% Ni) the low temperature spontaneous magnetization is located in magnetic polarization clouds of large total moment -- roughly 8-11 Bohr magnetons -- and extending over many atoms. The existence of these clouds was indicated by a forward peak in the neutron scattering cross-section which would not occur if the magnetization were uniform. Similar results were reported for weakly ferromagnetic Rh-Ni.

Observation of Curie-Weiss behavior in the susceptibility of paramagnetic Cu-Ni alloys[82] has shown that these polarization clouds persist well into the paramagnetic range. High field saturation values of magnetization obtained for the same Cu-Ni samples at low temperatures[83] were combined with the Curie-Weiss coefficients obtained from susceptibility measurements to give values for the moments of polarization clouds in paramagnetic samples comparable to those deduced by Hicks et al. for weakly ferromagnetic samples. Hence, one concludes that the total moment of such a cloud shows little variation either above or below the critical Ni composition, but the concentration of clouds increases with Ni content.

Kouvel and Comly[82] note a correlation between the concentration of clouds and the probabilities that a

lattice site in fcc Cu-Ni will be occupied by a Ni atom and have either 10 to 12 or 11 to 12 Ni nearest neighbors. (The correlated quantities are each considered as a function of Ni concentration). On this basis they suggest that the clouds are nucleated at highly local Ni-rich regions, and that it is the aligning forces between neighboring clouds which give rise to ferromagnetism as the cloud concentration is increased. They suggest, further, that "the exchange-induced moments in the atomically disordered matrix around each nucleating site are probably situated only at the Ni atoms,[84] and vary in magnitude with their proximity to the nucleating sites as well as with their local atomic environment." In this sense they are analogous to polarization clouds which had been observed earlier in dilute Pd-Fe[85], in which nucleation occurs about the Fe sites, and the distribution of moments induced on surrounding Pd sites could be more readily determined.

However, systems like Pd-Fe and systems like Cu-Ni and Rh-Ni are different in the following sense. In the former, moments are induced at Pd sites, since the Pd host is highly exchange enhanced, so that only dilute concentrations of the impurity are required for nucleation of polarization clouds. In the latter systems, where moments occur only at the Ni sites, impurity-impurity interactions between Ni atoms are necessary if polarization clouds are to form, so that more than

dilute concentrations of Ni are required. This is true by definition, since the dilute regime is considered to be the range of impurity concentrations sufficiently small so that impurity-impurity interactions can be neglected. In systems like the Cu-Ni[86] and Rh-Ni, by contrast, there is an absence of the kinds of behavior discussed in Section IV-A (*e.g.* resistivity minimum and giant thermopower peak) associated with magnetic moment formation at dilute impurity concentrations.

Unlike the dilute impurity problem, which has been the subject of an extensive corpus of theoretical literature, the question of giant moment clouds and associated properties in concentrated magnetic alloys has thus far been treated predominantly on a phenomenological basis. It is therefore an accurate reflection of the state of the art to proceed with a discussion of some observed physical properties of giant moment systems, and after, to touch on some recent theoretical developments.

Further experimental support for the existence of giant moment clouds is provided by the low-temperature behavior of the specific heat C. In both Cu-Ni[87,88] and Rh-Ni[89] an "upturn" in the C/T vs. $T^2$ graph as $T \to 0$ is noted for paramagnetic alloys. Schröder[90] attributed the upturn for Cu-Ni to ferromagnetic clusters as early as 1961. He suggested that these clusters (which one

could take to be giant moment clouds) behave like a system of independent oscillators and can be described by the Einstein Specific heat for such a system, which above the Einstein temperature (below 1.4°K for Cu-Ni) is essentially constant. Hence, a specific heat of the form $C=A+\gamma T+\beta T^3$ is assumed (the latter two terms giving the conduction electron and lattice specific heats) and is found to fit well with the data. Bucher et al.[89], on the other hand, found that their low temperature Rh-Ni data could be fit to an expression of the form $C_V=\gamma T+\beta T^3+bT^3 \ln T$, where the last term is expected from electron-paramagnon interactions in the "uniform enhancement" picture.[43] Finally, Robbins et al.[88] found that either expression could be fit to their Cu-Ni data, but that the RMS deviations are consistently lower for the cluster or giant moment cloud expression. Moreover they noted that plastic deformations of their samples increased the observed upturn, and that this change could be reversed by re-annealing. They argued that this effect could not be explained on the basis of electron-paramagnon interactions, but that one could account for the increase in the anomaly by assuming that the number of clusters or clouds is increased "when the clusters are subdivided as a result of deformation by slip (i.e. the passage of dislocations through them)."

Of particular interest is the resistivity behavior

of these systems. Measurements of resistivity in Cu-Ni and Rh-Ni have been made for a broad range of concentrations. The results reported by Houghton, Sarachik and Kouvel[91] for Cu-Ni alloys ranging from 30 to 50 at.% Ni are seen in Fig. 10. The critical concentration is 44 at.% Ni. A resistivity minimum is seen between 50 and 80°K, depending on concentration. A maximum at a higher temperature is noted, and then a second minimum at around 600°K, slightly below the Curie temperature of pure Ni. These authors suggested that the rise in resistivity below 600°K is associated with the formation of giant polarization clouds, which give rise to a spin-disorder scattering term in the resistivity.

The low temperature minima shown in Fig. 11,[92] as well as negative magnetoresistances reported by the same authors,[92] resemble the behavior of Cu with dilute transition metal impurities, such as Fe and Cr, which carry local magnetic moments. As has been noted, however, dilute Cu-Ni alloys do not exhibit localized moment behavior, and the effect observed by Houghton et al. in concentrated Cu-Ni alloys seems to extrapolate to zero at about 27 at.% Ni. Moreover, as is seen in Table 2, also due to Houghton et al., both $\Delta\rho(\Delta T)$ -- defined as the difference between the resistivities at 1.75 and 20°K -- and $\Delta\rho(\Delta H)$ -- defined as the difference between the resistivities at zero field and 50 kiloGauss -- vary

linearly with the cloud concentration c deduced from the susceptibility data of Kouvel and Comly.[82]

In contrast, Fig. 12 shows the resistivity data reported by Houghton et al. for Rh-Ni[93], in which no such structure as that seen in Cu-Ni is observed. Hence, while both systems show similar evidence of giant moment clouds on the basis of neutron scattering cross-sections and susceptibility and specific heat measurements, Cu-Ni shows resistivity behavior which can be related by phenomenological arguments to the giant moment clouds, whereas the resistivity of Rh-Ni behaves quite differently.

Theoretical calculations of physical properties based on a giant moment picture have only recently begun to appear. At this point it should be noted that on the basis of the phenomenology, it has been concluded that the giant moment clouds exist, that they nucleate about locally Ni-rich regions, and that at sufficiently large cloud concentrations, aligning forces between clouds give rise to ferromagnetism. However, no conclusions were drawn as to the mechanism of nucleation or the nature of the aligning forces between polarization clouds.

The aligning forces between clouds, but not the nucleation mechanism, were treated by Fibich and Ron[94], who proposed a model for the susceptibility of paramag-

netic Cu-Ni. In this model the clouds interact via the itinerant electrons. An electron interacts with a cluster only when it is very close to one of the constituent Ni atoms. It is assumed that the intracluster aligning forces correlate the Ni atoms very strongly, so that itinerant electrons interact with the magnetic moment of each cluster as a whole rather than with its atomic constituents. The interactions between clouds is shown to exhibit Ruderman-Kittel type oscillations, with a wavelength of the order of the cluster size. On this basis the authors obtain a Curie-Weiss contribution to the susceptibility, of the form $\frac{B}{T-\theta}$, where $B=\frac{CM}{3k_B}$, C is the cluster concentration, and M the magnetic moment per cluster. Both B and $\theta$ decrease with decreasing Ni concentration and $\theta$ becomes negative when the Ni concentration is low. This is in qualitative agreement with the measurements of Kouvel and Comly, although a good numerical fit is not obtained.

Fibich and Ron[95] also calculated a Kondo-like minimum in the resistivity arising from a cluster of spins, again considering an itinerant electron to interact with the cluster as a whole. However, Levin and Mills[96] point out that this calculation neglects the spatial separation between spins in the cluster and they therefore consider it a poor approximation.

A model for the formation of magnetic moments in Cu-Ni was proposed by Robbins *et al.*[97] The linear

decrease [98,99] in the average atomic moment of ferromagnetic Cu-Ni with decreasing Ni content was for a long time interpreted as resulting from the filling of a rigid d-band by the extra electron of Cu, so that below critical Ni concentration the d-band is completely filled. Robbins et al. point to an extensive amount of experimental evidence, including much of what has been discussed in this section, indicating that this is not the case, but rather that permanent moments exist well into the paramagnetic range, the number of d holes per Ni atom stays roughly constant at all concentrations, and the Ni solute atoms give rise to a high density of virtual bound d-states at and just below the Fermi surface. In analogy with the interpretation of the behavior of several other alloy systems, in which the moment of one type of atom is considered to depend on the composition of its nearest neighbor environment, Robbins et al. proposed that the spin moment on a Ni atom in Cu-Ni must depend on its local environment, as specified by the number of Ni atoms among its nearest and second-nearest neighbors. They express the average moment per Ni atom in the alloy as $\bar{\mu}(x) = \sum_{n=0}^{12} \sum_{m=0}^{6} P_{n,m}(x)\, \mu_{n,m}$, where $x$ is the atomic fraction of Ni in the alloy, $P_{n,m}(x)$ is the probability for a given $x$ that a Ni atom will have n nearest and m second-nearest Ni neighbors, and $\mu_{n,m}$ is the moment assigned to a Ni atom with n nearest and m second-

nearest Ni neighbors. With reasonable choices for the values of the $\mu_{n,m}$, a good fit is obtained to experimentally determined values of $\bar{\mu}$.[98,99] Moreover, on the basis of these $\mu_{n,m}$ values, a moment of $8\mu_B$ per giant moment cloud is estimated to require about 30 Ni atoms per cloud, in rough agreement with the observations of Hicks et al.[81] As noted earlier, this nearest-neighbor approach had also been suggested by Hicks et al. An approach similar to, but somewhat simpler than that of Robbins et al. is taken by Perrier et al.[100], who also obtain a reasonable fit to experimental data.

Aldred et al.[101] carry the near-neighbor model somewhat further, suggesting that the moment at a Ni atom is effectively reduced by the presence of a Cu atom as a nearest-neighbor because of the electronic screening of the larger nuclear charge of the Cu. This screening is largely localized within the Cu cell, but a small residue extends to nearest Ni neighbors. The net reduction of the Ni atom's moment arises from this screening, and to a lesser extent from the magnetic effect due to the replacement of a Ni nearest-neighbor by a Cu nearest-neighbor. Cooperative magnetic effects due to the reduction of the moments of other Ni nearest neighbors by the Cu atom become more significant and may have effects over more distant near-neighbor shells as the Cu concentration is increased.

The most extensive theoretical treatment of giant

moment clouds to date is that of Levin and Mills.[96] On the basis of a model of the type discussed above, in which the giant moment clouds arise from local environmental effects, the resistivity, neutron-scattering cross-section, and specific heat of giant moment systems are calculated, and the results applied to Cu-Ni.

These authors proceed from a Hamiltonian of the form

$$H = -2\sum_{i,j} J^{dd}\vec{S}_i\cdot\vec{S}_j - \mu_B\sum_i \vec{H}\cdot\vec{S}_i - \sum_{i,e} J^{sd}\vec{S}_i\cdot s_e\,\delta(\vec{R}_i-\vec{R}_e)$$

The first term represents the ferromagnetic Heisenberg exchange interaction between near-neighbor spins; i.e. it is an intracluster term. The second term is an intercluster term, given in terms of a magnetic field H which is the sum of the anisotropy field and the internal molecular field which results from ferromagnetic alignment of the polarization clouds. The intercluster interaction is neglected in the paramagnetic regime. The last term represents an interaction between the conduction electrons and the localized spins. Hence this approach differs from that of Fibich and Ron in that it considers intracluster effects and that it treats the conduction electrons as interacting with component spins of the polarization cloud rather than with the cloud as a whole.

This Hamiltonian is treated in a Born approximation calculation in which the transition rate $\frac{1}{\tau}(\vec{k},\sigma\rightarrow\vec{k}',\sigma')$ is obtained for conduction electrons scattered by localized spins. This in turn is used to obtain the resistivity. The neutron-scattering cross section is obtained from

spin cross-correlation functions of the form $\langle S_i^{\alpha}(t)\, S_j^{\beta}(0)\rangle$ ($\alpha,\beta=x,y,z$). The specific heat per atom arising from the localized spins is obtained from $C_V=\frac{1}{N}\frac{d\langle E\rangle}{dT}$, where $\langle E\rangle$ is the expectation value of the energy of the localized spin system.

Noting that it is difficult to obtain analytical expressions for these quantities, the authors do obtain explicit results in certain regimes.

In the paramagnetic regime with $\vec{H}$ taken as zero, it is found that the spin disorder resistivity $\rho$ decreases with increasing temperature where $k_F a \lesssim 2.0$ in fcc lattices, i.e. when the electron wavelength $\lambda=\frac{2\pi}{k_F}$ is long compared to the lattice constant, which represents the separation between spins in a cloud, and interference effects are unimportant. At low temperatures ($k_B T \ll J^{dd}$, where $J^{dd}\approx 105^{\circ}K$ for CuNi), the spins in the cloud remain strongly correlated as the cloud tumbles about, and the electron-scattering cross-section is proportional to $\langle(\sum_i \vec{S}_i)^2\rangle=NS(NS+1)$. At high temperatures ($k_B T \gg J^{dd}$) the individual spins move in an uncorrelated way and scatter independently. The scattering cross-section is proportional to $\sum_i \langle S_i^2\rangle=NS(S+1)$ and is a factor of N smaller, and hence the cluster resistivity decreases with increasing temperatures. This accounts for the high temperature minimum in Cu-Ni.

In agreement with the observations of Hicks et al.[81], Levin and Mills find that the neutron scat-

tering cross-section $\frac{d\sigma}{d\Omega}$ peaks in the forward direction. This is of physical significance in the resistivity behavior. A further result obtained by Levin and Mills is that if terms of third order in $J^{sd}$ are retained in calculating the transition rate when $k_BT \ll J^{dd}$ (so that the spin clusters are in a correlated ground state and rotate rigidly from one N+1-degenerate ground state energy level to another) a Kondo-like minimum occurs in the resistivity. (This is the low temperature minimum observed in Cu-Ni). However, the size of this minimum is suppressed relative to a Kondo minimum resulting from a single spin of the same magnitude, and the suppression is more pronounced as the cloud increases in size, so that the Kondo divergence of $\rho$ must disappear when $N \to \infty$. This suppression comes about because there is a forward peak in the differential cross section for the scattering of electrons from large clusters in the first Born approximation, and in the cross-section for the scattering of electrons into intermediate states in the second Born approximation. Forward scattering does not contribute to the resistivity ($\rho \sim 1-\vec{k}\cdot\vec{k}'=0$ when $\vec{k} // \vec{k}'$). The size of this minimum is also diminished as the parameter $k_Fa$ is increased.

Finally, in disagreement with Schröder[90] and Robbins et al.[88], Levin and Mills find that the cluster contribution to the specific heat is probably not temperature independent, but rather in the ferromagnetic

regime it increases slowly with temperature and in the paramagnetic regime it decreases somewhat more rapidly with temperature.

These authors treat Cu-Ni specifically using as parameters a cluster size of 50 atoms and a spin of $\frac{1}{2}$ for each Ni atom (this assumes exactly one d-hole per Ni atom). The clusters are all assumed to be in the most closely packed configuration, and are all assumed to be in the same local magnetic field $\vec{H}$. Reasonable semi-qualitative agreement with experimental results is obtained for the resistivity, elastic neutron-scattering, and the low-temperature specific heat of Cu-Ni.

No comparable treatment is available for Rh-Ni.

B. Thermoelectric Power in Giant Moment Systems: Background

To date, no theoretical calculations of thermoelectric power have been published for concentrated magnetic alloys characterized by giant moment clouds. Moreover, relatively little published experimental data exists for these systems. We know of no published thermopower measurements for Rh-Ni prior to the present work. Some measurements have been made on Cu-Ni, but not for all ranges of temperature and concentration.

As early as 1926, measurements of the thermopower of Cu-Ni relative to Pt between 0 and 1000°C were published by Chevenard[102] for fourteen samples ranging in concentration from pure Ni to pure Cu. An anomalous bend in the plots of $S_{Cu-Ni}-S_{Pt}$ vs. T is noted at about 450°C and is most pronounced in the 40 to 60% Ni concentration range. The thermopowers are large and negative. At temperatures below the bend, the magnitude of the thermopower increases monotonically with temperature. At temperatures above the bend, the magnitude of the thermopower remains roughly constant or decreases slightly with temperature. Recent measurements, however, taken over a broad range of concentrations between 200°K and 900°K by Ahmad and Greig[103], show a monotonic increase in the magnitude of the thermopower with a gradual decrease in the magnitude of the slope over the entire range. There is no sign of the pronounced

bend observed by Chevenard. The difference cannot be accounted for by the fact that the earlier measurements were taken relative to Pt, since $S_{Pt}$ is itself monotonic over the entire temperature range of interest[104], and its magnitude increases much less rapidly than that of $S_{Cu-Ni}$.

Low temperature thermopower measurements were performed on Cu-Ni by Schroeder et al.[86], but only for low Ni concentrations. These authors measured the thermopower of Cu-Ni between 4.2 and 300°K for samples containing from 0 to 17.1% Ni. In this concentration range, for Ni concentrations sufficiently large for the phonon drag peak of pure Cu to be completely suppressed, the thermopower behavior was observed to be completely monotonic. Similarly, low temperature measurements for Ni with dilute amounts of Cu (0-5 at.%)[105] showed that at 5 at.% Cu the thermopower peak in Ni was completely suppressed and the thermopower varied monotonically with temperature.

More recently, Zrudsky and Showalter[106] measured the low-temperature thermopower of CuNi samples containing 6.2, 11.6, and 23.6 at.% Ni and presented their data as a function of Ni concentration at several fixed temperatures. At each of the temperatures considered, the thermopower varied linearly with Ni concentration.

Prior to the present work, no low-temperature thermopower measurements have been published for Cu-Ni

in the nearly ferromagnetic and weakly ferromagnetic regimes of Ni concentration.

C. Thermoelectric power in Giant Moment Systems: Experimental Results and Conclusions

We have measured the thermoelectric power between 4.2 and 300°K in Cu-Ni and Rh-Ni for a broad range of Ni concentrations straddling the critical concentration for ferromagnetism in each system. These measurements had a twofold motivation -- to see what effect the giant polarization clouds would have on the thermoelectric power in the nearly ferromagnetic and weakly ferromagnetic regimes, and to see whether the differences observed in the resistivity behavior of Cu-Ni and Rh-Ni would be paralleled by similar differences in the behavior of the thermoelectric power of the two systems.

Thermopower data for Cu-Ni was taken for samples containing from 30 to 50 at.% Ni. The critical concentration is 44 at.%Ni. The results as a function of temperature between 4.2 and 300°K for several samples are displayed together for comparison in Fig. 13. The origins for the several curves have been uniformly displaced by 5$\mu$V/°K in the vertical direction for clarity. Plots for individual samples between 4.2 and 100°K, the range of primary interest, are shown in somewhat more detail in Figs. 14-21. A contribution which peaks at about 50°K is in evidence over most of the concentration range. This extra contribution is largest near the critical concentration of 44% Ni and is greatly

diminished at the extremes of the concentration range, just as was true of the extra low temperature contribution to the resistivity of Cu-Ni.

As mentioned in part B of this section, Zrudsky and Showalter[106] reported thermopower data for Cu-Ni over the same temperature range but for much lower Ni concentrations. For the concentrations they considered, they found no extra term at low temperatures. In Fig.22, the circled points represent the data of Zrudsky and Showalter. Plotting their data for 6.2, 11.6, and 23.6 at.% Ni as a function of Ni concentration at fixed temperatures they find that over the concentration range considered, the thermopower varies linearly with concentration at each temperature. Our data for higher Ni concentrations, designated by uncircled points, are shown on the same plot. For comparison, we have also plotted the 300°K data of Ahmad and Greig[103] for a broad range of Ni concentrations (data points enclosed in squares) and the 300°K data of Schroeder et al.[86] for very low Ni concentrations. Clearly, the linear behavior observed by Zrudsky and Showalter does not extend to the very low Ni concentrations considered by Schroeder et al. However, the data of Schroeder et al. do appear to continue smoothly into the data of Zrudsky and Showalter at higher concentrations.

We have extended the straight lines determined by Zrudsky and Showalter's data. On the higher

temperature (200°K and 297°K) plots, our data follows these straight lines for the lower compositions and falls below at higher Ni concentrations. This decreasing slope is also seen in Greig's 300°K data and seems reasonable, since the magnitude of the thermopower (-S) must eventually drop down to the value for pure Ni. On the lower temperature plots, however, it seems that, due to the extra contribution which we noted on our S vs. T plots, the values of -S start rising above the straight line well below the critical concentration of 44 at.% Ni, then drop back toward or below the straight line above the critical concentration. One notes further that this anomaly has essentially disappeared at 200°K, so that these plots give a measure of the effective temperature range of the additional term.

As can be seen in Fig. 22, the numerical values of our 297°K data seem to be a reasonable extrapolation of the data of Zrudsky and Showalter for lower Ni concentrations, which in turn fits well with the data of Schroeder et al. at still lower concentrations. However, they differ somewhat from the values obtained at 300 K by Ahmad and Greig. These authors note that constantan, $Cu_{0.55}Ni_{0.45}$, falls within the concentration range considered, and has a comparable thermopower. Actually, the thermopower of constantan is commonly tabulated relative to copper, since the two materials are often

used together as a thermocouple. Its value at 300 K, when corrected for $S_{Cu}$[108] is about -39.3 $\mu$V/°K. This is slightly lower in magnitude than the values of -40.1 $\mu$V/°K obtained by Ahmad and Greig and about 7 $\mu$V /°K lower than our own. However, compositions for commercial thermocouple grade constantan are in fact varied according to the material with which the constantan is to be coupled, and constantan produced for use with copper (Instrument Society of America code TN) contains 2% Mn[109]. The various constantans do not have the same thermal EMF characteristics[110]. Considerable differences may therefore be reasonably expected between thermopower values obtained for pure Cu-Ni samples and values obtained for commercial constantan.

Our 300°K data agrees considerably better with the data of Chevenard after corrections are made for the fact that Chevenard's measurements were obtained relative to platinum (Chevenard's data has appeared in works by other authors[111] without mention of the fact that the measurements were relative to Pt. While the plots of $S_{Cu-Ni}$ versus Ni concentration presented by these authors retain the correct shape, the numerical values are incorrect.)

It seems reasonable that the differences among the room temperature values obtained by various authors can be attributed at least in part to differences in metal-

lurgy. Legvold et al.[112] have noted that the low temperature resistivity values for a freshly annealed sample with 44 at.% Ni differed somewhat from values obtained for a sample with a three-year shelf life. The additional low-temperature resistivity contribution was present in both cases. The authors attributed the difference in numerical values to abnormal Ni cluster growth during the shelf-life of the sample. With this in mind, we re-annealed our $Cu_{58}Ni_{42}$ sample to see if similar differences were observable in the thermopower of Cu-Ni. Our original measurements were on samples with roughly a 4 year shelf life.

Fig. 23 shows our thermopower data for the same sample before and after annealing. The higher temperature values for both samples are the same to within the experimental error of 1 to 2%. If the differences noted previously among the room temperature measurements of various authors do arise from metallurgy, we can at least assume that the metallurgical factors involved are not simply a question of shelf life.

More importantly, the freshly annealed sample retains the extra low temperature contribution. The effect is lessened but not substantially, and it remains the most prominent feature of the thermopower behavior of Cu-Ni in the range of concentrations we have considered.

The extra thermopower contribution seems consistent with the Levin and Mills calculation of a Kondo-like minimum in the low-temperature resistivity of giant moment systems. If this Kondo-like viewpoint is correct, it does not seem unreasonable to expect that a thermopower contribution of the sort typical of Kondo systems should also arise, peaking roughly at a Kondo temperature determined from the resistivity data. Since the size of the resistivity minimum due to a polarization cloud is suppressed relative to a minimum due to a single spin of the same magnitude, one would also expect the thermopower peak due to polarization clouds to be correspondingly suppressed. Unfortunately, while one can subtract the host metal thermopower from that of the alloy in dilute magnetic alloys to determine the behavior of S due to impurities, a similar analysis for concentrated magnetic alloys would require finding the difference between the thermopower of Cu-Ni with and without polarization clouds. Clearly this cannot be done. However, on a rough qualitative basis our thermopower measurements for Cu-Ni are not inconsistent with an interpretation in analogy to the thermopower behavior of dilute Kondo systems.

The fact that the temperature at which the extra thermopower contribution appears to peak varies very little with composition is also consistent with the

thermopower behavior exhibited by dilute Kondo systems. It may also reflect the fact that, while the cloud concentration increases with increasing Ni, the size of an individual cloud remains roughly constant. This suggests the possibility of a characteristic energy and a corresponding characteristic temperature.

For the $Cu_{50}Ni_{50}$ sample (Fig. 21) there appears to be a slight but abrupt change in the slope at about 40°K, which is the Curie point $T_C$ for that concentration as given by Hicks et.al.[81] There has been some recent interest in cusp-like anomalies of this sort occurring in $\frac{dS}{dT}$ and also in $\frac{d\rho}{dT}$[103] in ferromagnetic metals and alloys which arise from short-range thermal fluctuations in the spin system.[113] A logarithmic[113] or exponential[103] drop is observed empirically in $\frac{1}{\rho}\frac{d\rho}{dT}$ and $\frac{1}{S}\frac{dS}{dT}$ above and below $T_C$. Theoretical calculations based on critical fluctuations give a satisfactory account of these resistive[114] and thermoelectric[115] anomalies.

The scatter of data points makes it unclear whether a similar effect is occurring in our more weakly ferromagnetic samples. It should be noted, however, that this is an effect which occurs at $T_C$, which drops to zero at the critical Ni concentration. It is therefore a distinctly different effect than the extra contribution which occurs at a roughly constant temperature over our concentration range.

Our data for Rh-Ni is shown in Fig. 24. Data for

the several samples are displayed together for comparison. The origins are uniformly displaced by $4\mu V/^{\circ}K$ for clarity. The thermopower was measured between 4.2 and 300°K in Rh-Ni samples containing from 56 to 64 at.% Ni. The critical concentration is 63 at.%. Data for the 4.2-100°K range is shown in more detail in separate plots in Figs. 25-28. First and foremost, we note the absence of any additional low temperature contribution such as was seen in Cu-Ni, and we correlate this with the fact that the additional low temperature resistivity term seen in Cu-Ni was also absent in Rh-Ni.

The lack of structure observed in the thermopower behavior of Rh-Ni is nevertheless surprising. Despite the fact that the resistivity of Cu-Ni shows considerably more structure than that of Rh-Ni, some interesting low temperature behavior has been noted in the latter system. Houghton et al.[93] observed a low temperature transition from $T^2$ to T dependence analogous to that observed in local spin fluctuation systems, and discussed at length in Section IV. These authors suggest, therefore, that the observed behavior may arise from spin fluctuations associated with Ni atoms in nearly critical local environments.

Hence, while the resistivity of Cu-Ni exhibits Kondo-like behavior at low temperature, the low-temperature resistivity of Rh-Ni behaves markedly like that of

a spin fluctuation system. Interestingly, among dilute alloys, Cu-Fe shows classic Kondo behavior, whereas, as was noted in Section IV, the behavior of Rh-Fe is well described by spin fluctuation theory, which suggests a certain consistency among alloys with the same host transition metal.

If one carries this analogy further, however, one might expect that, just as one finds an extra thermopower contribution associated with the Kondo-like resistivity minimum in Cu-Ni, one should find a thermopower peak in Rh-Ni analogous to those found in dilute nearly-magnetic alloys characterized by local spin fluctuations. The $T^2$-to-T resistivity transition occurs at $\frac{1}{4}T_S$ in the Kaiser and Doniach[2] model. The resistivity data of Houghton et al. suggests that $T_S$ goes through a minimum at the critical concentration but is about $20^oK$ for $Rh_{44}Ni_{56}$, and even higher for $Rh_{36}Ni_{64}$. A thermopower peak would then be expected either at $\frac{1}{4}T_S$, as in Pd-Ni, or at $T_S$, as in Ir-Fe and Rh-Fe.(See Sec. IV-D.) We find no evidence of such a peak. It must be noted, however, that the low-temperature resistivity anomaly in Rh-Ni, in addition to being qualitatively different, is also orders of magnitude smaller than that in Cu-Ni. Thus, since the extra thermopower contribution is small compared to the background in Cu-Ni, it is quite conceivable that there may be an extra low

temperature thermopower term in Rh-Ni as well which we have not been able to detect within the accuracy of our measurements.

While we find no evidence of a peak of the type described above, we do note a change in slope at about 5°K for $Rh_{36}Ni_{64}$ (Fig. 28) which may be the same kind of anomaly discussed previously with regard to $Cu_{50}Ni_{50}$.

Returning now to a comparison of Rh-Ni and Cu-Ni, it should be noted that the thermopower of Rh-Ni is positive, whereas that of Cu-Ni is negative. This can be explained using arguments by Fletcher and Greig[116], based on the $\frac{d \ln N_d}{d\epsilon}$ term which dominates the diffusion thermoelectric power of transition metals. These authors noted that alloying another metal with a transition metal such as Ni will increase or decrease the thermopower according as the number of empty d-levels is increased or decreased, so that increasing the concentration of a metal to the left of Ni on the periodic table, such as Rh, will make the thermopower of the alloy more positive or hole-like, and increasing the concentration of a metal to the right of Ni, such as Cu, makes the thermopower more electron-like or negative. (The thermopower of pure Ni is negative.) The analytic form of these arguments presumes a rigid band model, which is inapplicable in giant moment systems. In Cu-Ni, for example, the number of holes per Ni atom does not change

appreciably with Ni concentration[84], and, as Robbins et al.[97] point out the contribution per Ni atom to $N_d$, the density of d-states at the Fermi surface, for alloys with less than 30 at.% Ni, as estimated from specific heat measurements[87], is only slightly less than that of pure Ni. Nevertheless, the total contribution to $N_d$ from all the Ni atoms decreases with decreasing Ni concentration and the character of $N_d$ is increasingly determined by the other component of the alloy, so that the arguments of Fletcher and Greig should still have qualitative validity for Cu-Ni and Rh-Ni.

A final point of contrast between the Cu-Ni and Rh-Ni systems is that the thermopower values for Rh-Ni, apart from sign, are more than a factor of three smaller than the Cu-Ni values for comparable concentrations and temperatures. What may be more significant, however, is that the thermopower values for Rh-Ni are further removed from the pure Ni values[117] than are the values for Cu-Ni.

To reiterate, though, the major difference is that, while both systems exhibit giant moments, an additional low-temperature term is observed in the thermopower of Cu-Ni, while Rh-Ni exhibits no such term. An analogous contrast was seen between the low-temperature resistivity behavior in the two systems. Both effects appear to occur for roughly the same range of concentrations and temperatures. As with the additional resistivity term,

we believe the additional term in the thermoelectric power of Cu-Ni to be a magnetic term which, since it is not observed at very low Ni concentrations, seems to be related to the presence of giant moment clouds. It should be recalled that the relationship between the additional resistivity term and the giant moment clouds in Cu-Ni is supported experimentally by the observations of Houghton et al.[92] that $\Delta\rho(\Delta H)$ and $\Delta\rho(\Delta T)$ (defined in Sec. IV-A) vary linearly with cloud concentration. It is also consistent with the Levin and Mills calculation of a Kondo-like minimum in the resistivity of giant moment systems, which suggests that one might also expect a Kondo-like thermopower peak. It is puzzling, therefore, that in Rh-Ni, which is also a giant moment system, the transport properties behave strikingly differently than they do in Cu-Ni. We believe that further theoretical work in this regard is desirable.

One alternate viewpoint should be mentioned. A recent paper by Ahmad and Greig[118] reports data for the resistivity of $Pd_{60}Ag_{40}$ between 4.2 and 900°K, and finds its behavior as a function of temperature to be similar to the resistivity behavior of $Cu_{65}Ni_{35}$ over the same range of temperatures. For Pd-Ag the observed effects cannot be due to giant moment clouds, and the following argument is applied. The high resistivity of pure Pd follows from the high probability of scattering conduction s-electrons into a narrow d-band in which the density of

states at the Fermi surface is large. The rapid decrease in density of states with increasing energy results in a decreased probability that electrons will be scattered by phonons into the d-band at higher temperatures. In Pd alloys, that part of the impurity resistivity arising from s-d scattering is similarly modified with temperature. In both cases the modifying factor is $(1-AT^2)$[119], where $A = \frac{\pi^2 k_B^2}{6}\left[3\left(1-\frac{1}{n(E)}\frac{dn(E)}{dE}\right)^2 - \frac{1}{n(E)}\frac{d^2n(E)}{dE^2}\right]_{E=E_F}$. Hence, in Pd-Ag the low temperature impurity resistivity $\rho_0(T)$ is given by $\rho_0(T) = \rho_0(0)(1-AT^2)$, which, in combination with an ideal resistivity that increases monotonically with temperature, results in a low-temperature minimum. At higher temperatures, the ideal resistivity is linear in T and the temperature dependence of the negative impurity resistivity term drops to a lower power dependence than $T^2$ as it must in order that the impurity resistivity not become negative. This change in T-dependence of the impurity resistivity can thus, in combination with the linear term, give rise to a second, higher-temperature minimum.

Pure Ni, like pure Pd, has a large resistivity which may be similarly attributed to a high density of d-states at the Fermi surface. Ahmad and Greig argue that since Cu-Ni alloys in the mid-range of compositions show the same resistivity behavior as does $Pd_{60}Ag_{40}$, their resistivity behavior can be explained by similar arguments. They contend that the absence of this behavior

in Rh-Ni makes scattering from giant moment clouds a less likely explanation for the observed behavior.

The following points can be made in regard to this argument:

1) The most pronounced low-temperature resistivity minimum in the Pd-Ag series occurs for $Pd_{60}Ag_{40}$[121]. The most pronounced low-temperature minimum in the Cu-Ni series occurs near $Cu_{56}Ni_{44}$ and is more than twice as deep as that occuring at $Cu_{65}Ni_{35}$, which Ahmad and Greig use as their basis for comparison. It is at least an order of magnitude greater than the minimum in $Pd_{60}Ag_{40}$. Moreover, while the high-temperature minimum in $Cu_{65}Ni_{35}$ is about twice as large as that of $Pd_{60}Ag_{40}$, the most pronounced high-temperature minima for Cu-Ni occur in the weakly ferromagnetic regime and are again roughly an order of magnitude greater than the corresponding minimum in $Pd_{60}Ag_{40}$.

2) While there are unfortunately no low temperature thermopower measurements available for the middle range of Pd-Ag concentrations to compare with our Cu-Ni measurements, it is known that the concentration dependence of the room temperature thermopower differs markedly in the two systems.[111,86] (See Fig. 29.) Coles[111] notes that curves of room temperature resistivity vs. composition for the two systems show similar differences. The Pd-Ag curve can be analyzed[122] into s-s and s-d

scattering contributions. The former contribution follows a c(1-c) dependence on the concentration c of one component, and the latter contribution is zero for Ag concentrations sufficiently large so that the d-band is completely full. The Cu-Ni curve does not admit to this simple analysis. This is not surprising since, as noted earlier, a rigid band treatment is invalid for Cu-Ni.

3) In a recent letter, Greig[123] acknowledges that while magnetic clusters could not be the cause of the Pd-Ag behavior they seem to be the most likely explanation for the Cu-Ni behavior, although he still considers the similarity between the resistivities in the two systems "something of a fly in the ointment." Interestingly, an opposite tack is taken by Edwards et al.[121] who conjecture that the Pd-Ag resistivity behavior arises from spin fluctuations in the local regions of exchange enhancement (non-critical), in rough analogy to the local critical exchange enhancement associated with giant moment clouds in Cu-Ni. These authors cite experimental evidence that the Pd and Ag d-states do not interact strongly and that the Pd d-states lie closer to the Fermi surface. They suggest that the Pd d-band broadens with increasing Pd concentration, and d-state holes emerge at the Fermi band at 50 at.% Pd. "Pockets of holes" will occur at the Fermi level, at

locally Pd-rich regions, characterized by an enhanced local d-spin susceptibility, and it is these, the authors argue, that are responsible for the resistivity behavior.

Whether or not this picture is valid for Pd-Ag, we feel that the arguments previously given support our contention that the resistivity and thermopower of Cu-Ni are associated with the occurrence of giant moment clouds, especially in light of the difference between the Cu-Ni and Pd-Ag systems noted in points (1) and (2) above. There remains the difficulty of explaining the differences between the transport behavior of Cu-Ni and Rh-Ni, and as indicated earlier, we believe there is a need for further theoretical work in this regard.

## VI. SUMMARY

We have measured the thermoelectric power between 4.2 and 300°K in one dilute (Ir-Fe) and two concentrated (Cu-Ni and Rh-Ni) magnetic alloys.

In the case of Ir-Fe, the most prominent feature of our results is an impurity-induced peak which increases in magnitude but does not broaden significantly with increasing Fe concentration. The peak occurs at the spin-fluctuation temperature $T_S$ determined by Kaiser and Doniach to be 28°K from resistivity data. The shape of the peak is similar to that observed in Pd-Ni and in contradistinction to what one expects for Kondo systems. Moreover, it is considerably removed from a Kondo temperature on the order of 100°K determined from susceptibility data. We conclude that the observed behavior is attributable to spin fluctuations, whereas the Kondo-Nagaoka picture does not give a satisfactory account of our observations. However, the Ir-Fe peak occurs at $T_S$, whereas the Pd-Ni peak occurs at $T_C \approx \frac{1}{4} T_S$, a characteristic temperature marking roughly the transition from $T^2$ to T dependence in the resistivity. We believe that further theoretical work is needed in this regard.

In our measurements on Cu-Ni and Rh-Ni, two concentrated magnetic alloy systems characterized by the existence of giant polarization clouds, we observe an extra low temperature contribution to the thermopower of Cu-Ni for a broad range of compositions straddling

the critical Ni concentration for ferromagnetism. The thermopower of Rh-Ni over a similar range of concentrations exhibits no extra contribution. We correlate our observations with the fact that an extra low temperature contribution occurs in the resistivity of Cu-Ni in the same range of concentrations, while no similar contribution is observed in the resistivity of Rh-Ni.

We have noted that the low-temperature resistivity in Cu-Ni shows Kondo-like behavior whereas the low-temperature resistivity of Rh-Ni shows the same T-dependence observed in dilute alloys characterized by local spin fluctuations. Interestingly, dilute Cu-Fe is a Kondo system, whereas dilute Rh-Fe is a local-spin-fluctuation system. Lederer and Mills calculated a Kondo-like minimum in Cu-Ni due to giant polarization clouds rather than single impurities as in dilute systems. This suggests that interpreting the extra contribution to the thermopower as a Kondo-like peak is not unreasonable. However, nothing analogous to the thermopower peak observed in dilute local spin fluctuation systems is observed in Rh-Ni, though we recognize the possibility that such an effect may simply be too small to have been detected within the accuracy of our experiment.

The difference in the transport behavior of Cu-Ni and Rh-Ni, both systems characterized by giant moment clouds and showing similar magnetic properties, is strik-

ing. A full understanding of these differences awaits further theoretical work.

## APPENDIX A: EXPERIMENTAL PROCEDURE

A brief outline of the experimental procedure was presented in Sec. III. The details of our procedure are given in this appendix.

### A. Samples

The Cu-Ni samples were the same samples used by Houghton *et al.*[92] for their resistivity measurements The samples were in the form of thin bars (roughly .75" x .04" x .04") cut from the same cold-worked ingots as those used by Kouvel and Comly[81,82], to measure susceptibility, and were similarly annealed and water-quenched. More specifically, the ingots as prepared by Kouvel and Comly were induction-melted and chill-cast under argon. Before being cut to shape, they were severely cold-rolled to break up any gross chemical inhomogeneity such as one associates with the dendritic structure of a cast alloy. The samples were then cut, annealed at 1000°C for 3 days, and water-quenched. The samples cut by Houghton *et al.* were similarly annealed and water-quenched.

The Rh-Ni samples were from the same source and were similarly prepared. These were also in the form of thin bars, typically about .80" x .04" x .03".

When it became necessary for us to re-anneal some of the Cu-Ni samples (See Sec. V-C), the samples were etched in nitric acid and washed with water then with

acetone. They were then annealed at 900°C in a vacuum of $10^{-6}$mm for 2 days in a set-up such as that shown schematically in Fig. 30. Before quenching, helium was bled gradually into the vacuum system until a pressure slightly greater than one atmosphere was reached, in order to prevent oxidation of the samples when the annealing system was opened to the atmosphere. The samples were then quenched as quickly as possible in a mixture of ice and salt-water.

The Ir and Ir-Fe samples were the same ones used by Sarachik for her resistivity measurements[54]. They were thin bars, typically .40" x .04" x .02". The alloys were prepared by arc melting the constituent elements in an arc furnace. High-purity elements were used. As Sarachik points out, "the consistency of sample preparation is demonstrated by the fact that the excess resistivity per percent Fe was found to be the same for Ir containing ½ and 1 at.% Fe."[54]

The Pd samples used for checking the accuracy of the thermopower measurements (See part C of this appendix) were prepared by the present author by arc-melting 99.99% pure palladium sponge into loaf-shaped ingots in an arc furnace under an argon atmosphere. Rod-shaped samples (roughly 1.00" x .045" x.025") were then cut from the ingots on a surface grinder with thin alumina blades.

B. Experimental Apparatus

The apparatus we used to measure thermoelectric power consists basically of three components -- the sample holder, the electronics, and the cryostat (plus vacuum system).

(1) The Sample Holder: A schematic diagram of the sample holder is shown in Fig. 31. The inset shows how the sample holder fits into the cryostat. The sample sits within an evacuated sample chamber (A in the diagram) and is anchored to the projecting portion of an OFC copper flange of large thermal mass (B). Immediately above the copper flange and in direct thermal contact with it is a chamber filled with activated charcoal (C) which is used in achieving the ambient temperature. (See notes on cryogenics below).

Several lines of metal tubing (D,E) provide uninterrupted vacuum-tight paths from the sample chamber through the top flange of the sample holder and out of the cryostat. Line 1 in the diagram is a vacuum line. Lines 2, 3, and 4 carry the electrical leads. Copper refrigerator tubing is used for the portions of these lines (E) passing through the charcoal chamber in order to maximize thermal contact between the charcoal and the sample chamber. Above the charcoal chamber, the copper tubing is soldered to the portions of the lines (D) which continue up to the top flange and out

of the cryostat. Thin-walled stainless steel tubing is used for the latter (¼"OD for line 1, 3/16"OD for 2, 3, and 4) to minimize thermal links with room temperature.

The copper portion of the vacuum line (1) is bent and joined to the stainless steel through a copper block (F). The bend functions as a radiation baffle. (The continuation G of the stainless steel tubing below the block is not part of the vacuum system and serves only for structural solidity.) The stainless steel tubing passes at intervals through thin brass flanges which serve as further radiation baffles. Styrofoam (I) surrounds the tubing below the top flange to further diminish thermal contact with room temperature.

Vacuum sealing of the sample space is achieved as follows. An indium O-ring seal (J) is used where the can (K) used to enclose the sample chamber (A) is joined to the OFC copper flange (B). The ends of the stainless steel tubes where the leads emerge (points 5, 6, and 7 in diagram) are sealed with Epoxy Adhesive 907 (made by Miller-Stephenson Chemical Co.)

Fig. 32 shows the activated charcoal chamber and the portion of the OFC flange which is enclosed in the sample chamber in greater detail. Labeling is the same as in Fig. 1. To prevent undesired electrical contacts, all copper surfaces within the sample chamber are coated

with General Electric 7031 adhesive and insulating varnish. The adhesive is thinned with an alcohol-toluene mixture and several coats are applied. After each application, the coated parts are dried in an oven for an hour at 100°C and then allowed to cool before the next coat is applied.

All leads entering the sample are then wound around the cylindrical projection (M) of the copper flange (which acts as a heat sink),and then around either of the two teflon posts (N) before being brought into contact with the sample. This allows us to introduce greater lengths of wire to maximize the thermal resistance of the leads. In addition, winding the leads about the copper heat sink assures that they are firmly anchored thermally to the ambient temperature.

All copper leads entering the sample holder are Leeds and Northrup best thermocouple grade #30 copper wire, which were found to minimize extraneous thermal voltages. The constantan used throughout is from Omega Engineering.

The sample is mounted and the various leads brought into contact with it as shown in Fig. 33. The teflon posts are omitted from this diagram for clarity. The sample is clamped to the heat sink as shown, so that the contact with the voltage lead (I) at point a is a pressure contact. The other voltage lead (V) also serves

as an element of the differential thermocouple which measures $\Delta T$. Leads IV, V and VIII are for the differential thermocouple, and leads II and III form one junction of the absolute thermocouple.

All thermocouple junctions are spot-welded. One junction of the differential thermocouple is then in turn spot-welded to the sample at point c. The other is attached to the heat-sink in close proximity to the sample at b, using the 7031 as an adhesive. The coating of 7031 on the heat sink allows good thermal contact while maintaining electrical insulation. One junction of the absolute thermocouple (which measures the ambient temperature) is anchored to the heat sink at d in the same manner. The other is immersed in an ice-and-water mixture (outside the cryostat) which provides a reference temperature.

A 42-ohm carbon resistor (f) with the insulation removed serves as a heater for imposing a temperature gradient across the sample. The resistor is wrapped in a single layer of cigarette paper, which is attached with 7031 varnish, and anchored to a small copper block g using the same varnish. The intent is once again to maintain good thermal contact while providing electrical insulation. The copper block is then soft-soldered to the sample at e. To insure that the sample is the major heat path from heater to heat sink, the heat is connected by lengths of #40 copper wire to the more substantial leads.

Outside the sample chamber (P in Fig. 31), 6 feet of 50 ohm/foot stainless steel wire (from Sigmund Cohen) are wrapped around the charcoal chamber and serve as a heater for raising the ambient temperature. (In practice, the ambient temperature rose quickly enough so that for ordinary runs the ambient heater was rarely used.) A carbon resistor resting on top of the charcoal chamber acts as a liquid $He^4$ level detector.

(2) Electronics: Fig. 34 shows a block diagram of the electronics, showing all lead connections. The section of the diagram above the horizontal dotted line shows the electronics outside the cryostat. The section of the diagram below the dotted line shows the circuitry within the sample chamber. Identifying letters and numbers here represent the same features as in Fig. 33. Junctions b and d are in thermal contact with but electrically insulated from the sample.

A DC power supply (Power designs Precision Power Source Model 2005) connected between VI and VII sends a small current through the resistor f, and the consequent Joule heating produces a temperature difference $\Delta T$ across the sample. The thermovoltage $\Delta V$ produced by $\Delta T$ across the sample (relative to copper -- see part C of this appendix) is measured directly between I and V using a Keithley #148 nanovoltmeter. The thermovoltage produced by $\Delta T$ in the Cu-constantan differential thermocouple is measured between IV and V using the same

nanovoltmeter. As will be seen in part C of this appendix, this latter thermovoltage is a measure of $\Delta T$.

The ambient temperature is determined by measuring the thermovoltage between junction d (anchored to the heat sink) and junction g (immersed in the ice-water mixture) of the absolute thermocouple. This measures the temperature difference between the ambient temperature and $0^{\circ}C$. Since these thermovoltages are on the order of thousands of microvolts, and since changes in ambient temperature between readings may represent a change of only a few microvolts, four-place accuracy is required in measuring these thermovoltages. For this reason a Leeds and Northrup K-3 Universal Potentiometer is used, and is connected between II and IX. The K-3 is in turn connected to a null detector which has microvolt accuracy or better. (At various times, a 147 Nanovolt Null Detector, a 149 Milli-Microvoltmeter, and a 150AR Microvolt Ammeter, all by Keithley Instruments, proved satisfactory for this purpose.)

Not shown in Fig. 34, since they connect with nothing within the sample chamber, are the following instruments: (1) a Kepco regulated DC power supply, which connects to the ambient heater, (2) a Simpson meter which connects to the carbon resistor used as a Liquid $He^4$ level detector, and (3) a Vacuum instrument Corporation cold cathode discharge gauge for measuring the pressure in the vacuum system which includes the

sample space.

3. Cryogenics and Vacuum System

The sample holder was designed to fit into the inner chamber of a commercial Sulfrian cryostat of standard design. Liquid helium is transferred until the level rises above the top of the charcoal chamber. A sharp rise in the resistance of the carbon resistor which serves as a level detector indicates when this has occurred.

The openwork section of the outer wall of the charcoal chamber (See Fig. 32), through which the chamber is filled, is screened in with copper mesh screening which allows access to the helium bath. When the helium is boiled off, the high heat of adsorption associated with the helium adsorbed by the charcoal prevents a rapid rise in the ambient temperature. When the temperature increases to 77°K, further increases in temperature may be halted (if desired) or slowed by the introduction of suitable quantities of liquid nitrogen to the inner chamber. Adsorption of nitrogen plays the same role in this temperature range that adsorption of helium does at lower temperatures.

The sample space is evacuated by an air-cooled diffusion pump to a pressure of about $5 \times 10^{-6}$mm of Hg.

C) Operating Procedure and Analysis of Data

The system is first pre-cooled with liquid nitrogen, and then sufficient liquid helium to cover the charocal chamber is transferred into the inner space of the cryostat. The resistance of the level detector increases from about 60$\Omega$ at above nitrogen temperature to about 4200$\Omega$ when it is immersed in liquid helium.

When sufficient time has elapsed (a few minutes) for thermal equilibrium to be reached within the sample chamber, the voltage across the absolute thermocouple is read, and is taken to be the thermovoltage between 4.2°K and 273°K (0°C) for a given run. Typically this value is 6255$\mu$V$\pm$3$\mu$V, depending somewhat on the run. The reading is then re-normalized (as are all subsequent ambient temperature readings) to be 0 at 0 K, in agreement with the calibration tables of Powell et al.[107], which we have used for our Cu-constantan thermocouples throughout.

The assumption that the sample is at 4.2°K when the charcoal chamber is immersed in helium is supported by the observation that the absolute thermocouple reading is unaffected if helium exchange gas is introduced into the sample space.

The power supply to the heater at the end of the sample is then turned on to impose a temperature gradient. Typical power supply settings (which may vary from sample to sample) range from about .50 volts maximum at 4.2°K

(when the heater resistance is about 2500Ω)to about .20 volts or less at room temperature (when the heater resistance is about 40 ). Hence, typical power inputs range from 0.1 mW at 4.2K to 1 mW at room temperature. The power supply setting for any given data reading was determined on an ad hoc basis to produce a suitable temperature difference, typically between 0.1 and 0.2 K.

For a typical data point, the ambient temperature T was obtained from the absolute thermocouple reading using the calibration tables of Powell et al. For each ambient temperature T, we then use the tables to find the thermopower $\frac{dV}{dT}$ of the Cu-constantan thermocouples for that temperature. We meanwhile get a reading for the thermocouple voltage across the differential thermocouple (denoted hereafter by $\Delta T(\mu V)$) and obtain the temperature difference in K(denoted hereafter by $\Delta T(^{o}K)$)using the fact that $\Delta T(^{o}K) = \frac{\Delta T(\mu V)}{dV/dT}$. We then obtain a value for $\Delta V$ directly in microvolts and can thus determine $S(=\frac{\Delta V}{\Delta T})$ in $\mu V/K$ at our ambient temperature.

Some aspects of the above procedures for finding S require further explanation. First of all, even when the power supply is off, $\Delta V$ and $\Delta T$ ($\mu V$) as read directly from the nanovoltmeter are not typically zero. It is not at all clear how much of the non-zero readings $(\Delta V)_o$ and $(\Delta T)_o$ are due to an actual temperature gradient and how much are due to extraneous thermovoltages in the leads running up to room temperature. However, it was

observed that if $\Delta V$ was plotted against $\Delta T$ for a fixed ambient temperature T and a varying temperature difference, one obtained a straight line, the slope of which could be taken as the thermoelectric power S. In practice, several temperature gradients were imposed for only a few ambient temperatures, to insure that we were in fact obtaining a straight line. For other temperatures, we simply measured $(\Delta V)_0$ and $(\Delta T)_0$ and then the values of $\Delta V$ and $\Delta T$ with a single non-zero power supply setting ( $(\Delta V)_1$ and $(\Delta T)_1$ respectively). The values of $\Delta V$ and $\Delta T$ used to calculate S are then given by $\Delta V=(\Delta V)_1-(\Delta V)_0$ and $\Delta T=(\Delta T)_1-(\Delta T)_0$.

Our procedure of taking S(T) to be the slope of $\Delta V$ vs. $\Delta T$ for several values of $\Delta T$ at a given T in order to avoid having to get rid of $\Delta V_0$ and $\Delta T_0$ electronically can be justified on two grounds. First, whatever part of $\Delta V_0$ and $\Delta T_0$ is attributable to an actual temperature difference across the sample will not alter the slope. Second, whatever part of $\Delta V_0$ and $\Delta T_0$ is attributable to extraneous thermovoltages in the leads between the ambient temperature and room temperature should not be affected significantly by the imposition of a temperature difference across the sample which is typically a few orders of magnitude smaller than the difference between T and room temperature.

Another factor in the determination of S which needs further explanation is the fact that the S we

determined by taking $S=\frac{\Delta V}{\Delta T}=\frac{(\Delta V)_1-(\Delta V)_0}{(\Delta T)_1-(\Delta T)_0}$ is not the absolute thermoelectric power of the sample, but rather the thermoelectric power of the sample relative to the thermocouple grade copper lead, i.e. $S_{measured}=S_{sample}-S_{Cu}$. Thus the absolute thermopower of the sample, which is our ultimate object, is given by $S_{sample}=S_{measured}+S_{Cu}$.

The values used for $S_{Cu}$ in calculations are essentially those given by the $S_{Cu}$ vs. T curve reported by Gainon and Sierro[124]. That the values they report are also applicable to our own copper leads is supported by the following:

To ensure that we were obtaining correct data for the samples we were investigating, we first performed our measurements on pure palladium, for which the thermoelectric power has been reported between 4.2°K and room temperature by several authors.[104,125] Our measurements reproduced published data to within 1 to 2%, after correcting for $S_{Cu}$. This is a routine matter at temperatures in the liquid nitrogen range and above, where thermopower measurements on various copper samples are generally in good agreement. At lower temperatures however, $S_{Cu}$ is highly sensitive to impurities, as is strikingly pointed out by Gold et al.[108] For example, the pronounced negative low temperature Kondo peak resulting from the introduction of small amounts of iron is well known. In this temperature range, however, the $S_{Cu}$ values required to give good agreement between

our data and published Pd data were essentially those reported by Gainon and Sierro. Their measurements were made on thermocouple grade copper leads used for thermopower measurements, and therefore were for copper wire of comparable purity to our own.

Our ability to reproduce the Pd data also gave us empirical justification for another aspect of our procedure. Each time the sample heater was turned on to produce a temperature gradient, some time was necessary for a quasi-steady state to be attained, so that if $(\Delta V)_0$ and $(\Delta T)_0$ were measured at time t, $(\Delta V)_1$ and $(\Delta T)_1$ were measured at $t + \Delta t$, where $\Delta t$ might be anywhere from 30 sec. or less at the bottom of our temperature range to 7 or 8 min. at room temperature. Since the ambient temperature changes slightly during the interval $\Delta T$, the background signals $(\Delta V)_0$ and $(\Delta T)_0$ change also. For this reason, after the heater is switched off at $t + \Delta t$, a second measurement of $(\Delta V)_0$ and $(\Delta T)_0$ is made at time $t + 2\Delta t$. The values of $(\Delta V)_0$ and $(\Delta T)_0$ used to obtain $\Delta V$ and $\Delta T$ are an average of their values at t and $t + 2\ t$. The fact that we can reproduce known results using this method seems to be sufficient justification for the method.

An indication of the rate at which the ambient temperature changes in different temperature ranges is given in Table 3. The rate of temperature increase

is sufficiently rapid to introduce a significant error in our measurements only between about 150 and 250°K and for about 3 or 4°K above about 24°K. An accurate picture of this latter range is obtained by repeated measurements and fitting to adjacent temperature ranges (which is quite simple for a range this small.) Somewhat larger errors are permissible for the 150-250°K range since none of the salient features of the S vs. T curves for the samples we have considered occur in this range.

After each few runs with unknown samples, we ran the Pd again to verify that we were still obtaining accurate measurements. Moreover, to make sure our data for the unknown samples was reproducible, each unknown sample was run at least twice. A greater number of runs was undertaken if the second run did not reproduce the first to within 1 to 2%.

It was found in the course of our early checks for reproducibility that our results were considerably affected by the repeated mechanical manipulation of the ends of the copper leads which came in contact with the samples. Such manipulation was necessary each time a fresh sample was mounted. This difficulty was largely eliminated by cutting off the battered ends of the leads and removing the insulation from adjacent fresh lengths each time a new sample was mounted. It was always possible to do this since the large lengths of wire wound around the teflon posts could be unwound when

the leads no longer reached the sample.

## REFERENCES


1. P. Lederer and D. L. Mills, Phys. Rev. 165, 837 (1968).

2. A. B. Kaiser and S. Doniach, Intern. J. Magnetism 1. 11 (1970).

3. N. Rivier and M. J. Zuckermann, Phys. Rev. Letters 21. 904 (1968)

4. D. K. C. MacDonald, Thermoelectricity: An Introduction to the Principles, Wiley, New York, 1962.

5. R. P. Huebener, in Solid State Physics (F. Seitz, D. Turnbull, and H. Ehrenreich, Eds.), Vol. 27, p. 63, Academic Press, New York, 1973.

6. On p. 9 of Ref. 4, it is noted that S may be understood as an entropy per unit charge of the conduction electrons. The entropy must be zero at T=0. Taking $dS=dQ/T=CdT/T$, one identifies Q with the Peltier heat $\pi$ and C with the Thomson heat $\mu$ which Thomson called a "specific heat of electricity." from the above, one gets $\pi=T \cdot S$ and $\mu=T\frac{dS}{dT}$.

7. J. W. Christian, J.-P. Jan, W. B. Pearson and I. M. Templeton, Proc. Roy. Soc. A 245, 213 (1958)

8. J. M. Ziman, Principles of the Theory of Solids, Cambridge University, Press, Cambridge, 1964.

9. J. M. Ziman, Electrons and Phonons, Clarendon Press, Oxford, 1962.

10. M. Bailyn, Advan Phys. 15, 179 (1966).

11. J. M. Ziman, Electrons in Metals: A Short Guide to the Fermi Surface, Taylor and Francis, London, 1963.

12. M. Bailyn, Phys. Rev. 126, 2040 (1962).

13. G. J. Van den Berg, in Progress in Low Temperature Physics (G. J. Gorter, Ed.) Vol. 4, Chap. 4, North Holland Publishing Company, Amsterdam, 1964.

14. M. D. Daybell and W. A. Steyert, Rev. Mod. Phys. 40, 380 (1968).

15. A. A. Abrikosov, Sov, Phys. Uspekhi 12, 168 (1969).

16. J. Kondo, in Solid State Physics (See Ref. 5), Vol. 23, p. 183, 1969.

17. A. J. Heeger, in Solid State Physics (See Ref. 5), Vol. 23, p. 283, 1969.

18. K. Fischer, in Springer Tracts in Modern Physics (Ed. G. Hohler) p. 2, Springer-Verlag, Berlin, 1970.

19. The entire contents of Magnetism (G. T. Rado and H. Suhl, Eds.), Vol. V, Academic Press, New York, 1973, is devoted to this problem.

20. J. Friedel, Nuovo Cimento Supplement 7, 287, (1958).

21. A. Blandin and J. Friedel, J. Phys. Rad. 20, 160 (1959).

22. J. Friedel, in Metallic Solid Solutions (J. Friedel and A. Guinier, Eds.), Chap. XIX, Benjamin, New York, 1963.

23. P. W. Anderson, Phys. Rev. 124, 41, (1961).

24. E. C. Stoner, Rep. Prog. Phys. 11, 43, (1948).

25. J. R. Schrieffer, City College Papers No. 10, The City College, New York, 1969.

26. J. Kondo, Prof. Theor. Phys. 32, 37, (1964).

27. J. R. Schrieffer, and P. A. Wolff, Phys. Rev. 149, 491 (1966).

28. K.-D. Schotte, Z. Physik 235, 155 (1970).

29. A. A. Abrikosov, Physics 2, 5 (1965).

30. Y. Nagaoka, Phys. Rev. 138, A1112 (1965).

31. J. Bardeen, L. N. Cooper, and J. R. Schrieffer, Phys. Rev. 108, 1175 (1957).

32. H. Suhl and D. Wong, Physics 3, 17 (1967).

33. H. Suhl, Phys. Rev. 138, A515 (1965); Physics 2, 39 (1965); Phys. Rev. 141, 483 (1966).

34. D. R. Hamann, Phys. Rev. 158, 570 (1967).

35. P. E. Bloomfield and D. Hamann, Phys. Rev. 164, 856 (1967)

36. P. W. Anderson and G. Yuval, in Ref. 19, p. 217.

37. J. R. Schrieffer, J. Appl. Phys. 38, 1143 (1967).

38. A. D. Caplin, Phys. Letters 26A, 46 (1967).

39. A. D. Caplin and C. Rizzuto, Phys. Rev. Letters 21, 746 (1967).

40. W. F. Brinkman and S. Engelsberg, Phys. Rev. 169, 417 (1968).

41. J. R. Schrieffer, J. Appl. Phys. 39, 642 (1968).

42. D.K.Wohlleben and B.R.Coles, in Ref. 19, p. 3.

43. S.Doniach and S.Engelsberg, Phys. Rev. Letters 17, 750 (1966).

44. D.L.Mills, M.T.Béal-Monod and P.Lederer, in Ref. 19, p. 89.

45. T. Izuyama, D.J.Kim and K.Kubo, J. Phys. Soc. Japan 18, 1025 (1963).

46. N.F.Berk and J.R.Schrieffer, Phys. Rev. Letters 17, 433 (1966).

47. H.Suhl, Phys. Rev. Letters 19, 442,(1967).

48. M.Levine and H.Suhl, Phys. Rev. 171, 567 (1968).

49. M.Levine, T.V.Ramakrishnan, and R.Weiner, Phys. Rev. Letters 20, 1370 (1968).

50. S.Q.Wang, W.E.Evenson, and J.R.Schrieffer, Phys. Rev. Letters 23, 92 (1969).

51. D.Shaltiel, J.H.Wernick and H.J.Williams, Phys. Rev. 135, 1346 (1964).

52. A.I.Schindler and C.A.Mackliet, Phys. Rev. Letters 20, 15,(1968).

53. A. I.Schindler and M.J.Rice, Phys. Rev. 164, 759 (1967).

54. M.P.Sarachik, Phys. Rev. 170, 679 (1968).

55. B.R.Coles, Phys. Letters 8, 243 (1964).

56. The linear variation of the resistivity with T is for temperatures sufficiently high for the paramagnon number to vary as T. This may be understood in direct analogy to the linear variation with T of the resistivity due to electron-phonon interactions in the range of temperatures where phonon number is linear in T, since both phonons and paramagnons are bosons.

57. A.B.Kaiser, Phys. Rev. B 3, 3040 (1971).

58. N.Rivier, M.Sunjic, and M.J.Zuckermann, Phys. Letters 28A, 492 (1969).

59. D.L.Mills and P.Lederer, J. Phys. Chem. Solids 27, 1805 (1966).

60. N.Rivier and V.Zlatić, J. Physics F 2, L87 (1972).

61. E.Babić, R.Krsnik, B.Leontić,Z.Vučić,I.Zorić, and C.A.Rizzuto, Phys. Rev. Letters 27, 805 (1972).

62. For example see:
A.Narath and H.T.Weaver, Phys. Rev. Letters 23, 233 (1969); L.Dworin, Phys. Rev. Letters 26, 1372 (1971); C.Rizzuto, E.Babic, and A.M.Stewart, J. Phys. F 3, 825 (1973).

63. P.W.Anderson and G.Yuval, in Ref. 19, p. 217.

64. D.R.Hamann and J.R.Schrieffer in Ref. 19, p. 237.

65. P.W.Anderson, G.Yuval, and D.R.Hamann, Phys. Rev. B 1, 4464 (1970).

66. M.Daybell, in Ref. 19, p. 121.

67. J.Kondo, Prof. Theor. Phys. 34, 372 (1965).

68. K.Fischer, Phys. Rev.158, 613 (1967).

69. A.B.Kaiser, private communication.

70. G.S.Knapp, J. Appl. Phys. 38, 1267 (1967).

71 C.L.Foiles and A.I.Schindler, Phys. Letters 26A, 154 (1968).

72. H.Nagasawa, J.Phys.Soc,Japan 25, 691 (1968).

73. J. E. Graebner, R. J. Schutz, F.S.L. Hsu, J.J. Rubin, W. A. Reed, and R. J. Higgins, Bull, Am. Phys. Soc., Series II 19, 304 (1974).

74. J.R.Cooper. E. Babić, and C. Rizzuto, to be published.

75. T.H.Geballe, B.T.Matthias, A.M.Clogston, H.J. Williams, R.C.Sherwood, and J.P.Maita, J. Appl. Phys. 37, 1181 (1966).

76. G. Chouteau, R. Fourneaux, R. Tournier, and P. Lederer, Phys. Rev. Letters 21, 1082 (1968).

77. S. Engelsberg, W. F.Brinkman, and S. Doniach, Phys. Rev. Letters 20,1040 (1968).

78. M.V.Vedernikov, Advan. Phys. 18, 337 (1969).

79. P. Lederer and D.L.Mills, Phys. Rev. Letters 20, 1036 (1968).

80. C.A.Mackliet, A.I.Schindler, and D.J.Gillespie, Phys. Rev. B1, 3283 (1970).

81. T.J.Hicks, B. Rainford, J.S.Kouvel, G.G.Low, and J.B.Comly, Phys. Rev. Letters 22, 531 (1969).

82. J.S.Kouvel and J.B.Comly, Phys. Rev. Letters 24, 598 (1970).

83. S. Foner and E.J.McNiff, Jr., unpublished.

84. N.D.Lang and H. Ehrenreich, Phys. Rev. 168, 605 (1970).

85. G.G.Low and T.M.Holden, Proc. Phys. Soc. 89, 119 (1966).

86. P.A.Schroeder,R. Wolf, and J.A.Woollam,Phys. Rev. 138, A105 (1965).

87. G.L.Guthrie, S.A.Friedberg, and J.E.Goldman, Phys. Rev. 113, 45 (1959).

88. C.G.Robbins, H. Claus, and P.A.Beck, J. Appl. Phys. 40, 2269 (1969).

89. E. Bucher, W.F.Brinkman, J.P.Maita, and H.J.Williams, Phys. Rev. Letters 18, 1125 (1967).

90. K. Schröder, J. Appl. Phys. 32, 880 (1961).

91. R.W.Houghton, M.P.Sarachik, and J.S.Kouvel, Phys. Rev. Letters 25, 238 (1970).

92. R.W.Houghton, M.P.Sarachik, and J.S.Kouvel, Solid St. Comm. 8, 943 (1970).

93. R.W.Houghton, M.P.Sarachik, and J.S.Kouvel, Solid St. Comm. 10, 369 (1972).

94. M. Fibich and A. Ron, Phys.Rev. Letters 25, 296 (1970).

95. M. Fibich and A. Ron, J. Physique 32, Colloq. C1, C1-748 (1971).

96. K. Levin and D.L.Mills, to be published.

97. C.G.Robbins, H. Claus, and P.A.Beck, Phys. Rev. Letters 22, 1307 (1969).

98. S.A.Ahern, M.J.C.Martin, and W. Sucksmith, Proc. Roy. Soc. (London) Sec. A 248, 145 (1958).

99. A.J.P.Meyer and C. Wolff, Compt. Rend. 246, 576 (1958).

100. J.P.Perrier, B. Tissier, and R. Tournier, Phys. Rev. Letters 24, 313 (1970).

101. A.T.Aldred, B.D.Rainford, T.J.Hicks, and J.S. Kouvel, Phys. Rev. B 7, 218 (1973).

102. P. Chevenard, J. Inst. Metals 36, 39 (1926).

103. H.M.Ahmad and D. Greig, to be published (I).

104. N. Cusack and P. Kendall. Proc. Phys. Soc. 72, 898 (1958).

105. D. Greig and J.P.Harrison, Phil. Mag. 12, 71 (1965).

106. D.R.Zrudsky and A.B.Showalter, Phys. Letters 45A, 105 (1973).

107. R.L.Powell, M.D.Bunch, and R.J.Corruccini, Cryogenics 1, 139 (1961).

108. A.V.Gold, D.K.C.MacDonald, W.B.Pearson and I.M. Templeton, Phil. Mag. 5, 765 (1960).

109. The author would like to acknowledge conversations about commercial constantan with Mr. John Berger of the Instrument Society of America, Pittsburgh, Pa., and Mr. E. Zysk of Engelhard Minerals and Chemicals, Menlo Park, N.J.

110. Standard Practices for Instrumentation, ISA-RP1, p. 13, Instrument Society of America, Pittsburgh, 1963.

111. B.R.Coles, Proc. Phys. Soc. B, 65, 221 (1952), and later reproduced in Ref. 9, p. 401.

112. S. Legvold, D.T.Peterson, P. Burgardt, R.J.Hofer, B. Lundell, and T.A.Vyrostek, to be published.

113. J.B.Sousa, M.R.Chaves, R.S.Pinto and M.F.Pinheiro, J. Phys. F. 2, L83 (1972).

114. M.E.Fisher, and J.S.Langer, Phys. Rev. Letters 20, 665 (1968).

115. G.A.Thomas, K. Levin, and R.D.Parks, Phys. Rev. Letters 29, 1321 (1972).

116. R. Fletcher and D. Greig, Phil. Mag. 17, 21 (1968).

117. F.J.Blatt, D.J.Flood, V. Rowe, P.A.Schroeder, and J.E.Cox, Phys. Rev. Letters 18, 395 (1967).

118. H.M.Ahmad and D. Greig, to be published (II).

119. B.R.Coles and J.C.Taylor, Proc. Roy. Soc. A, 267 (1962).

120. H. Jones, Handbuch der Physik 19, 227 (1956).

121. L.R.Edwards, C.W.Chen, and S. Legvold, Solid St. Comm. 8, 1403 (1970).

122. N.F.Mott and H. Jones, The Theory of the Properties of Metals and Alloys, Dover, New York, 1958.

123. D. Greig, Private Communication, Sept. 17, 1973.

124. D. Gainon and J. Sierro, Helvetica Acta Physica 43, 541 (1970).

125. R. Fletcher and D. Greig, Phys. Letters 17, 6 (1965).

126. J.C.Taylor and B.R.Coles, Phys. Rev. 102, 27 (1956).

| Alloy | $T_C$ (°K) | $T_S$ (°K) |
|---|---|---|
| Pd-Ni | 19 | 76 |
| Ir-Fe | 7 | 28 |
| Rh-Fe | $< 0.4$ | $< 1.6$ |

TABLE 1

| Alloy Comp. (at.% Ni) | $\rho$(1.75 K) ($\mu\Omega$-cm) | $\Delta\rho(\Delta T)$ ($\mu\Omega$-cm) | $\Delta\rho(\Delta H)$ ($\mu\Omega$-cm) | C (%) |
|---|---|---|---|---|
| 42 | 47.1 | 0.258 | 0.309 | 0.236 |
| 40 | 45.8 | 0.243 | 0.199 | 0.169 |
| 38 | 44.3 | 0.208 | 0.106 | 0.092 |
| 36 | 42.9 | 0.160 | 0.0566 | 0.045 |
| 34 | 39.5 | 0.102 | 0.0224 | 0.023 |
| 32 | 37.5 | 0.062 | 0.0117 | 0.012 |
| 30 | 34.4 | 0.032 | 0.0048 | -- |

TABLE 2

| T (°K) | $\frac{dT}{dt}$ (°K/minute) |
|---|---|
| 5 | 0.1 |
| 10 | 0.2- |
| 15 | 0.2 |
| 20 | 0.1 |
| 25 | 1.0 |
| 30 | 0.6 |
| 40 | 0.4 |
| 50 | 0.4 |
| 60 | 0.4 |
| 70 | 0.4 |
| 80 | 0.2 |
| 100 | 0.05 |
| 125 | 0.02½ |
| 145 | 0.5 |
| 160 | 0.8 |
| 175 | 0.8 |
| 200 | 0.7 |
| 245 | 0.4 |
| 260 | 0.3 |

TABLE 3

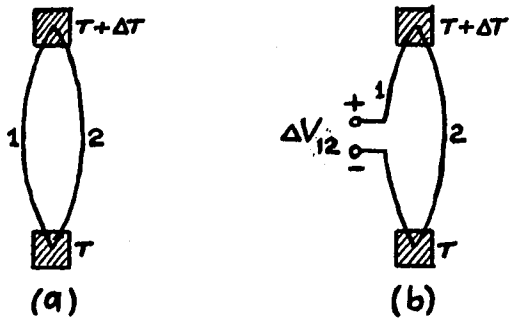


FIGURE 1: Basic Thermoelectric Circuits

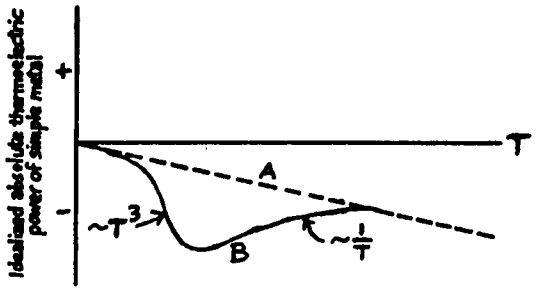


FIGURE 2

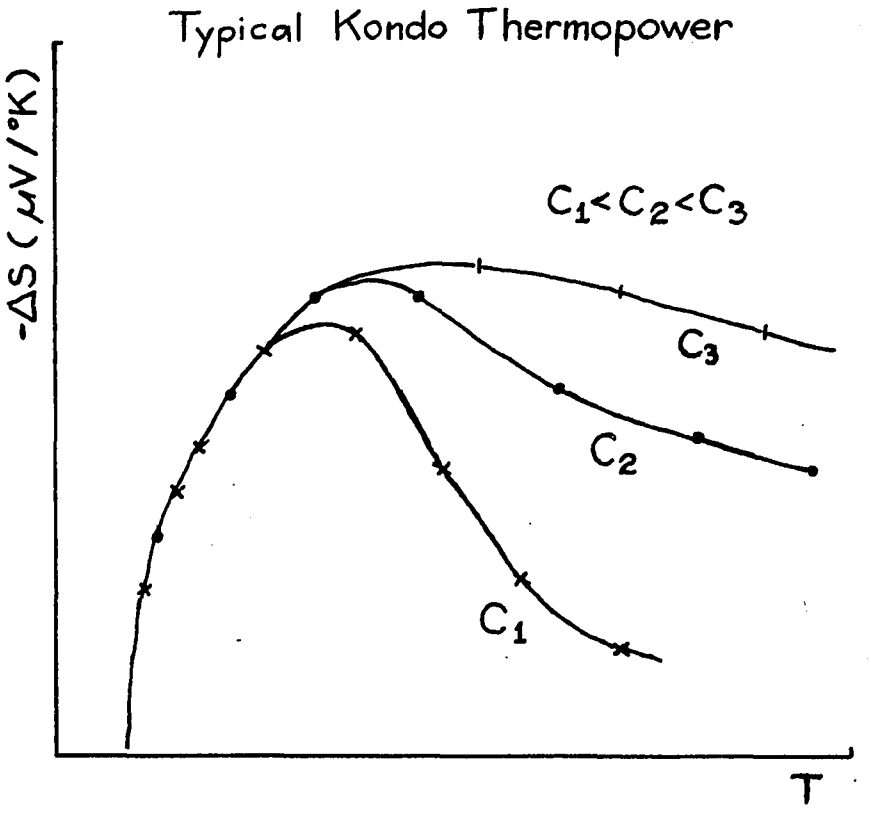


FIGURE 3

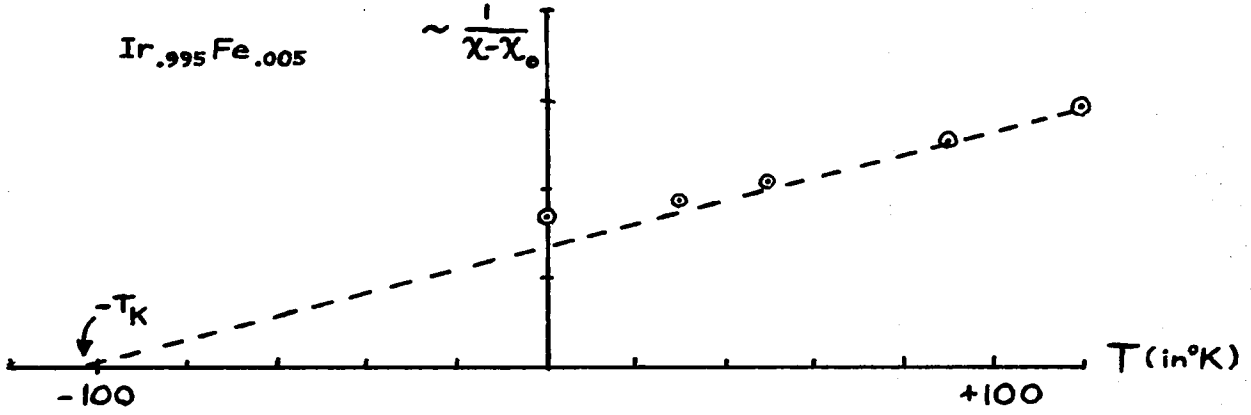


FIGURE 4

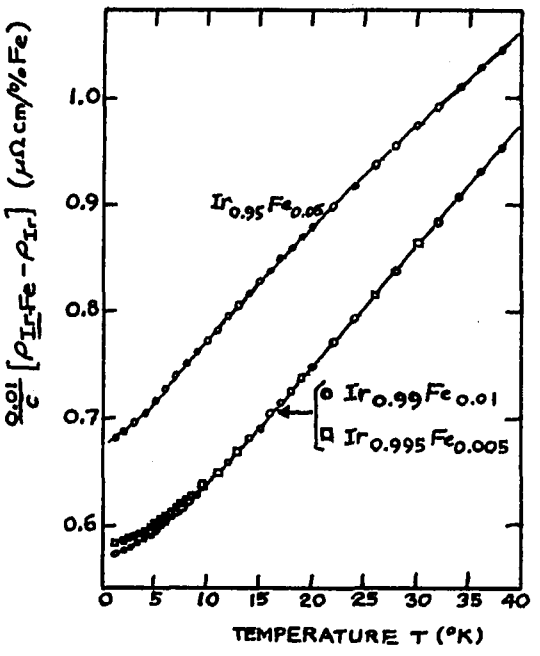


FIGURE 5

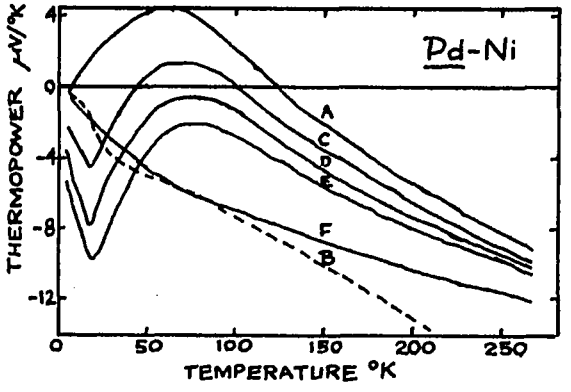


FIGURE 6

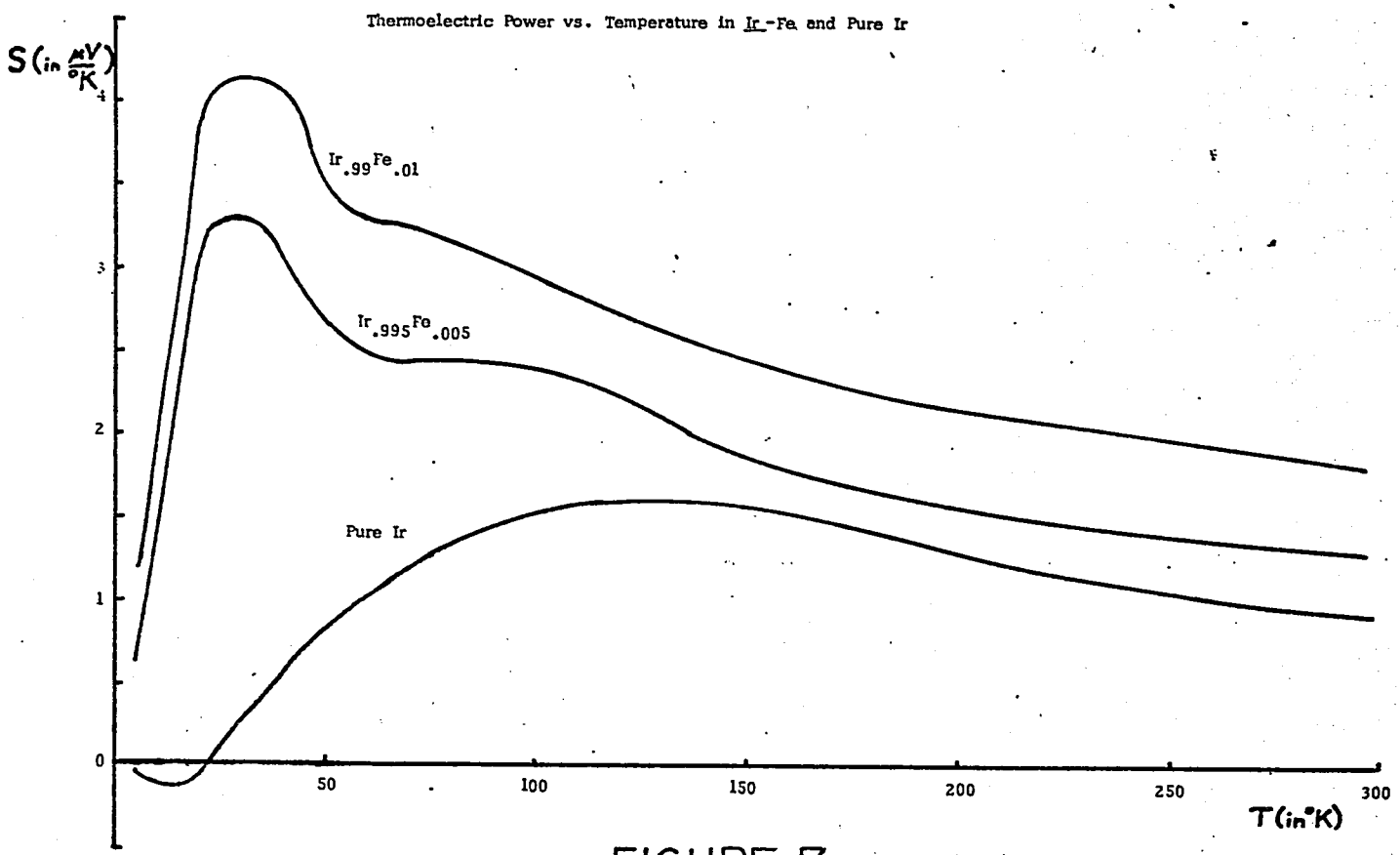
Thermoelectric Power vs. Temperature in Ir-Fe and Pure Ir
S(in μV/°K)
Ir.99Fe.01
Ir.995Fe.005
Pure Ir
0
1
2
3
4
50
100
150
200
250
300
T(in°K)

FIGURE 7a

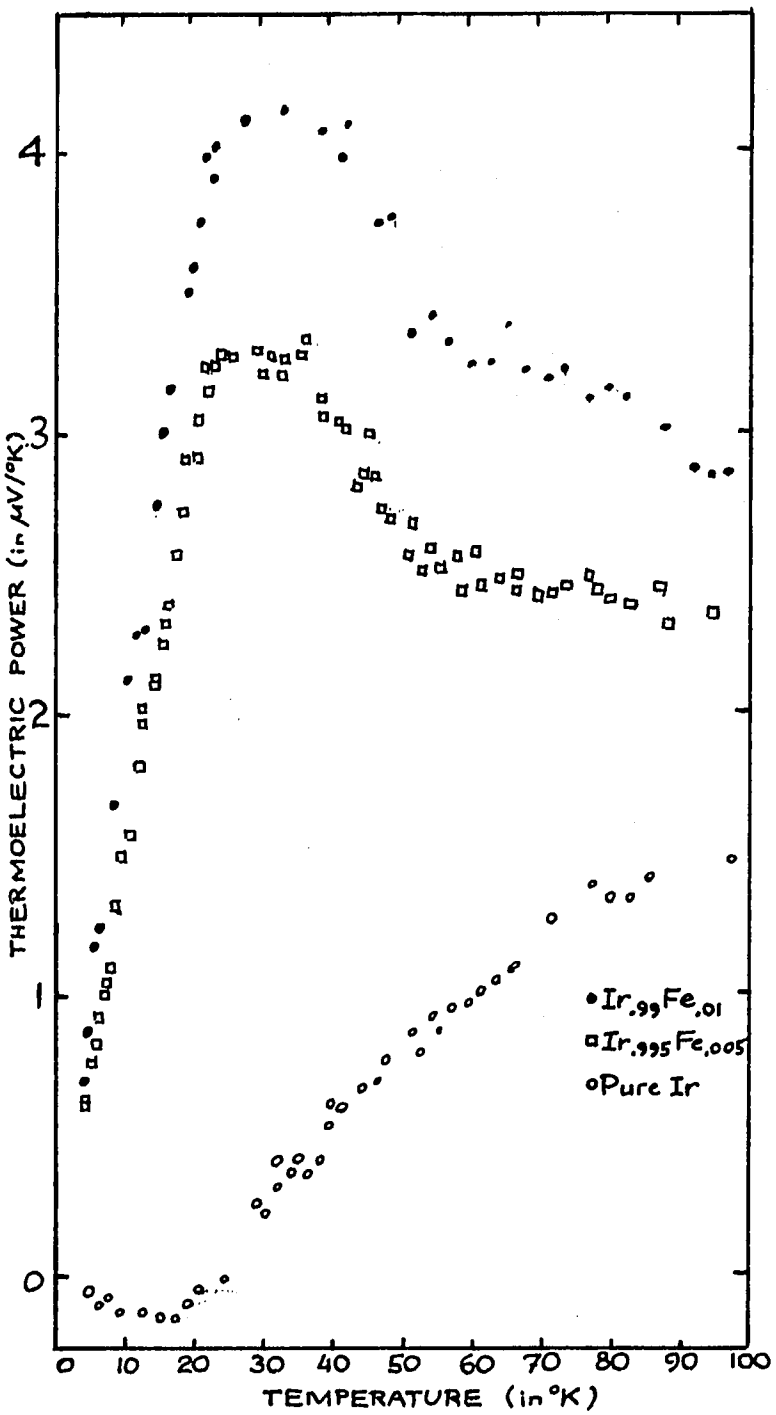
THERMOELECTRIC POWER (in μV/°K)
TEMPERATURE (in °K)
0
1
2
3
4
0
10
20
30
40
50
60
70
80
90
100
•Ir.99Fe.01
□Ir.995Fe.005
○Pure Ir

FIGURE 7b

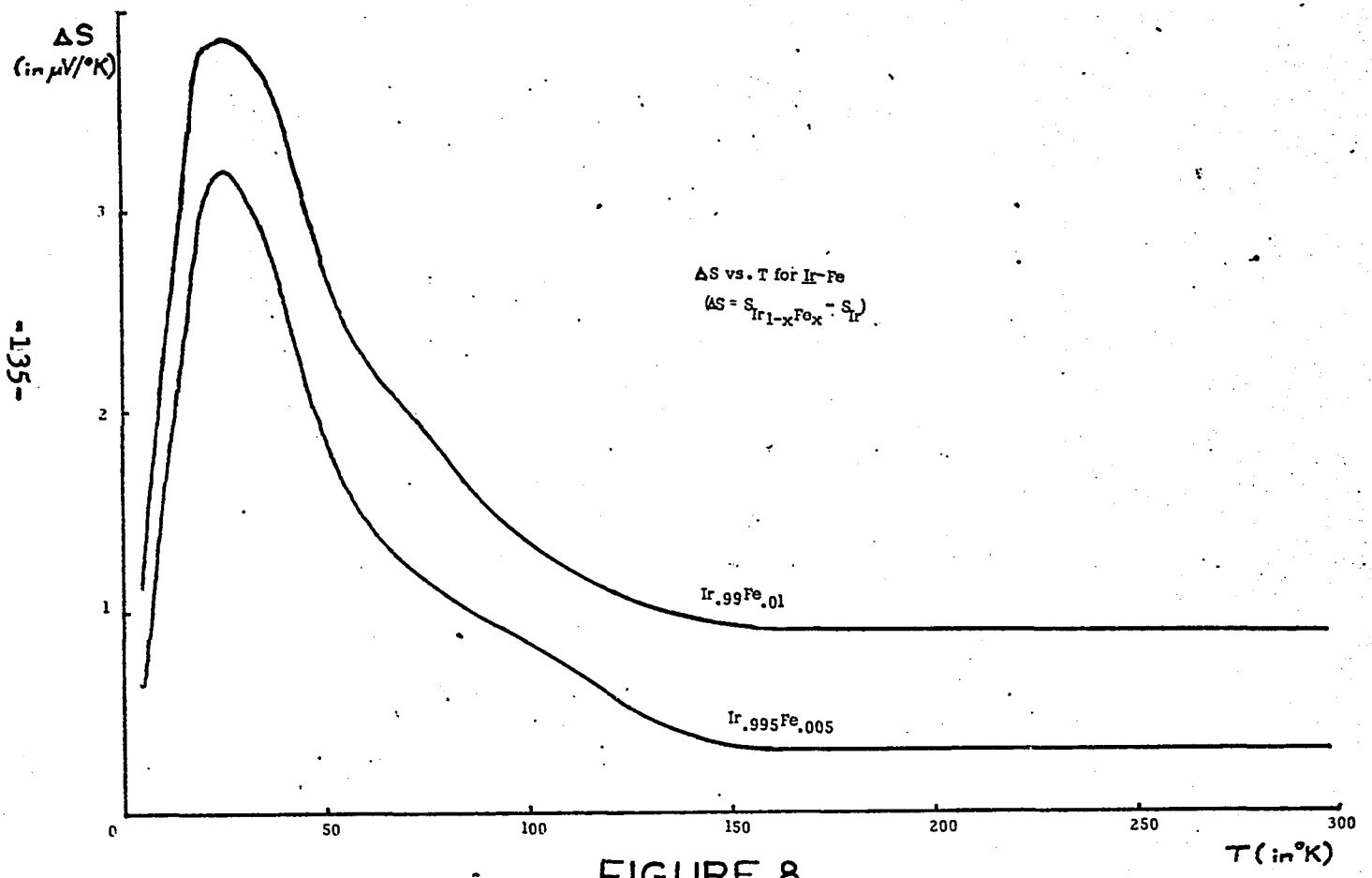
ΔS
(in μV/°K)
3
2
1
0
50
100
150
200
250
300
T (in °K)
ΔS vs. T for Ir-Fe
(ΔS = S_{Ir1-xFex} - S_Ir)
Ir.99Fe.01
Ir.995Fe.005

FIGURE 8

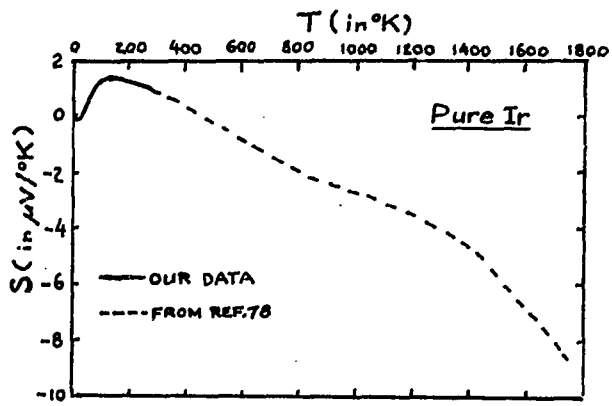
T (in °K)
0
200
400
600
800
1000
1200
1400
1600
1800
2
0
-2
-4
-6
-8
-10
S (in μV/°K)
Pure Ir
OUR DATA
FROM REF.78

FIGURE 9

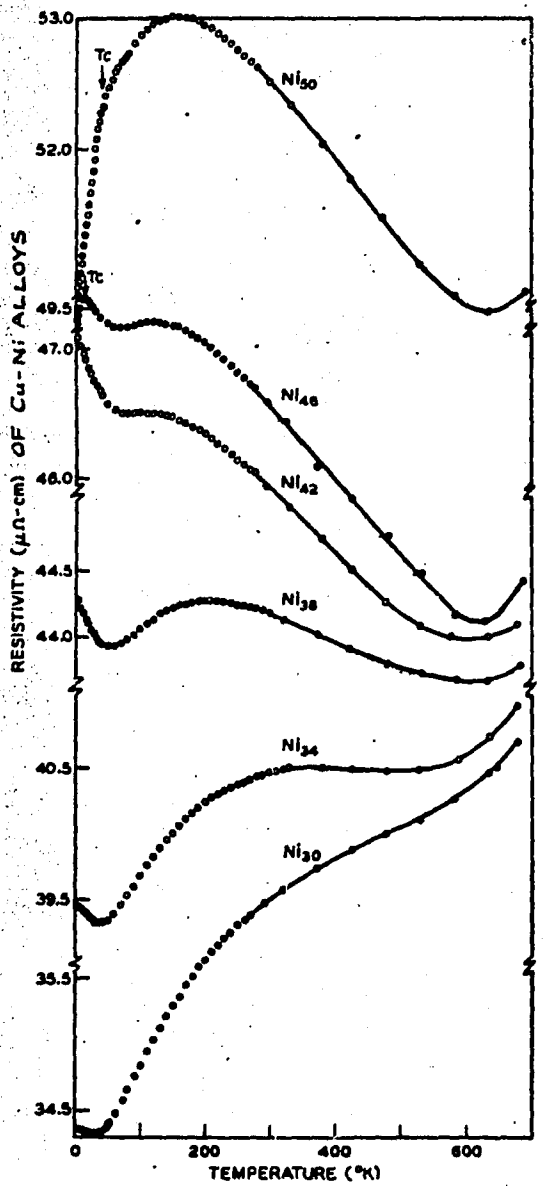
RESISTIVITY (μΩ-cm) OF Cu-Ni ALLOYS
TEMPERATURE (°K)
Tc
Tc
Ni50
Ni46
Ni42
Ni38
Ni34
Ni30
53.0
52.0
49.5
47.0
46.0
44.5
44.0
40.5
39.5
35.5
34.5
0
200
400
600

FIGURE 10

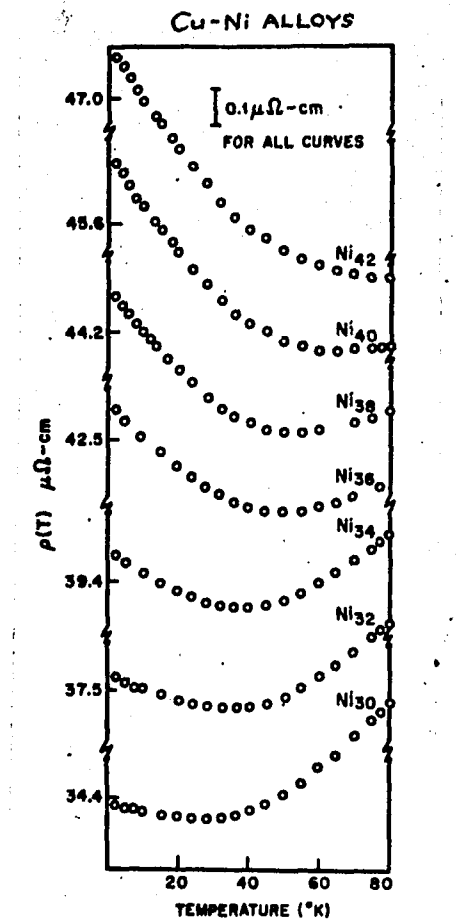


FIGURE 11

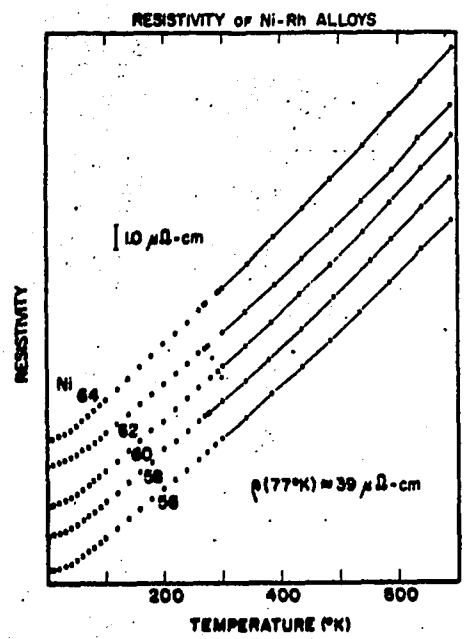


FIGURE 12

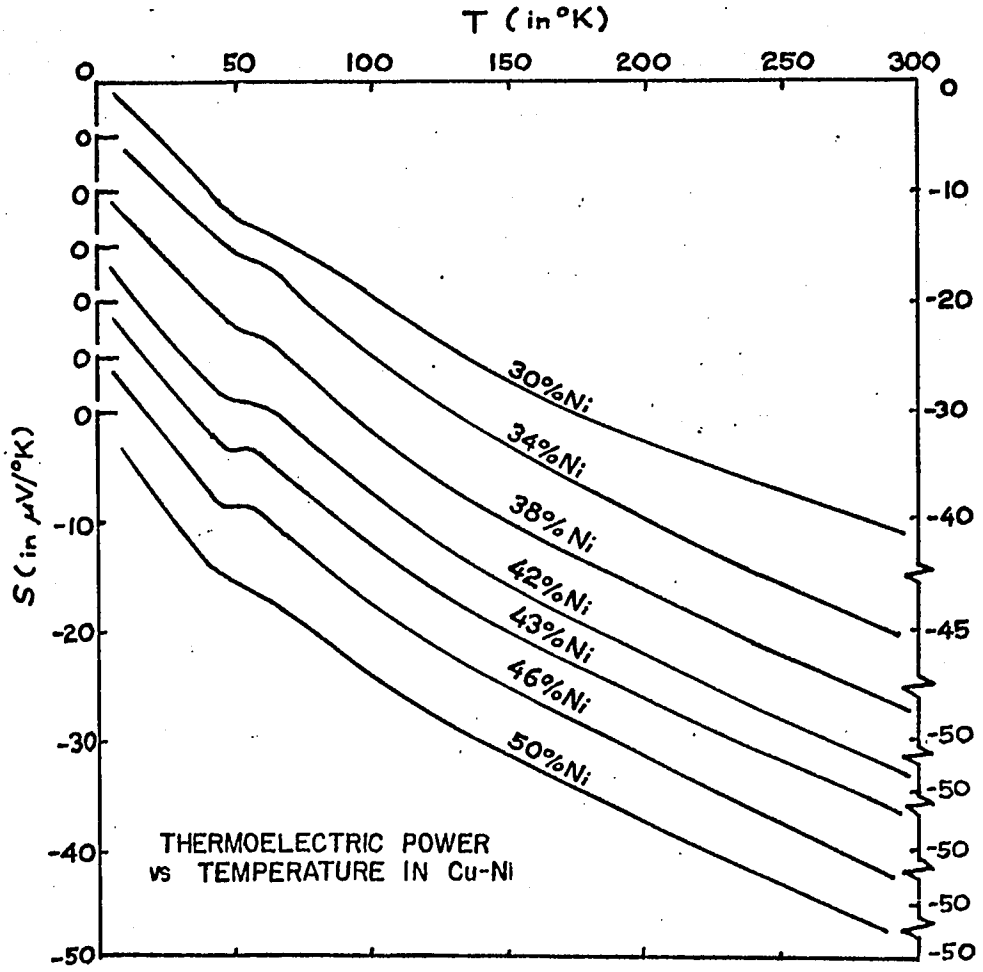
T (in °K)
0
50
100
150
200
250
300
S (in μV/°K)
0
-10
-20
-30
-40
-50
30%Ni
34%Ni
38%Ni
42%Ni
43%Ni
46%Ni
50%Ni
THERMOELECTRIC POWER
vs TEMPERATURE IN Cu-Ni

FIGURE 13

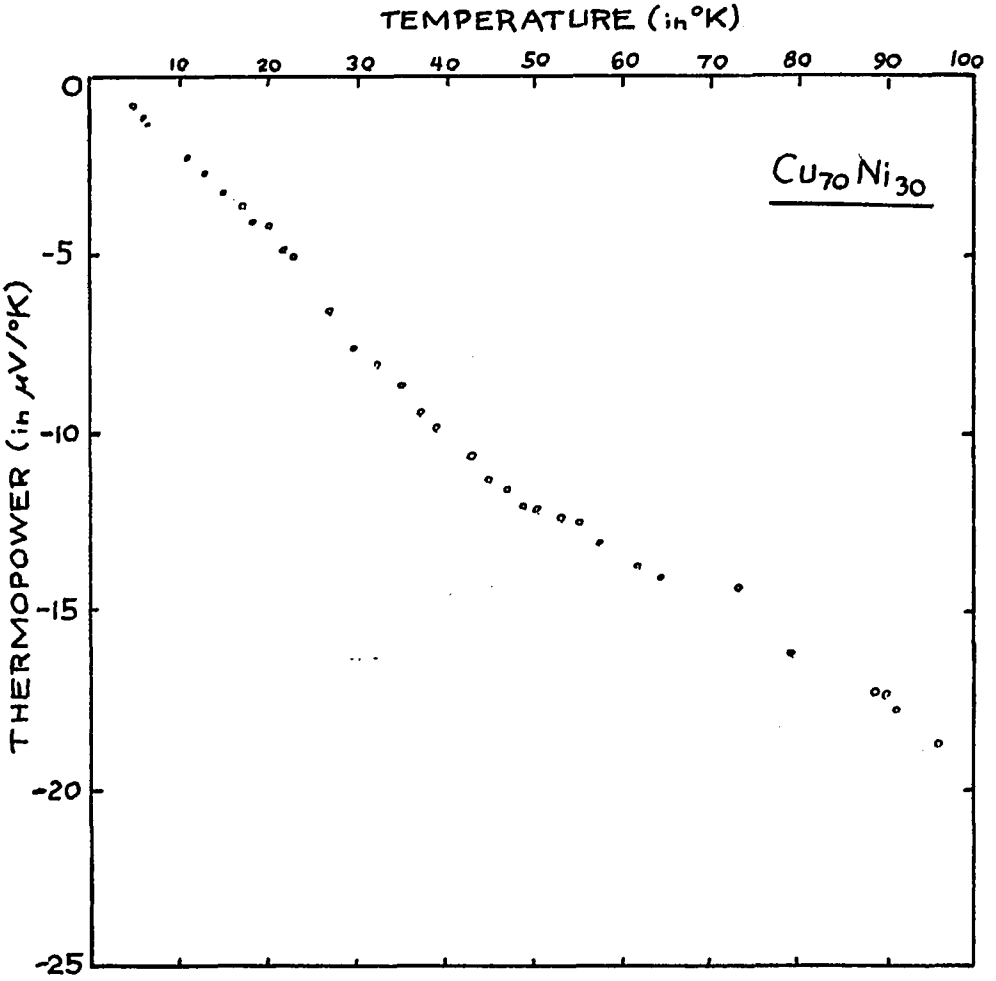
TEMPERATURE (in °K)
10
20
30
40
50
60
70
80
90
100
0
-5
-10
-15
-20
-25
THERMOPOWER (in μV/°K)
Cu70 Ni30

FIGURE 14

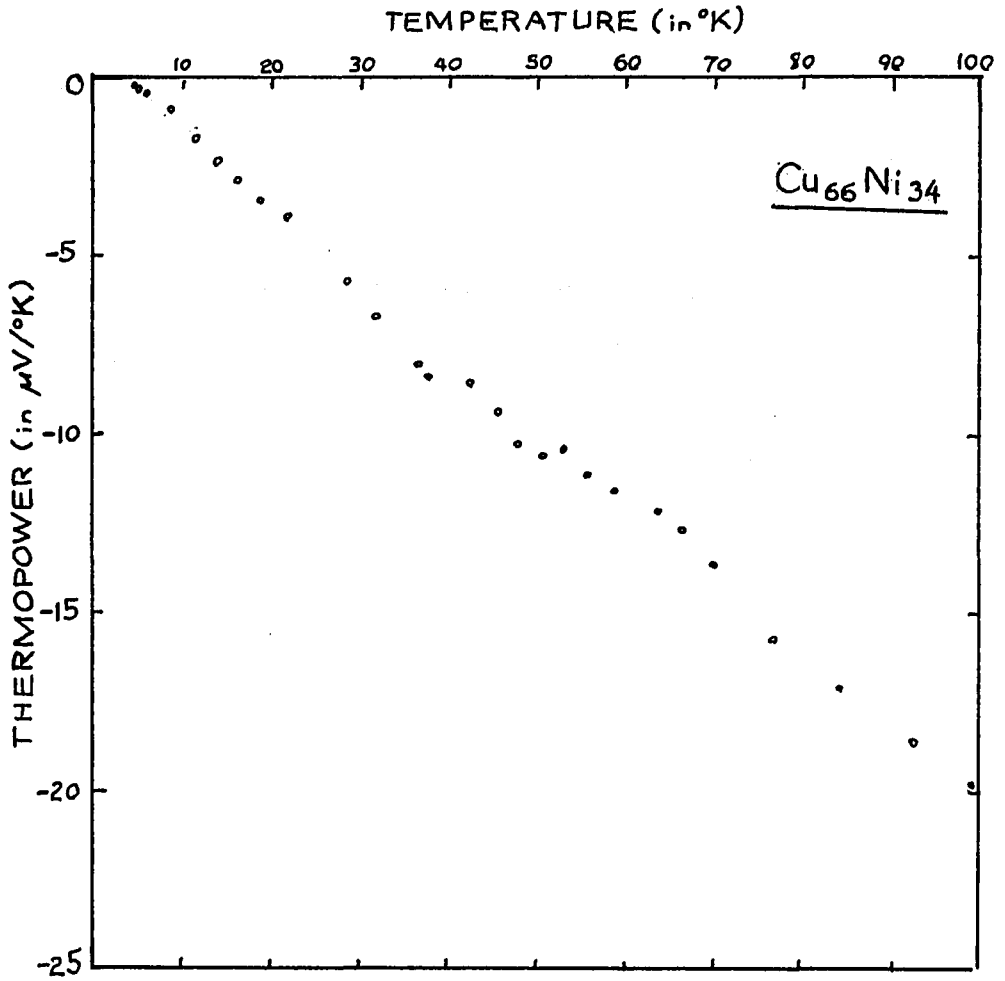
TEMPERATURE (in °K)
10
20
30
40
50
60
70
80
90
100
0
-5
-10
-15
-20
-25
THERMOPOWER (in μV/°K)
Cu66Ni34

FIGURE 15

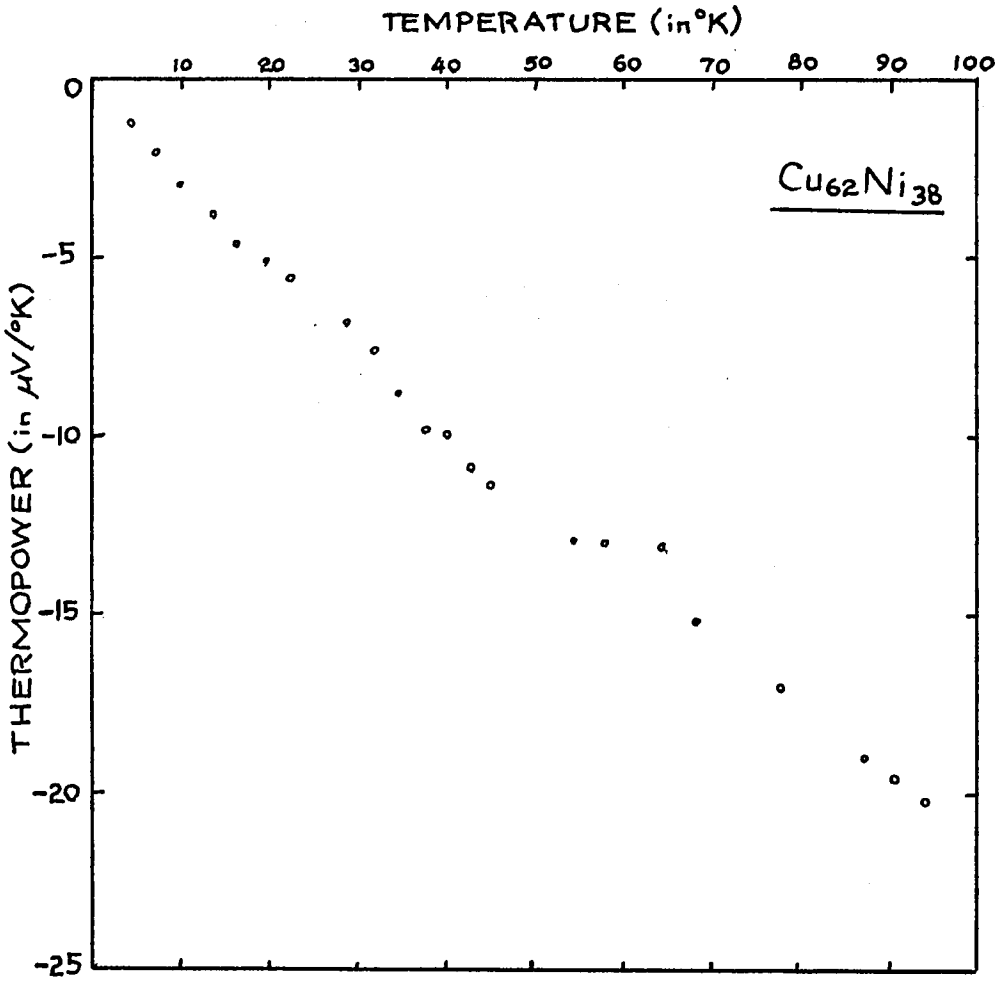
TEMPERATURE (in °K)
10
20
30
40
50
60
70
80
90
100
0
-5
-10
-15
-20
-25
THERMOPOWER (in μV/°K)
Cu62Ni38

FIGURE 16

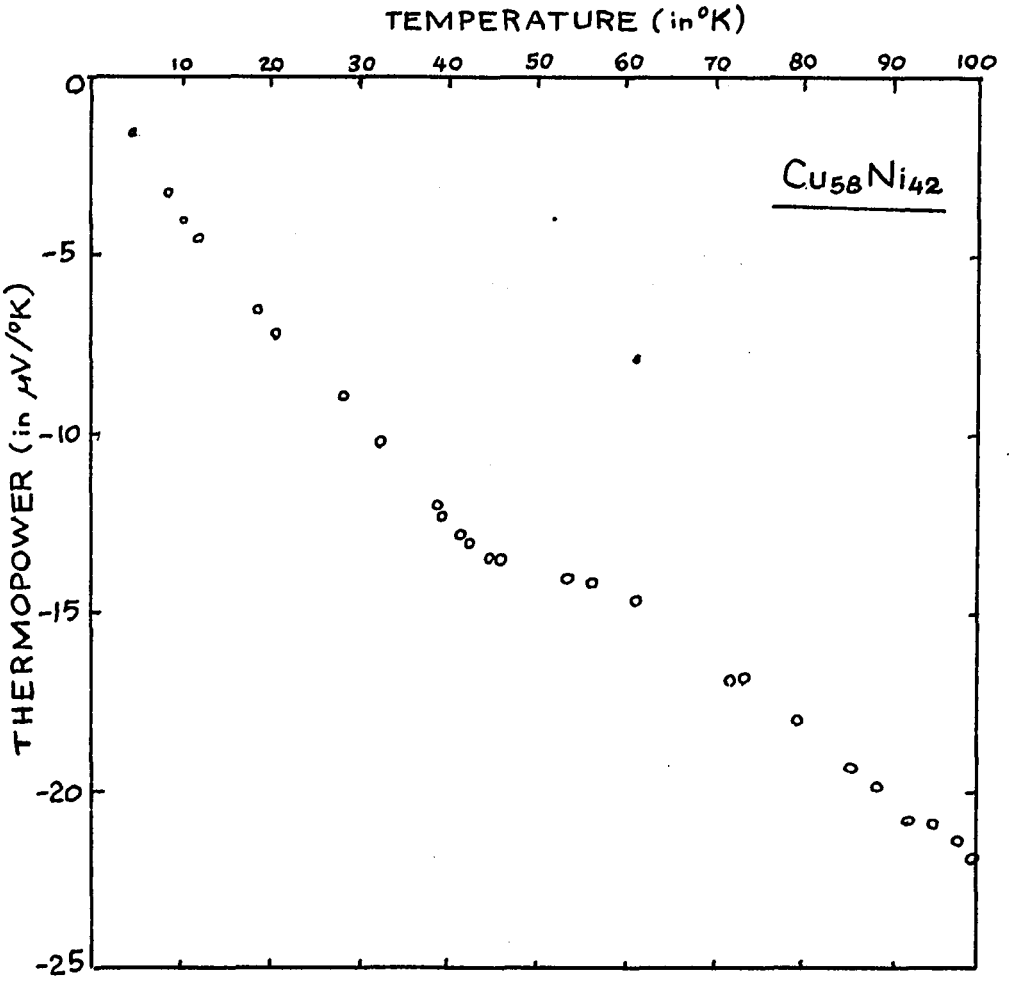
TEMPERATURE (in °K)
10
20
30
40
50
60
70
80
90
100
0
-5
-10
-15
-20
-25
THERMOPOWER (in μV/°K)
Cu58Ni42

FIGURE 17

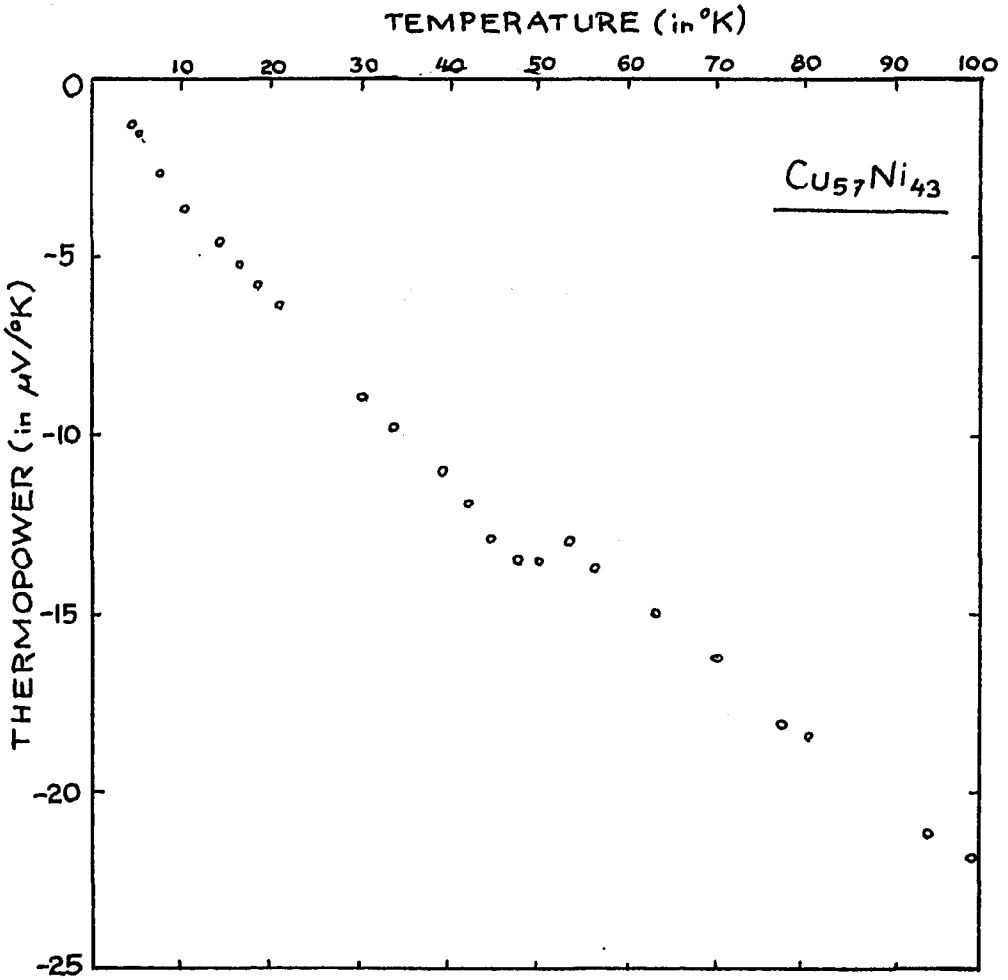
TEMPERATURE (in °K)
10
20
30
40
50
60
70
80
90
100
0
-5
-10
-15
-20
-25
THERMOPOWER (in μV/°K)
Cu57Ni43

FIGURE 18

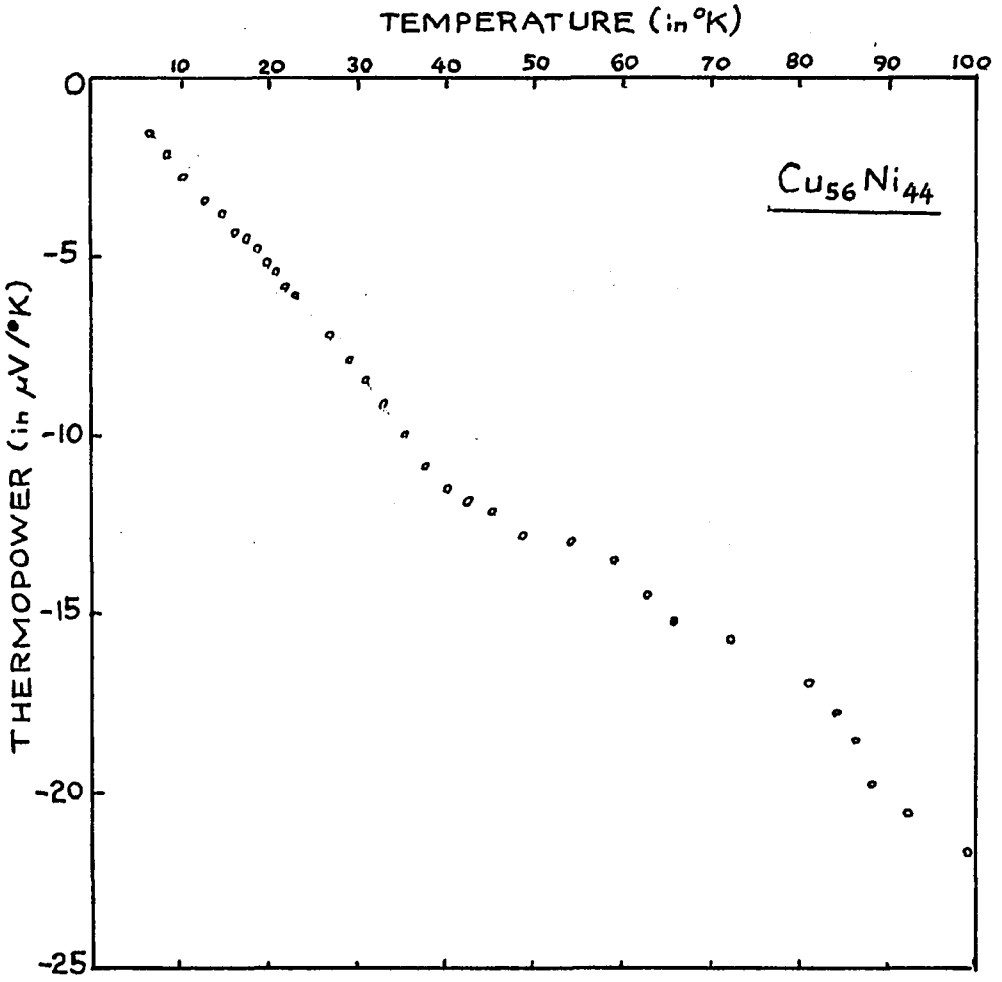
TEMPERATURE (in °K)
10
20
30
40
50
60
70
80
90
100
0
-5
-10
-15
-20
-25
THERMOPOWER (in μV/°K)
Cu56Ni44

FIGURE 19

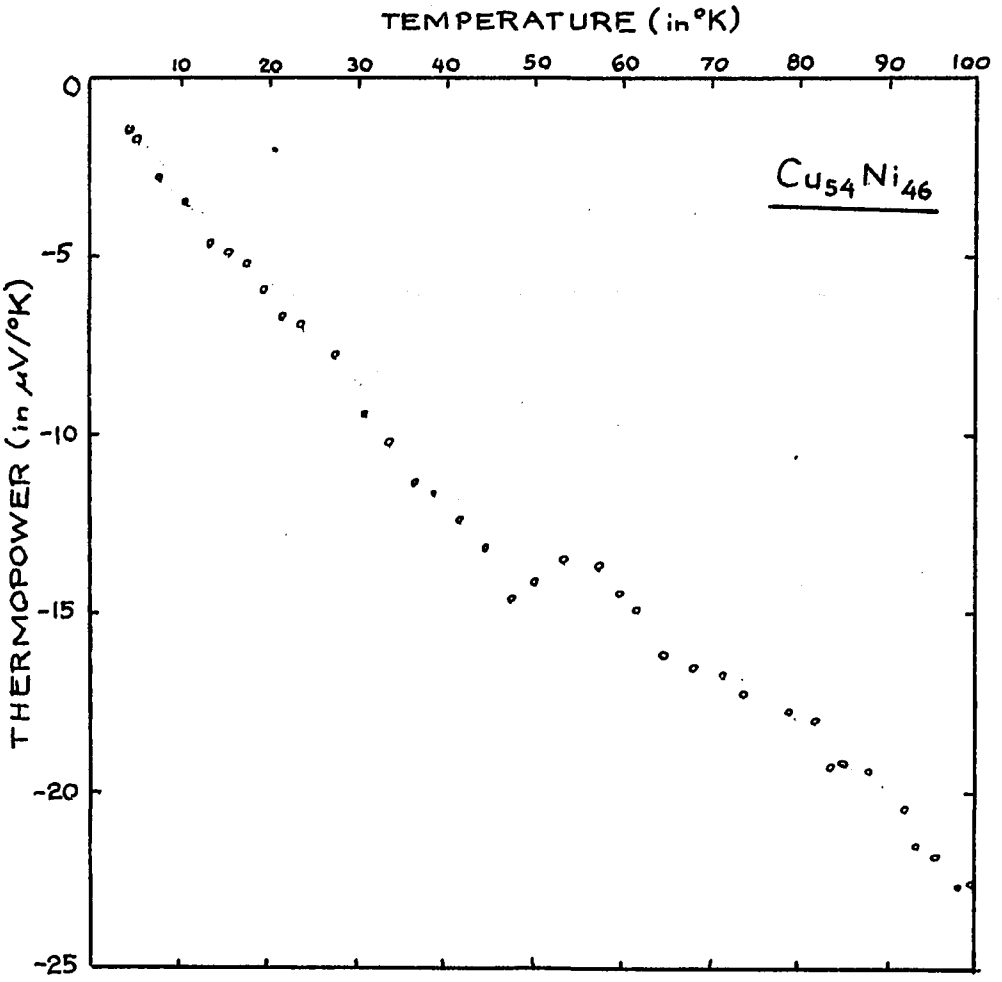
TEMPERATURE (in °K)
10
20
30
40
50
60
70
80
90
100
0
-5
-10
-15
-20
-25
THERMOPOWER (in μV/°K)
Cu54Ni46

FIGURE 20

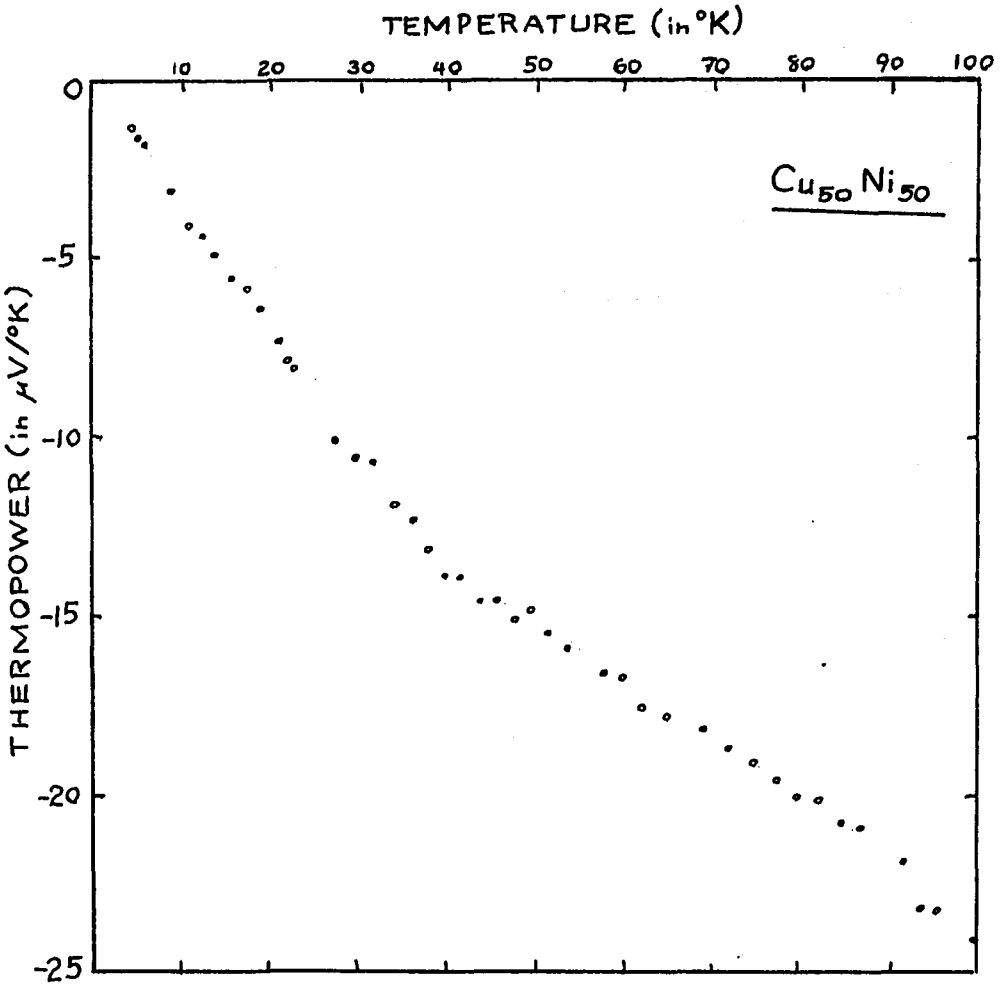
TEMPERATURE (in °K)
10
20
30
40
50
60
70
80
90
100
0
-5
-10
-15
-20
-25
THERMOPOWER (in μV/°K)
$Cu_{50}Ni_{50}$

FIGURE 21

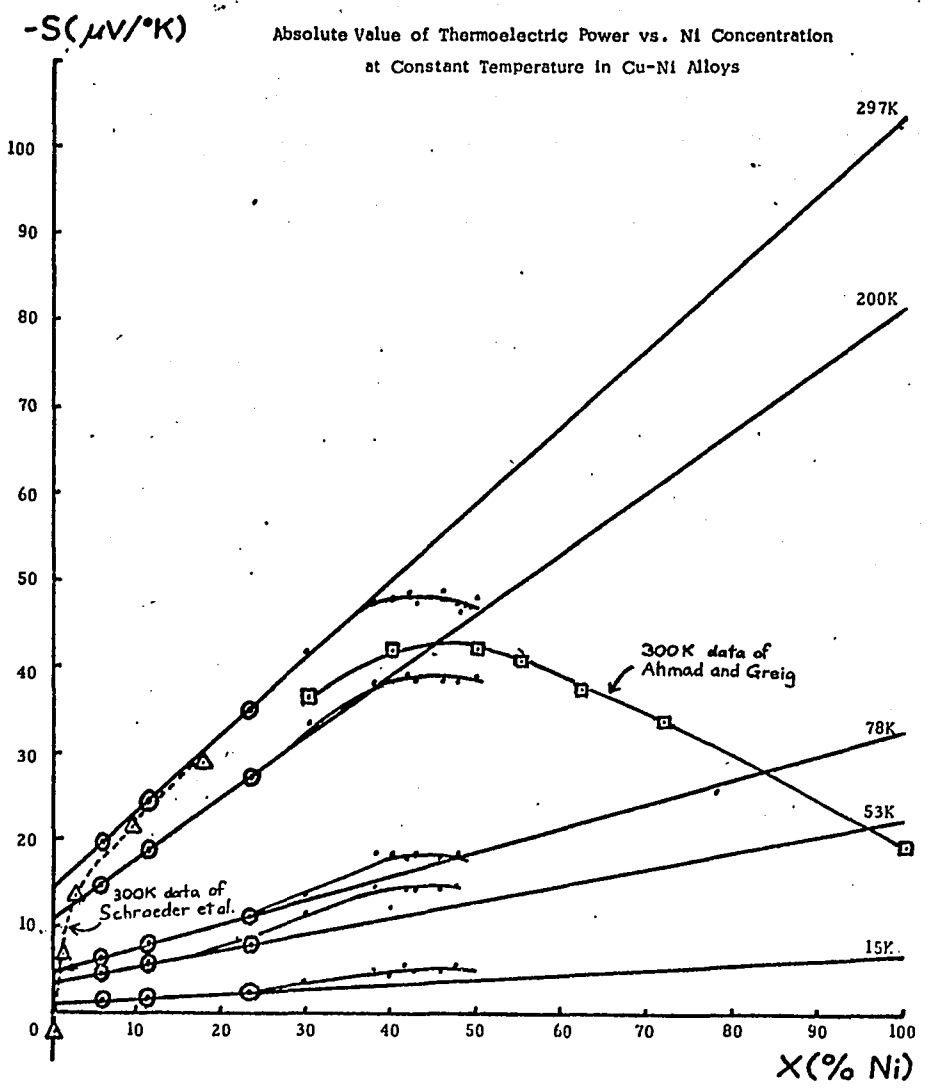
-S(μV/°K)
Absolute Value of Thermoelectric Power vs. Ni Concentration
at Constant Temperature in Cu-Ni Alloys
297K
200K
300K data of
Ahmad and Greig
78K
53K
300K data of
Schroeder et al.
15K.
0
10
20
30
40
50
60
70
80
90
100
X(% Ni)

FIGURE 22

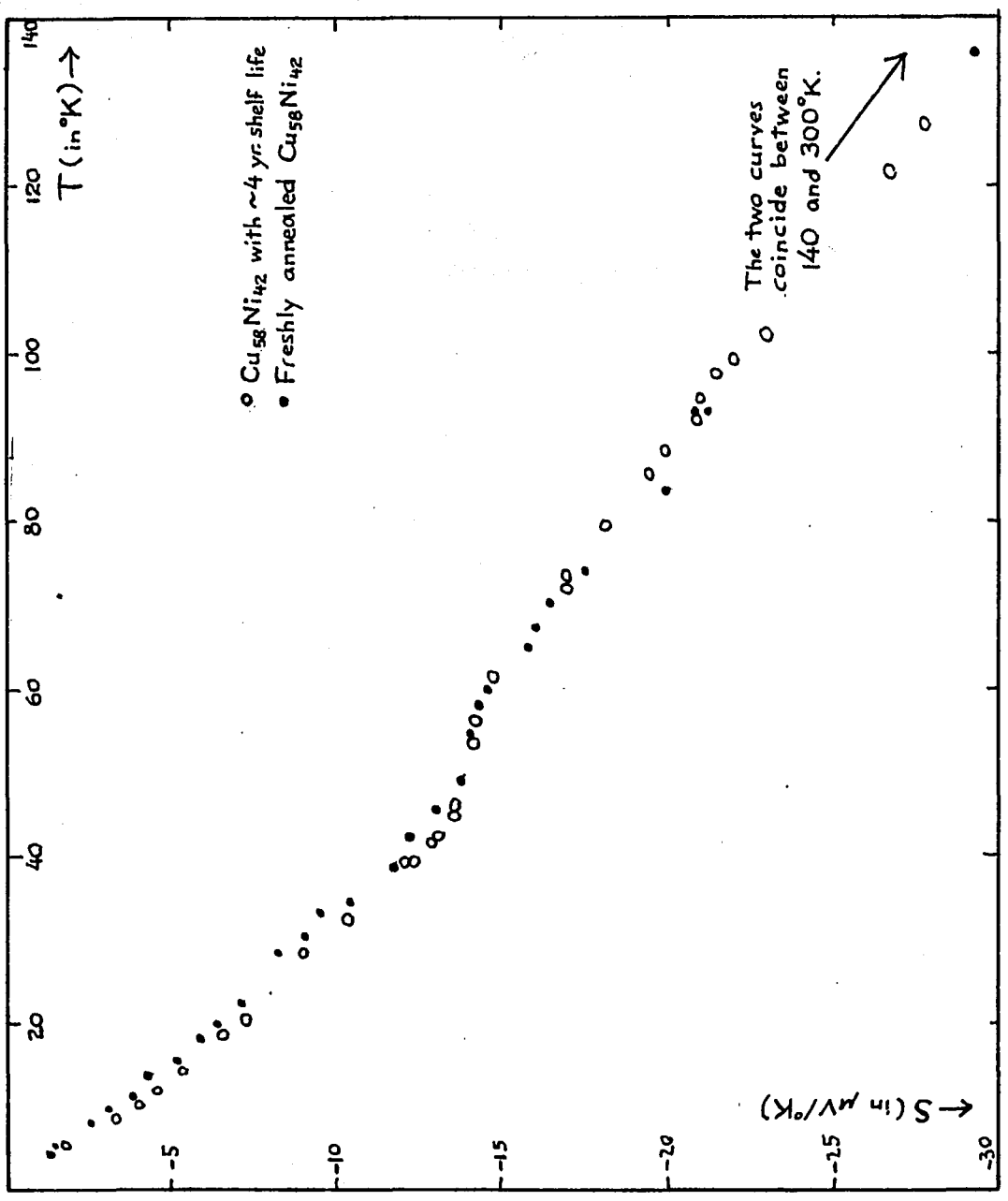
T (in °K) →
20
40
60
80
100
120
140
-5
-10
-15
-20
-25
-30
← S (in μV/°K)
o Cu58Ni42 with ~4 yr. shelf life
• Freshly annealed Cu58Ni42
The two curves coincide between 140 and 300°K.

FIGURE 23

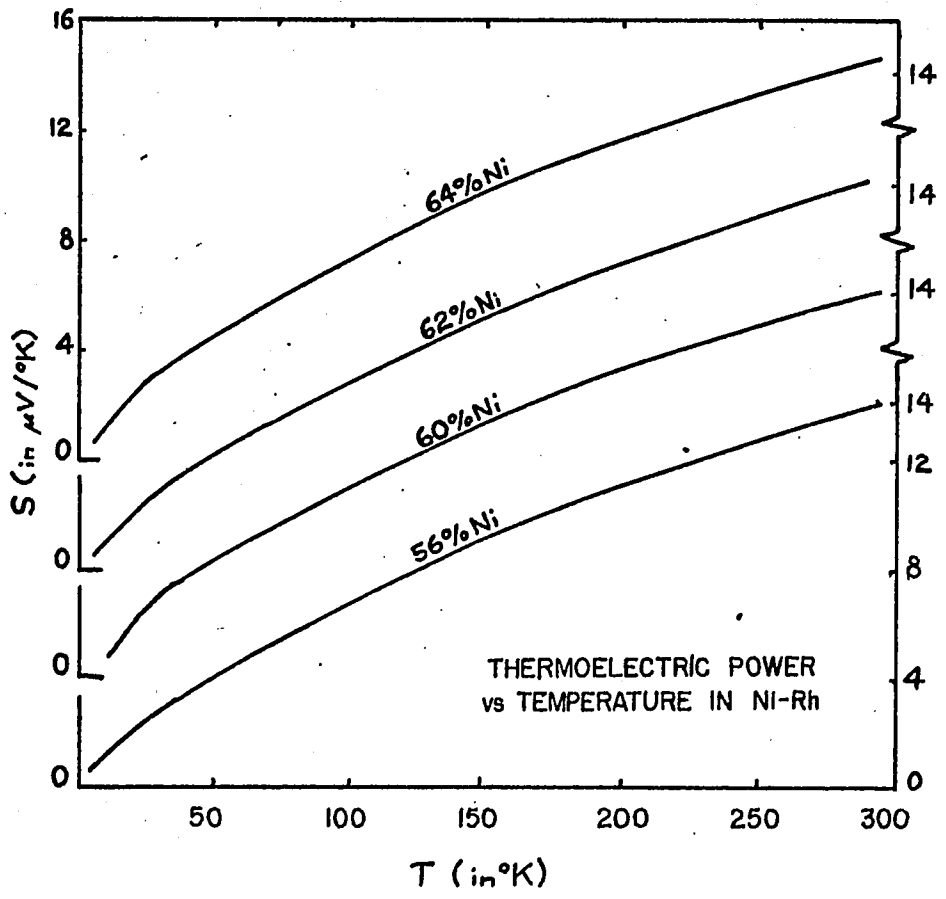
16
12
8
4
0
0
0
0
14
14
14
14
12
8
4
0
64%Ni
62%Ni
60%Ni
56%Ni
S (in μV/°K)
THERMOELECTRIC POWER
vs TEMPERATURE IN Ni-Rh
50
100
150
200
250
300
T (in °K)

FIGURE 24

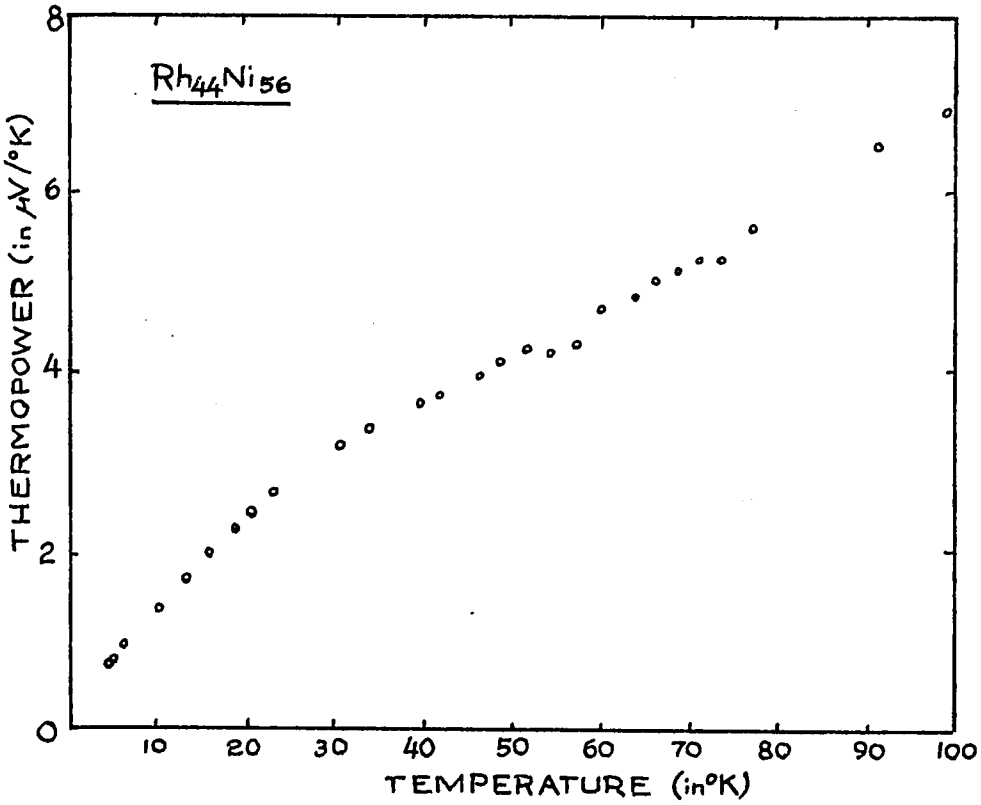
Rh44Ni56
THERMOPOWER (in μV/°K)
TEMPERATURE (in°K)
0
2
4
6
8
10
20
30
40
50
60
70
80
90
100

FIGURE 25

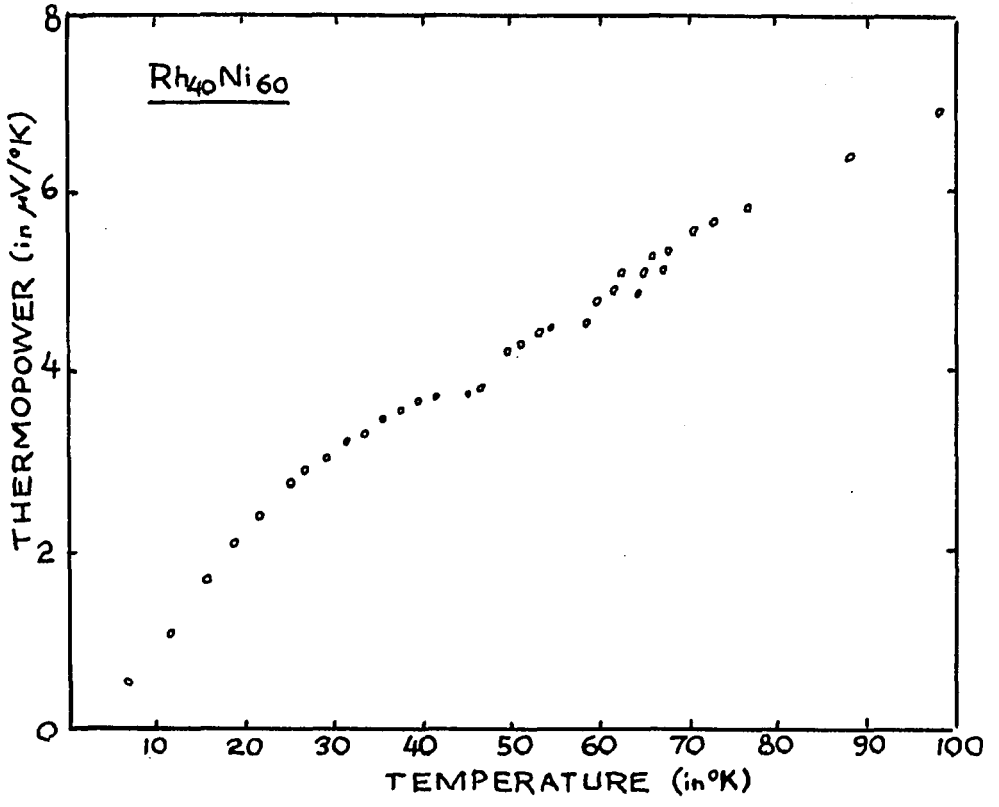
Rh40Ni60
THERMOPOWER (in μV/°K)
TEMPERATURE (in °K)
0
2
4
6
8
10
20
30
40
50
60
70
80
90
100

FIGURE 26

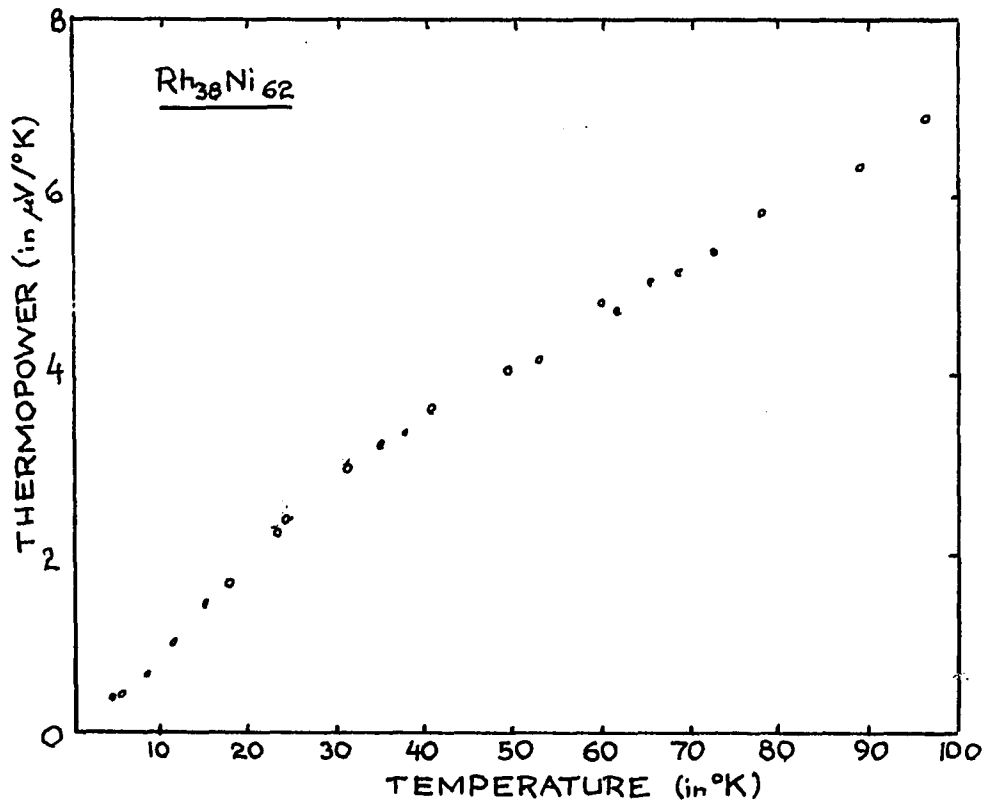
Rh38Ni62
THERMOPOWER (in μV/°K)
TEMPERATURE (in °K)
0
2
4
6
8
10
20
30
40
50
60
70
80
90
100

FIGURE 27

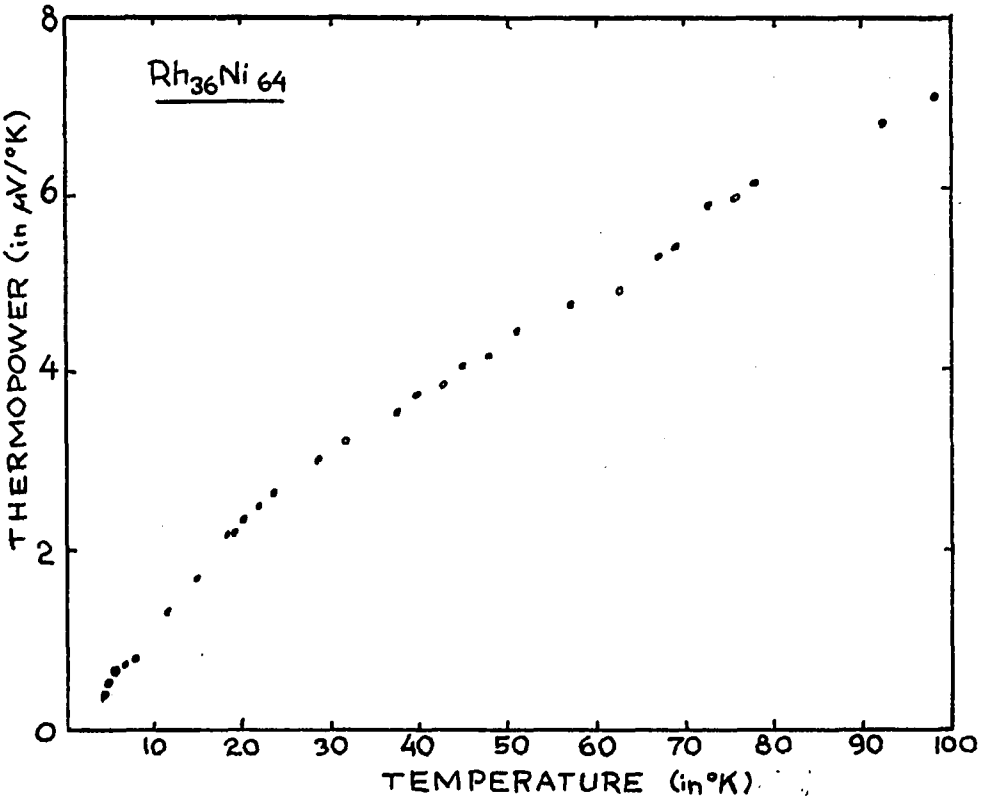
Rh36Ni64
THERMOPOWER (in μV/°K)
TEMPERATURE (in °K)
0
2
4
6
8
10
20
30
40
50
60
70
80
90
100

FIGURE 28

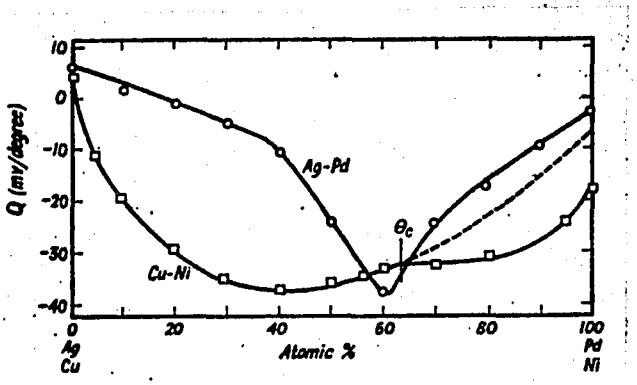


Thermopower of alloys of transition metals (Coles, 1951).

FIGURE 29

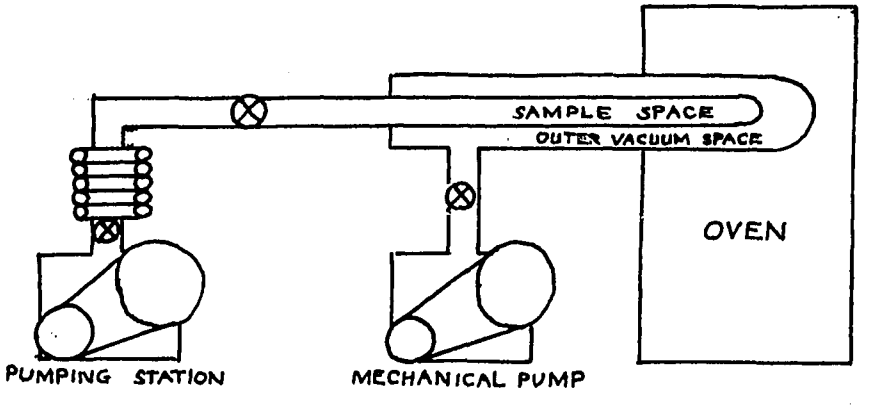


FIGURE 30

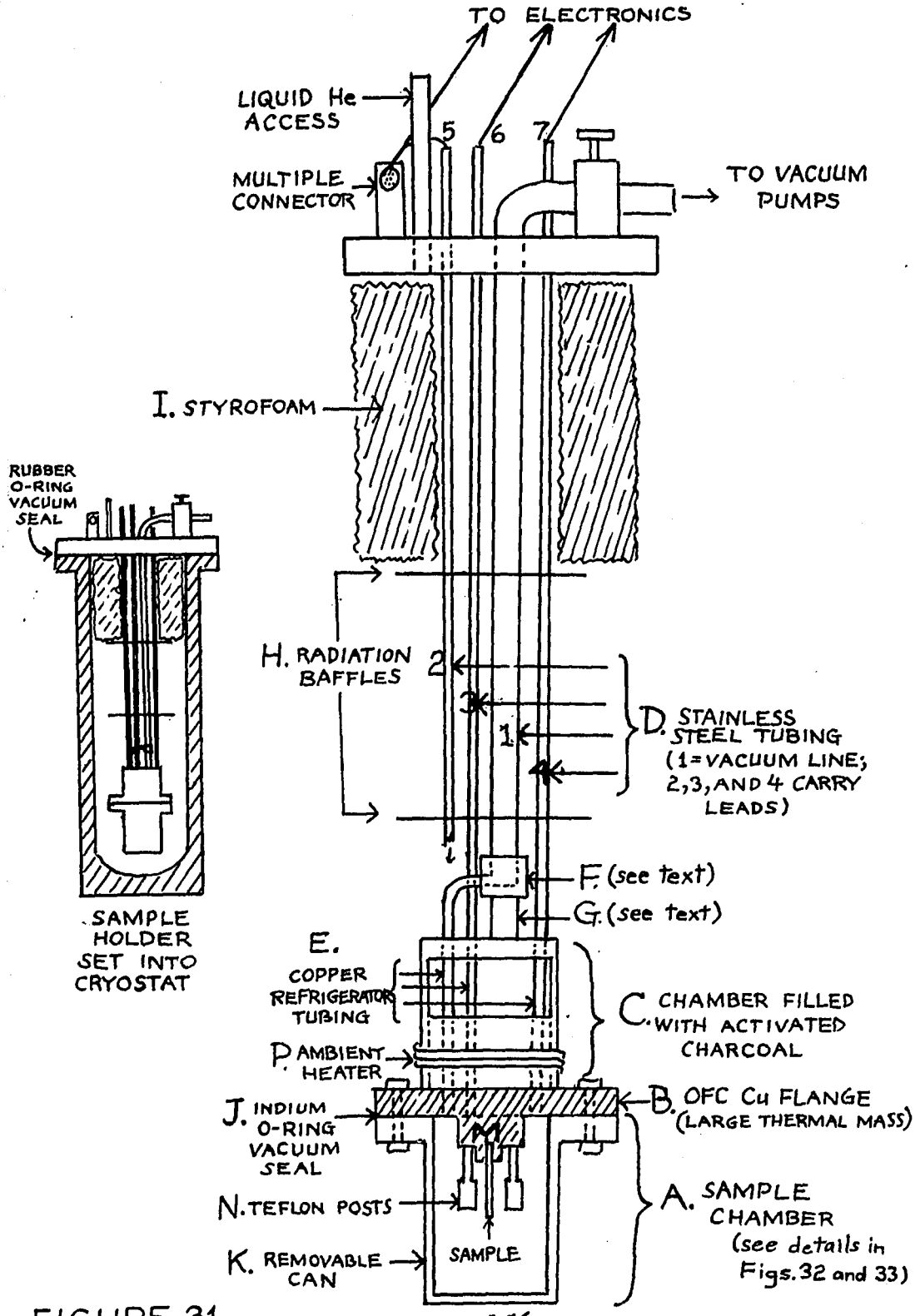
TO ELECTRONICS
LIQUID He ACCESS
MULTIPLE CONNECTOR
5
6
7
TO VACUUM PUMPS
I. STYROFOAM
RUBBER O-RING VACUUM SEAL
H. RADIATION BAFFLES
2
3
1
4
D. STAINLESS STEEL TUBING (1=VACUUM LINE; 2,3, AND 4 CARRY LEADS)
F. (see text)
G. (see text)
SAMPLE HOLDER SET INTO CRYOSTAT
E.
COPPER REFRIGERATOR TUBING
C. CHAMBER FILLED WITH ACTIVATED CHARCOAL
P. AMBIENT HEATER
J. INDIUM O-RING VACUUM SEAL
B. OFC Cu FLANGE (LARGE THERMAL MASS)
N. TEFLON POSTS
K. REMOVABLE CAN
SAMPLE
A. SAMPLE CHAMBER (see details in Figs. 32 and 33)

FIGURE 31

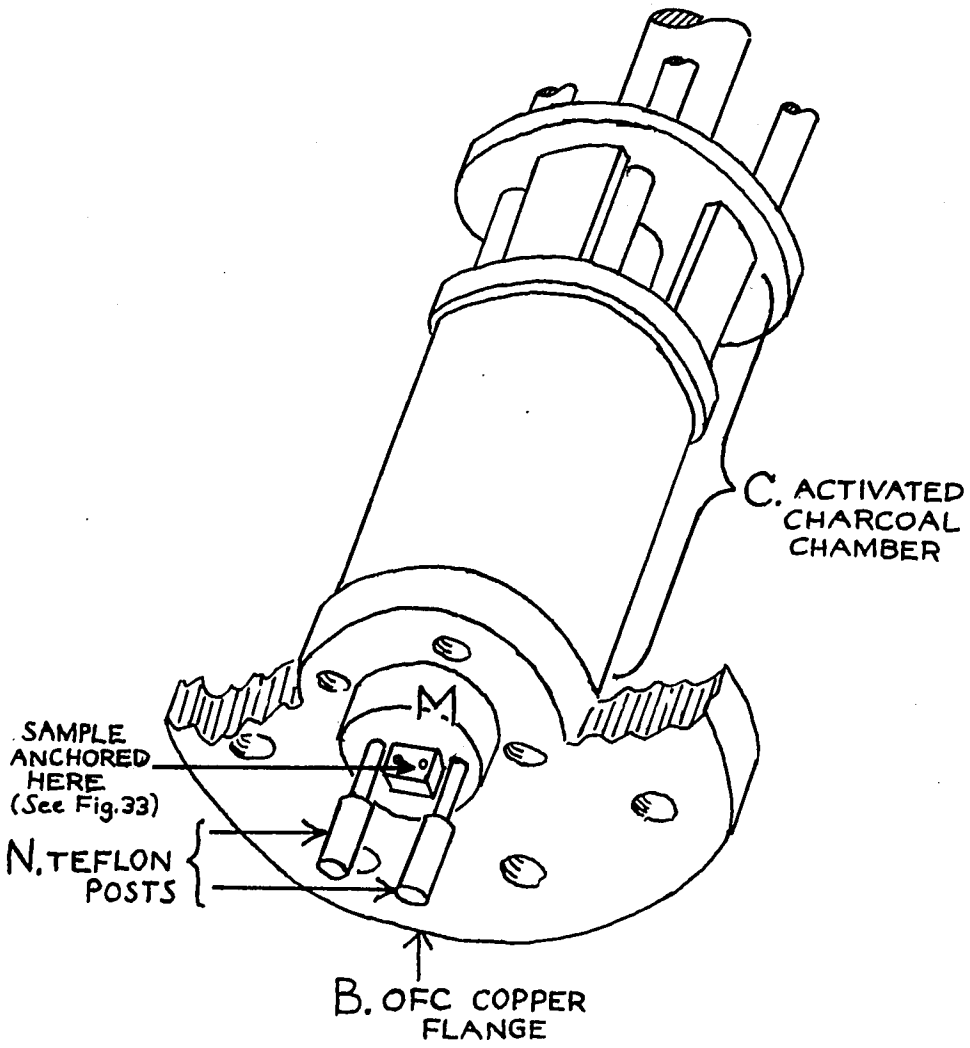
C. ACTIVATED CHARCOAL CHAMBER
M.
SAMPLE ANCHORED HERE (See Fig. 33)
N. TEFLON POSTS
B. OFC COPPER FLANGE

FIGURE 32

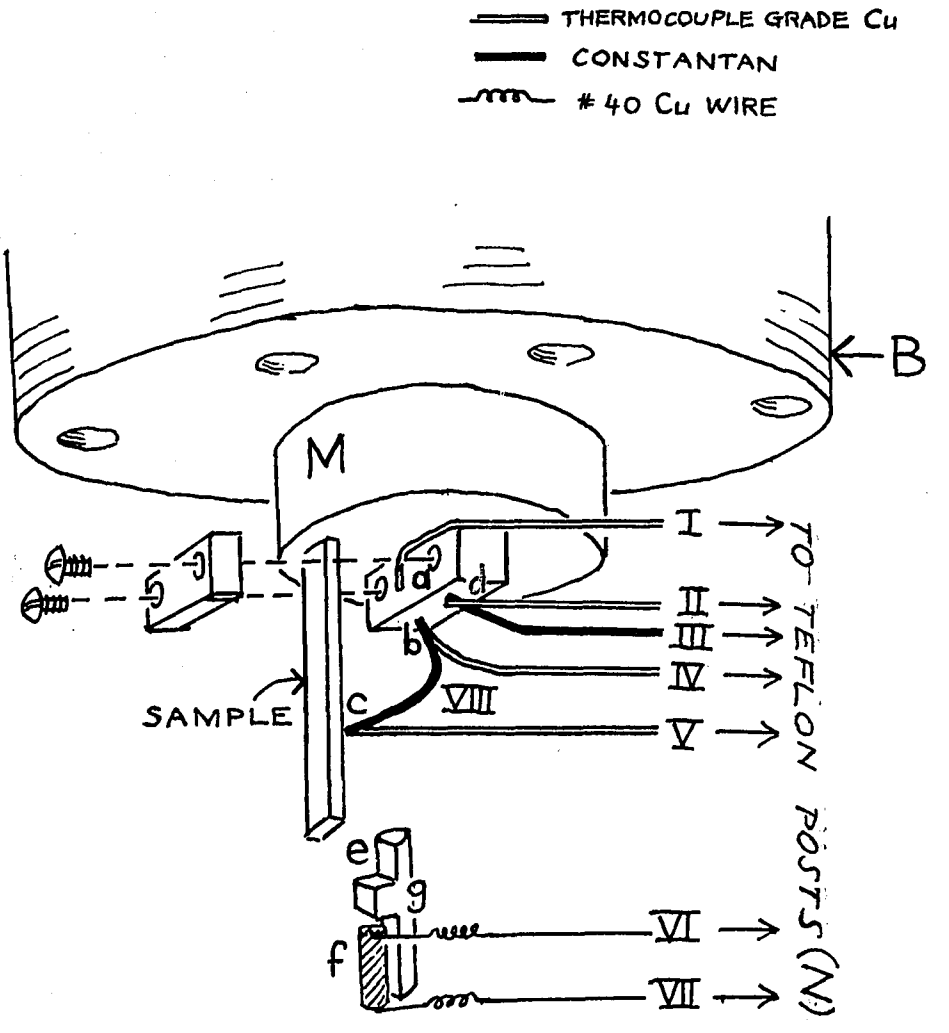
THERMOCOUPLE GRADE Cu
CONSTANTAN
# 40 Cu WIRE
B
M
I
II
III
IV
V
VI
VII
VIII
a
b
c
d
e
f
g
SAMPLE
TO TEFLON POSTS (N)

FIGURE 33

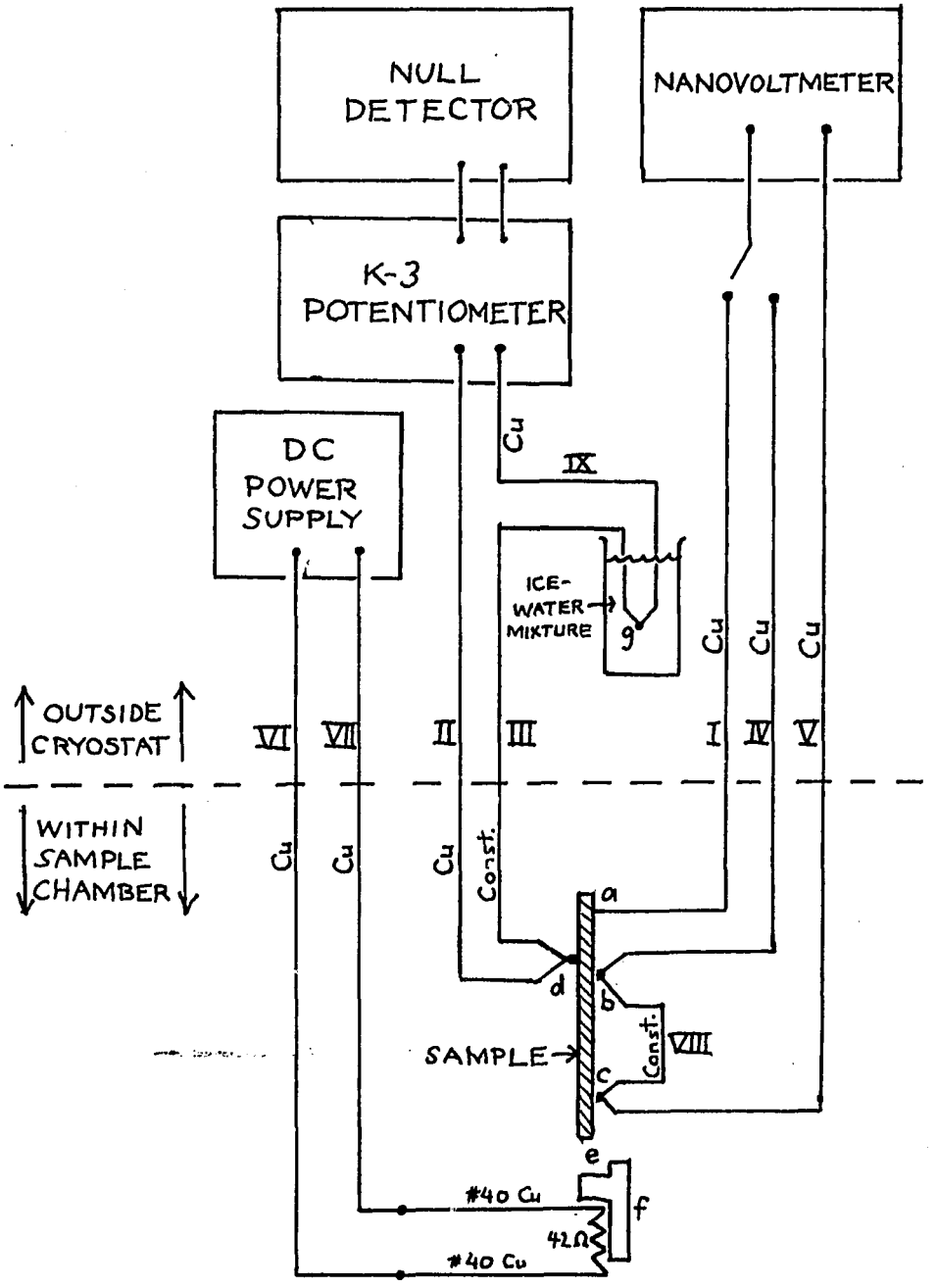
NULL DETECTOR
NANOVOLTMETER
K-3 POTENTIOMETER
DC POWER SUPPLY
Cu
IX
ICE-WATER MIXTURE
g
Cu
Cu
Cu
OUTSIDE CRYOSTAT
VI
VII
II
III
I
IV
V
WITHIN SAMPLE CHAMBER
Cu
Cu
Cu
Const.
a
d
b
Const.
VIII
SAMPLE
c
e
#40 Cu
f
42Ω
#40 Cu

FIGURE 34